Московский физико-технический институт (государственный университет)
Сколковский институт науки и технологий

ВЫПУСКНАЯ КВАЛИФИКАЦИОННАЯ РАБОТА
«Транспорт вдоль геликоидального края в присутствии магнитной примеси»
(магистерская диссертация)

Студент: Курилович Владислав Даниилович

Научный руководитель: Бурмистров Игорь Сергеевич, д. ф.-м. н.

Москва 2018

Moscow Institute of Physics and Technology (State University)
Skolkovo Institute of Science and Technology

MASTER'S THESIS
«Helical Edge Transport in the Presence of a Magnetic Impurity»

Student: Vladislav Kurilovich

Thesis advisor: Igor Burmistrov, Ph.D., D.Sc.

Moscow 2018

Acknowledgements

Contents

Chapter 1

Introduction

In the recent years, condensed matter systems which exhibit topologically non-trivial order received a lot of attention. A family of materials known as topological insulators is among the most prominent and well-established examples of those [1, 2, 3].

Topological insulators are novel semiconducting structures that behave as insulators in the bulk and, at the same time, are characterized by the existence of highly mobile electronic states propagating along the sample boundary. The emergence of such states stems from the non-trivial topology of the band structure which is induced in topological insulator materials by a strong spin-orbit interaction. These boundary states, commonly referred to as edge states in two-dimensional (2D) systems and surface states in three-dimensional (3D) systems, possess linear dispersion that spans the band gap. Spin-orbit coupling enforces spin-momentum locking of edge and surface states: the direction of their motion is rigidly tied with a spin degree of freedom.

Examples of 3D topological insulators include Bi_2Te_3, Bi_2Te_2Se, Sb_2Te_3, and many others [4]. The energy dispersion of surface states in these materials forms a Dirac cone which is spin-polarized in a helical way (see Fig. 1.1). The presence of such Dirac cone in 3D topological insulators was revealed experimentally via the angle-resolved photoemission spectroscopy measurements [5, 6].

In 2006, Bernevig, Hughes, and Zhang theoretically predicted [8] that 2D topological insulators can be realized in CdTe/HgTe/CdTe quantum wells (for the sketch of a realistic setup see Fig. 1.2).
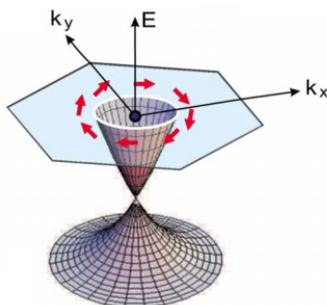

Figure 1.1: Surface states energy dispersion $E(\boldsymbol{k})$ for a 3D topological insulator. $E(\boldsymbol{k})$ forms a Dirac cone. For every $\boldsymbol{k}$ spin of the surface state (depicted in red) is perpendicular to its momentum. Consequently, the cone is spin-polarized helically. The image is adapted from [3].

It was shown that the topological state of a quantum well (QW) depends on the thickness d of the intermediate HgTe layer. If d is smaller than the critical value $d_c \simeq 6.3$ nm, then the QW is in a trivial regime. As the thickness increases, the gap between spatially quantized electron and hole bands of the heterostructure drops down and nullifies at $d = d_c$. For $d > d_c$ the gap opens up again, although the order of the bands gets inverted. As a result, the QW enters a topologically non-trivial phase which manifests itself in a presence of the edge states. This prediction was soon confirmed experimentally [9, 10]. Later, other examples of 2D topological insulators were discovered. Among them are InAs/GaSb heterostructures [11], bismuth bilayers [12], and WTe$_2$ monolayers [13].

The spectrum of the edge states of the 2D topological insulator consists of two linear branches that cross at the Γ-point (see Fig. 1.3). The branches bear a helical character: counter-propagating states have opposite spin projection on the direction perpendicular to the plane of the structure. This peculiar spin polarization gives rise to the quantum spin Hall effect – an analog of the quantum Hall effect in which the quantized spin current is transferred along the edge of the sample.

Time-reversal symmetry prohibits the elastic backscattering of the edge states by the potential (*non-magnetic*) disorder. Hence, even in the presence of the latter, the ideal ballistic current $I_0 = G_0 V$ ($G_0 = e^2/h$) is expected to propagate along the edge of the topological insulator under the applied voltage V.

Experiments conducted by the group of L. W. Molenkamp on CdTe/HgTe/CdTe quantum wells [9]
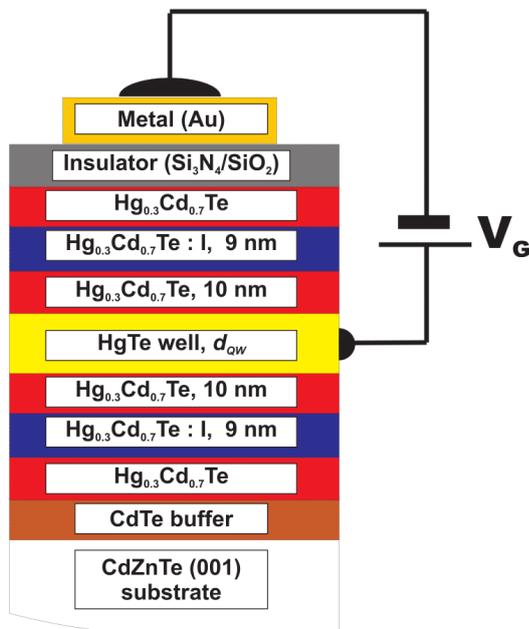
Figure 1.2: Sketch of a realistic experimental setup. Quantum well is formed by a thin HgTe layer surrounded by the layers of Hg$_{0.3}$Cd$_{0.7}$Te. The image is adapted from [7].
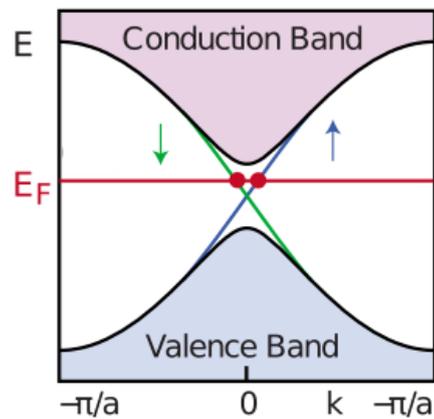
Figure 1.3: Sketch of the energy dispersion $E(k)$ of a two-dimensional topological insulator. The band gap is span by a pair of counter-propagating helical edge states. Electrons with a positive (negative) velocity have spin pointing up (down). The image is adapted from [3].

demonstrated the anticipated quantization of the conductance in the relatively short clean samples. Fig. 1.4 depicts the measured dependence of the resistivity on the gate voltage. Indeed, the conductance G of the devices with the length $l = 1\ \mu$m reaches the value of $2G_0$ when the chemical potential is tuned to lie inside the band gap (factor 2 appears because there are two edges in the Hall bar sample). However, the conductance of the longer samples (see curves I and II in Fig. 1.4, $l = 20\ \mu$m) turned out to be drastically lower.

Further studies revealed that the character of the helical edge transport in long samples is *diffusive* rather than ballistic. For instance, the experiments performed by the group of Z.D. Kvon on CdTe/HgTe/CdTe QWs with the length $l \geq 2$nm [14] showed the resistance exceeding the quantum $R_0 = 1/G_0$ by two orders of magnitude which scaled linearly with l (see Fig. 1.5). At the same time, the non-local measurements indicated that the current flowed along the edge and not through the bulk.

Remarkably, resistance obtained in [14] turned out to be almost temperature independent at low temperatures (see Fig. 1.6). The experiments with other 2D topological insulators, e.g. InAs/GaSb bilayers [11] and WTe$_2$ [13] monolayers, also demonstrated the conductance lower than the quantum in sufficiently long samples which exhibited weak temperature dependence.

The experimental observations triggered the intense theoretical research of the possible sources for the reduction of the conductance from the ballistic value. The efforts were additionally fuelled by the promises of technological applications of the topological insulators in spintronics. As a result, several mechanisms that could account for the discrepancy with the initial expectation of the quantized current were identified.

Local perturbations that violate time-reversal symmetry such as classical magnetic impurities give rise to spin-flip processes of the edge electrons and result in backscattering [15]. The backscattering mediated contribution to the current, hereinafter labeled by I_{bs}, is negative and, therefore, drives the conductance down from the quantized value G_0. Even if the time-reversal symmetry is
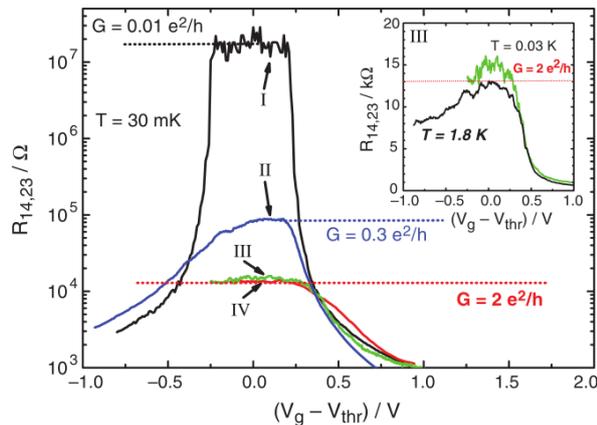
Figure 1.4: Resistivity as a function of gate voltage in a Hall bar geometry. Curves I and II correspond to the devices of the size $(20 \times 13.3)\ \mu$m^2 (length$\times$width). Curves III and IV are plotted for the device sizes $(1 \times 1)\ \mu$m^2 and $(1 \times 0.5)\ \mu$m^2 respectively. The plateaus in the middle correspond to the chemical potential pinned to the band gap. The image is adapted from [9].
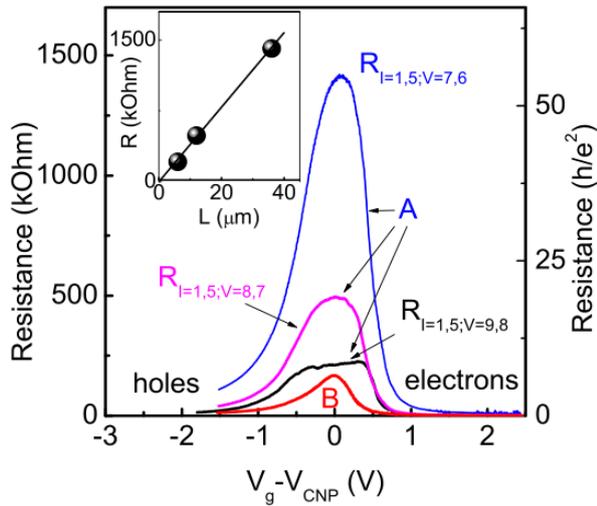
Figure 1.5: Resistance as a function of the gate voltage for the samples of the length $l = 2, 8, 32$ μm (black, purple, and blue curves respectively). Inset: resistance as the function of the device length. The image is adapted from [14].
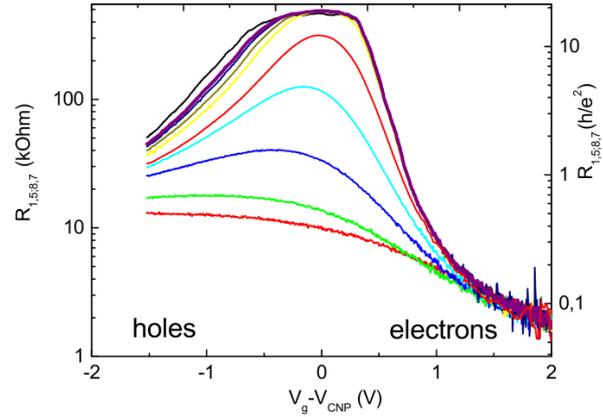
Figure 1.6: Resistance as a function of the gate voltage for the device of the length $l = 8$ μm at different temperatures. $T(K) = 62, 53, 40, 29, 19, 10, 4.2, 3.5, 3, 2.5, 1.5$ for the curves in the bottom-up order. The image is adapted from [14].

not broken electron-electron interaction may hinder the edge conductivity at finite temperature [16].

The deviations from the ballistic conductance may also arise due to the interaction of the helical electrons with charge puddles located near the edge of the topological insulator [17, 18]. Charge puddles are the metallic islands which are formed in semiconductor heterostructures with a narrow band gap due to the presence of the disorder potential. Created by the fluctuations in dopant density, this potential may locally push the Fermi level into the conduction or valence bands thereby forming the conductive regions, i.e. the puddles of charge.

A charge puddle located close to the boundary of the topological insulator acts as a quantum dot into which the helical electrons may tunnel. In the even valley regime of the Coulomb blockade, this quantum dot causes inelastic backscattering of the edge electrons and reduces the current from its ballistic value. However, the respective correction to the conductance strongly depends on temperature and, hence, cannot fully explain the experimental results presented in [14] and [11, 13].

The charge puddle in the odd valley regime behaves as a spin-1/2 magnetic impurity coupled to the edge electrons by almost isotropic exchange interaction. Such impurity is capable of flipping spins of the helical electrons and, thus, suppress the edge conductivity. Notably, in the linear regime the backscattering current I_{bs} is almost temperature independent provided that the temperature is larger than the Kondo temperature T_{K}.

The impurities with quantum dynamics may also be present in topological insulators due to contamination by the magnetic ions. A particular example of the latter is manganese ion Mn^{2+}

which, embedded in CdTe or HgTe, has a spin $S = 5/2$. The helical edge transport in the presence of a quantum magnetic impurity with $S = 1/2$ was studied in [19, 20, 21]. In these works, specific restrictive assumptions about the structure of the exchange interaction were made which are not generally justified.

The correction to the conductance mediated by the impurity with $S \geq 1/2$ was investigated recently in the work [22]. There, the backscattering current I_{bs} was evaluated in a wide region of voltages in the presence of Rashba interaction. However, the local magnetic anisotropy was fully disregarded. Such anisotropy inevitably exists in realistic systems for the impurities with spin $S > 1/2$. It may substantially alter the character of backscattering at low energies and, hence, cannot be always neglected.

In the present work, we investigate the transport properties of the edge of a 2D topological insulator weakly coupled to *a sole anisotropic magnetic impurity* with arbitrary spin S. The current flowing along the edge under the applied voltage V may be divided as $I = I_0 + I_{bs}$, where $I_0 = G_0 V$ is the ballistic current and I_{bs} is a *relatively small* negative correction to I_0 related to the impurity induced backscattering of helical electrons. Our goal in this thesis is to evaluate I_{bs} at any voltage V. Contrary to the previous works, we do not make any limiting assumptions about the matrix structure of the exchange interaction and develop a theory which is valid in the general case.

The outline of the thesis is as follows.

- In Chapter 2 we introduce the model of a 2D topological insulator with a magnetic impurity in it. There we focus on topological insulators based on CdTe/HgTe/CdTe quantum wells with the width $d > d_c$. First, we review the Bernevig-Hughes-Zhang Hamiltonian and describe bulk and edge electronic states within its framework. Then we present the exchange interaction Hamiltonian which governs the coupling between the electrons confined in the QW and the impurity. Ultimately, we derive the low-energy Hamiltonian for the helical electrons. We stress that the final formulation of the model (see Eq. (2.22)) is not limited to the topological insulators based on CdTe/HgTe/CdTe QWs only. It may be equally well applied to describe the edge transport in other 2D topological insulators, e.g. InAs/GaSb heterostructures and WTe$_2$ monolayers.

- In Chapter 3 we evaluate the backscattering current I_{bs} under the assumption of negligible anisotropy. We show that the problem of computing I_{bs} may be reduced to the determination of the stationary state of the magnetic impurity. To establish the latter we derive *the master equation* which controls the evolution of the reduced density matrix ρ_S of the impurity. With

its help, we describe the backscattering current at arbitrary voltage V. The results of this chapter are published in [23].

- In Chapter 4 we investigate the influence of local magnetic anisotropy of the impurity on the helical edge transport. The cases of uniaxial and non-uniaxial anisotropy are considered. In addition to that, we establish the conditions under which the anisotropy may be disregarded.

- The conclusions are presented in Chapter 5.

Throughout the thesis we use the units in which $k_B, \hbar, |e| = 1$.

Chapter 2

The model

In this chapter, we present and discuss the model of a 2D topological insulator with a magnetic impurity nearby its edge. The emphasis is made on topological insulators based on CdTe/HgTe/CdTe quantum wells albeit the resultant model is applicable to many other systems as well.

In section 2.1 we provide a low-energy description of the electronic structure of a 2D topological insulator based on (001) CdTe/HgTe/CdTe quantum well. We consider both edge and bulk states. In section 2.2 we discuss the way in which a localized magnetic moment embedded into the crystal lattice may be taken into account. Finally, in section 2.3 we derive the effective model for the edge states. The corresponding Hamiltonian describes the exchange interaction between the helical electrons and the magnetic impurity. A generalized version of such Hamiltonian may be employed to describe the helical edge transport in other physically relevant scenarios.

2.1   Bernevig-Hughes-Zhang Hamiltonian

In order to describe the low-energy physics of electron and hole states in a two-dimensional topological insulator based on (001) CdTe/HgTe/CdTe quantum well we employ the Bernevig-Hughes-Zhang Hamiltonian [8]. In the basis of spatially quantized states $|E_1, +\rangle, |H_1, +\rangle, |E_1, -\rangle, |H_1, -\rangle$[1] it has the block-diagonal form

$$H_{\text{BHZ}}(\boldsymbol{k}) = \mathcal{C}(k)I_{4\times 4} + \begin{pmatrix} h(\boldsymbol{k}) & 0 \\ 0 & h^T(-\boldsymbol{k}) \end{pmatrix}, \quad h(\boldsymbol{k}) = \begin{pmatrix} \mathcal{M}(k) & Ak_+ \\ Ak_- & -\mathcal{M}(k) \end{pmatrix}. \quad (2.1)$$

---

[1]The basis states are characterized by the angular momentum projection j_z on the direction z transversal to the plane of the topological insulator, i.e. for $|E_1, \pm\rangle$ the projection equals $j_z = \pm 1/2$ and for $|H_1, \pm\rangle$ $j_z = \pm 3/2$. For the explicit structure of the states see [8].

Here $I_{4\times 4}$ is a 4×4 identity matrix, T is the matrix transposition, $\boldsymbol{k} = (k_x,\ k_y)^T$ is a 2D wave vector in the plane of the topological insulator, $k = \sqrt{k_x^2 + k_y^2}$ is its absolute value, $k_{\pm} = k_x \pm i k_y$, and

$$\mathcal{C}(k) = C - Dk^2, \quad \mathcal{M}(k) = M - Bk^2. \tag{2.2}$$

The material parameters A, B, C, D, and M depend smoothly on the width d of the quantum well. We note that C describes the constant energy shift which can be absorbed in the energy redefinition. Hence, in what follows we omit it. For further reference, we mention that for the quantum well with the width $d = 7.0$ nm $A = 0.37$ eV $\cdot$ nm, $B = -0.69$ eV $\cdot$ nm^2, $D = -0.51$ eV $\cdot$ nm^2, and $M = -0.01$ eV [2].

The upper (lower) block of the Hamiltonian (2.1) describes the states with positive (negative) projection j_z of the angular momentum on the z-axis transversal to the plane of the topological insulator. The two blocks are connected by the time-reversal symmetry and are not mixed. The latter feature implies that all of the eigenstates of (2.1) may be divided into the two subsets: one includes states originating from the upper block – to indicate the positive projection of angular momentum we will denote such states by $\uparrow$ subscript – and the other consists of states coming from the lower block ($\downarrow$ subscript). Later, we will often refer to $\uparrow$ / $\downarrow$ index as pseudo-spin.

Under the assumption of the infinite sample, the Hamiltonian (2.1) may be readily diagonalized. For the spectrum of the conduction band one obtains $E_{\text{bulk},\uparrow/\downarrow}^{+}(\boldsymbol{k}) = \mathcal{C}(k) + \sqrt{\mathcal{M}^2(k) + A^2 k^2}$. Note the two-fold "spin" degeneracy with respect to $\uparrow$ / $\downarrow$ index. Similarly, the dispersion of the valence band is given by $E_{\text{bulk},\uparrow/\downarrow}^{-}(\boldsymbol{k}) = \mathcal{C}(k) - \sqrt{\mathcal{M}^2(k) + A^2 k^2}$. The expressions for $E_{\text{bulk},\uparrow/\downarrow}^{\pm}$ demonstrate that the parameter M controls the gap in the energy spectrum.

The gap M is positive for the quantum wells with $d < d_c \simeq 6.3$ nm and negative for the quantum wells with $d > d_c$ [8]. Thus, at $d = d_c$ the band inversion takes place. For $d > d_c$ the quantum well is in a topologically non-trivial regime and its Hamiltonian (2.1) cannot be matched adiabatically to vacuum. This feature reveals itself in a pair of counter-propagating gapless states localized near the edge of the sample.

In order to simplify the further discussion we note that the quadratic terms in the Hamiltonian (2.1) are not substantial for the discussion of transport properties of the helical edge. Hence, in the following we omit them and work with a *linearized* version of the Bernevig-Hughes-Zhang
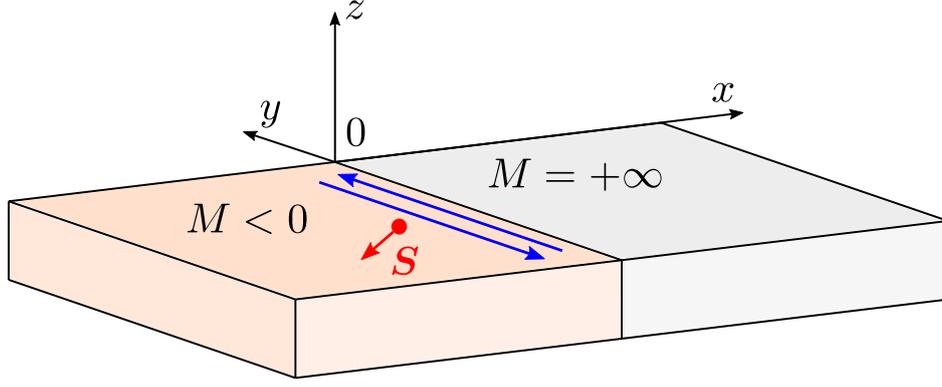
Figure 2.1: Sketch of the topological insulator in the considered model. Band inversion is realized at $x = 0$: $M(x)$ is a negative constant inside the topological insulator ($x < 0$) and $M(x) = +\infty$ in the topologically trivial region $x > 0$. The edge is directed along y. Two helical modes depicted with blue arrows propagate along it. The magnetic impurity with spin S is depicted in red. With changes the image is adapted from [25].

Hamiltonian:

$$H_{\text{BHZ}}(\boldsymbol{k}) = \begin{pmatrix} M & Ak_+ & 0 & 0 \\ Ak_- & -M & 0 & 0 \\ 0 & 0 & M & -Ak_- \\ 0 & 0 & -Ak_+ & -M \end{pmatrix}. \tag{2.3}$$

To account for the edge states in this model we adopt the approach of B.A. Volkov and D.A. Pankratov [24]. We suppose that the gap M is spatially dependent so that the band inversion is realized along the line $x = 0$. We take $M = M(x)$ as a negative constant inside the topological insulator ($x < 0$) and assume that $M(x) = +\infty$ in the topologically trivial region $x > 0$ (see Fig. 2.1).

In the presence of the edge the wave vector in the x-direction is not a good quantum number. Hence, in the Schrödinger equation k_x should be replaced by $-i\partial_x$. Yet, k_y is still a well-defined quantity. Solving $H_{\text{BHZ}}(-i\partial_x, k_y)\psi(\boldsymbol{r}) = E\psi(\boldsymbol{r})$ we show that there exists a pair of edge states connected by the time reversal symmetry of the following structure

$$\psi_{\text{edge},\uparrow}(\boldsymbol{r}, k_y) = \begin{pmatrix} 1 \\ i \\ 0 \\ 0 \end{pmatrix} \frac{e^{-|x|/\xi}}{\sqrt{\xi}} e^{ik_y y}\theta(-x), \quad \psi_{\text{edge},\downarrow}(\boldsymbol{r}, k_y) = \begin{pmatrix} 0 \\ 0 \\ 1 \\ -i \end{pmatrix} \frac{e^{-|x|/\xi}}{\sqrt{\xi}} e^{ik_y y}\theta(-x). \tag{2.4}$$

Here $\theta(x)$ is Heaviside step function, $\boldsymbol{r} = (x, y)^T$, and $\xi = A/|M|$ is a typical width of the edge states. For further estimates, we mention that for the quantum well with $d = 7.0\,\text{nm}$ the length scale $\xi \simeq 40$ nm. The presence of the absolute value $|x|$ in the exponents stresses that the topological insulator spans $x < 0$ half-plane. The states $\psi_{\text{edge},\uparrow}$ and $\psi_{\text{edge},\downarrow}$ are related to the upper and lower

14

blocks of the 4×4 Hamiltonian (2.3) respectively. Within the model (2.3) the dispersion of the edge states is *precisely* linear, $E_{\text{edge},\uparrow/\downarrow}(k_y) = \mp A k_y$. Notice that the parameter A plays the role of the edge states velocity along the y-direction. We emphasize that the sign of the velocity differs for the states with positive ($\uparrow$ subscript) and negative ($\downarrow$ subscript) pseudo-spin. This rigid connection between the pseudo-spin and the direction of motion of the helical electrons is the essence of the spin-momentum locking.

Next, we consider the bulk states in the model (2.3). We will employ the their structure explicitly while discussing the influence of the local magnetic anisotropy on the helical edge transport (see Chapter 4). We note that the bulk states are characterized by the 2D wave vector k even in the presence of the edge albeit in the this case k_x is restricted to the positive values only. It is convenient to introduce the following functions of k:

$$f_x^{\pm}(\boldsymbol{k}) = \frac{\left(Ak_{\pm} \pm i\left(\mathcal{E}(k) \mp |M|\right)\right)e^{ik_x x} + \text{c.c}}{2\sqrt{\mathcal{E}(k)\left(\mathcal{E}(k) + Ak_y\right)}}\theta(-x), \tag{2.5}$$

where c.c. stands for the complex conjugate and $\mathcal{E}(k) = \sqrt{M^2 + A^2 k^2}$. Then the wave functions of the bulk states may be expressed as [25]

$$\psi_{\text{bulk},\uparrow}^{\pm}(\boldsymbol{r},\boldsymbol{k}) = \begin{pmatrix} \pm f_x^{\pm}(\pm\boldsymbol{k}) \\ \pm i f_x^{\mp}(\pm\boldsymbol{k}) \\ 0 \\ 0 \end{pmatrix}\frac{e^{ik_y y}}{2\pi}, \quad \psi_{\text{bulk},\downarrow}^{\pm}(\boldsymbol{r},\boldsymbol{k}) = \begin{pmatrix} 0 \\ 0 \\ \mp f_x^{\pm}(\mp\boldsymbol{k}) \\ \pm i f_x^{\mp}(\mp\boldsymbol{k}) \end{pmatrix}\frac{e^{ik_y y}}{2\pi}, \tag{2.6}$$

The superscript $\pm$ distinguish between the conduction band ("+" superscript) and the valence band ("−" superscript). The energy spectrum is two-fold degenerate with respect to $\uparrow$ / $\downarrow$ index. It has a massive relativistic form $E_{\text{bulk},\uparrow/\downarrow}^{\pm} = \pm\mathcal{E}(k)$.

The dispersion of the bulk and edge states based on the Hamiltonian (2.3) is presented in Fig.
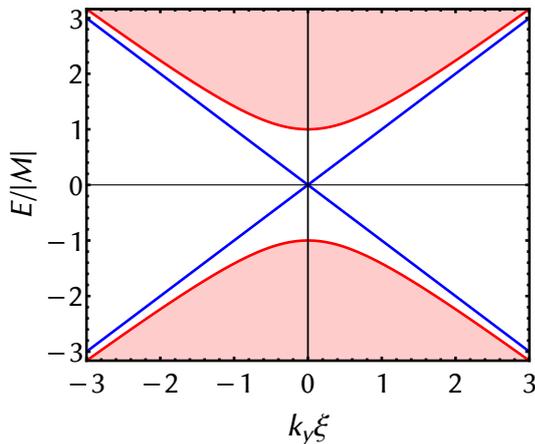
Figure 2.2: The dispersion of bulk and edge states in the model (2.3). The bulk states posses a relativistic massive spectrum $E_{\text{bulk},\uparrow/\downarrow}^{\pm}(\boldsymbol{k})$ which is depicted in red for $k_x = 0$ as a function of k_y. The edge states spectrum $E_{\text{edge},\uparrow/\downarrow}(k_y)$ is gapless (depicted in blue). The branch with a positive (negative) dispersion corresponds to the negative (positive) z-projection of pseudo-spin.

2.2. The bulk states spectrum asymptotically reaches the edge states branches without ever crossing them. This feature is but a consequence of the simplified linear model (2.3). In a more refined model (2.1) the edge states are defined in a finite interval of k_y only [26].

2.2 Electron-impurity interaction

In this section we discuss the interaction between the electrons confined in the (001) quantum well with a single spin-S magnetic impurity. As a possible physical realization of such impurity we keep in mind a manganese ion with $S = 5/2$ which is embedded either in HgTe or in CdTe lattice. We assume that the impurity is situated at some fixed point $\{x_0, y_0, z_0\}$ inside the quantum well (see Fig. 2.1) and interacts with the surrounding electrons *locally*. Projection of microscopically *isotropic* Heisenberg exchange interaction onto the states $|E_1, +\rangle, |H_1, +\rangle, |E_1, -\rangle, |H_1, -\rangle$ yields the following 4×4 electron-impurity Hamiltonian [22, 27]:

$$
H^{\mathrm{e-i}} = \begin{pmatrix} J_1 S_z & -i J_0 S_+ & J_m S_- & 0 \\ i J_0 S_- & J_2 S_z & 0 & 0 \\ J_m S_+ & 0 & -J_1 S_z & -i J_0 S_- \\ 0 & 0 & i J_0 S_+ & -J_2 S_z \end{pmatrix} \delta(x - x_0)\delta(y - y_0). \tag{2.7}
$$

Here $\boldsymbol{S}$ is the impurity spin operator and $S_\pm = S_x \pm i S_y$. The coupling constants J_0, J_1, J_2, and J_m are determined by the structure of the envelop functions of spatially quantized states $|E_1, \pm\rangle$, $|H_1, \pm\rangle$ and depend on z_0 only (for details, see [27]). Noticeably, for $z_0 = 0$, i.e. when the impurity is in the middle of HgTe layer, $J_0 = 0$ and $J_1 = J_m$.

2.3 Effective Hamiltonian of the helical edge

Now we obtain the effective 2×2 low-energy Hamiltonian for the edge states. To do that we project the 4×4 Hamiltonian (2.3) complemented by the electron-impurity interaction (2.7) onto the edge states subspace (2.4). As a result, we find (the summation over $i, j = x, y, z$ is assumed)

$$
H_{\mathrm{edge}} = H^{\mathrm{e}}_{\mathrm{edge}} + H^{\mathrm{e-i}}_{\mathrm{edge}}, \quad H^{\mathrm{e}}_{\mathrm{edge}} = -v k_y \sigma_z, \quad H^{\mathrm{e-i}}_{\mathrm{edge}} = \frac{1}{2\nu} \mathcal{J}_{ij} S_i \sigma_j \delta(y - y_0). \tag{2.8}
$$

Here σ_x, σ_y, and σ_z are the Pauli matrices in the edge states pseudo-spin[2] space $\uparrow$ / $\downarrow$. The presence of σ_z in $H_{\text{edge}}^{\text{e}}$ underscores the spin-momentum locking of the helical states. $v = A$ is the edge states velocity, $\nu = 1/(2\pi v)$ is the density of states per one edge mode, and $\mathcal{J}_{ij}$ is a matrix of *dimensionless* exchange coupling constants. The latter is given by [22, 23]

$$\mathcal{J} = \frac{2\nu}{\xi} e^{-2|x_0|} \begin{pmatrix} J_m & 0 & 2J_0 \\ 0 & J_m & 0 \\ 0 & 0 & J_z \end{pmatrix}, \qquad (2.9)$$

where $J_z = J_1 + J_2$.

For the sake of clarity, we rewrite the effective electron-impurity interaction explicitly:

$$H_{\text{edge}}^{\text{e-i}} = \frac{e^{-2|x_0|}}{\xi} \left\{ \frac{J_m}{2} \left(S_+\sigma_- + S_-\sigma_+ \right) + J_z S_z \sigma_z + J_0(S_+ + S_-)\sigma_z \right\}. \qquad (2.10)$$

Notice, that the first two terms in Eq. (2.10) – proportional to J_m and J_z – conserve the total "angular momentum" z-projection $S_z + \sigma_z/2$. In the processes mediated by $J_m \left(S_+\sigma_- + S_-\sigma_+ \right)/2$ term the impurity spin flips simultaneously with the spin of the incident electron. Due to the spin-momentum locking the latter changes its direction of motion and gets backscattered as presented in Fig. 2.3(a). $J_z S_z \sigma_z$ contribution neither changes the impurity spin nor does it flip the edge electron spin. Hence, it induces no backscattering along the helical edge. Strikingly, there is a $J_0(S_+ + S_-)\sigma_z$ term in Eq. (2.10) which allows for the processes that *do not conserve* $S_z + \sigma_z/2$, e.g. $|S_z = S - 1,\ \sigma_z = 1\rangle \to |S_z = S,\ \sigma_z = 1\rangle$. In such processes the z-projection of the edge electron spin does not change while the impurity spin gets flipped (see Fig. 2.3(b)). At the first glance, this feature might be somewhat surprising given the fact that the 4×4 electron-impurity Hamiltonian (2.7) was derived from the isotropic Heisenberg model. However, it would be too naïve to expect that the rotational invariance of the microscopic model was unaltered by the presence of the edge – a structure that breaks the respective symmetry. A particular manifestation of the rotational symmetry breaking is that the edge states $\psi_{\text{edge},\uparrow/\downarrow}$ do not possess a well-defined angular momentum, i.e. they are composed of the states with the angular momentum z-projection $j_z = \pm 3/2$ and the states with $j_z = \pm 1/2$. In Chapter 3 we will show that the processes which do not conserve $S_z + \sigma_z/2$ are of special importance for the evaluation of the backscattering current.

Later on, we will perform all of the calculations treating the dimensionless couplings as small parameters[3]: $\mathcal{J} \ll 1$. This assumption is commonly well-justified. For instance, for manganese

---

[2]In what follows we will often omit "pseudo" prefix although the edge states cannot be characterized by a well-defined spin projection.

[3]By $\mathcal{J}$ featured is various inequalities we understand the typical value of the matrix element $|\mathcal{J}_{ij}|$.
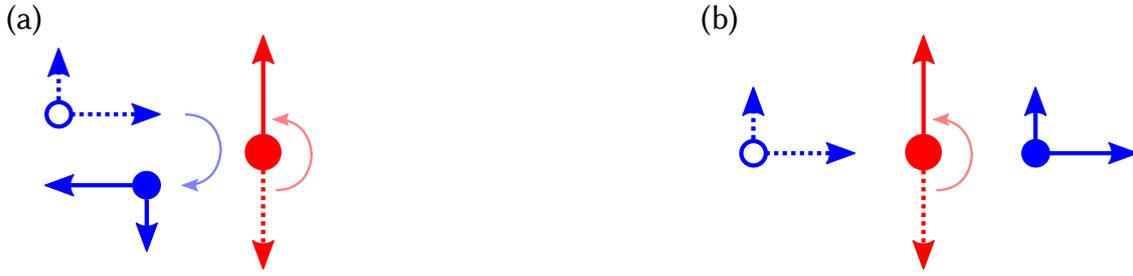
Figure 2.3: Two types of processes mediated by the exchange interaction between the edge states and the magnetic impurity. (a) Interaction due to $J_m \left(S_+ \sigma_- + S_- \sigma_+ \right)/2$ term. Both the impurity spin and the incident electron spin are flipped so that the z-projection of the total angular momentum $S_z + \sigma_z/2$ is conserved. (b) Interaction due to $J_0(S_+ + S_-)\sigma_z$ term. The impurity spin is flipped while the edge electron spin remains intact. The z-projection of the total angular momentum $S_z + \sigma_z/2$ is not conserved in the process.

impurities in the CdTe/HgTe/CdTe quantum well with the width $d = 7.0$ nm one estimates $J \sim 10^{-4} \div 10^{-3} \ll 1$ [23, 25, 27]. Furthermore, throughout the thesis, we will suppose that the matrix $\mathcal{J}$ has a general form which is not constricted to the simple structure (2.9). There are several reasons for that.

- Firstly, in a realistic CdTe/HgTe/CdTe based topological insulator the $\mathcal{J}$ matrix might have much more sophisticated structure than (2.9) due to the interface inversion asymmetry of the sample.

- Secondly, at sufficiently low temperatures T and voltages V, the renormalization of coupling constants alters the structure of the $\mathcal{J}$ matrix. Even if $\mathcal{J}$ has a simple form (2.9) at max $\{T, V\} \sim |M|$ at smaller energies this might not be the case.

- Last but not least, the Hamiltonian (2.8) with the matrix $\mathcal{J}$ of the general form is applicable to a broad spectrum of physical problems which goes far beyond magnetic impurities in CdTe/HgTe/CdTe based 2D topological insulators.

In the subsequent sections, we consider these points in details.

2.3.1 Bulk and interface inversion asymmetries

Using the Hamiltonian (2.3) we implicitly assumed that the CdTe/HgTe/CdTe quantum well the topological insulator is based on is symmetric with respect to inversion $z \rightarrow -z$. However, in realistic structures that is not the case. The tetrahedral symmetry group T_d of CdTe and HgTe does not include the inversion element (bulk inversion asymmetry). Furthermore, the upper and lower CdTe/HgTe interfaces of the heterostructure are non-equivalent on the microscopic level. In
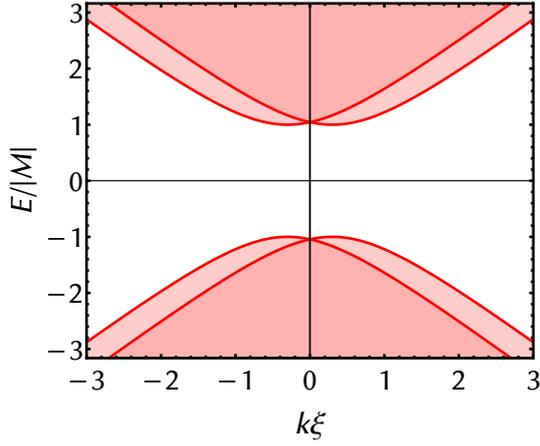
Figure 2.4: The dispersion of bulk states $E_{\text{bulk}}(k) = \pm\sqrt{M^2 + (Ak \pm \Delta)^2}$ for the Hamiltonian $H_{\text{BHZ}} + H_{\text{IA}}$. The spin degeneracy of H_{BHZ} is lifted by the presence of bulk and interface inversion asymmetries. The figure is plotted for $\Delta = 0.3|M|$.

(001) quantum well they are rotated by $90°$ with respect to each other (interface inversion asymmetry). Bulk and interface inversion asymmetries manifest themselves in the mixing between $|E_1, \pm\rangle$ and $|H_1, \mp\rangle$ states which lifts the two-fold degeneracy of the energy bands (see Fig. 2.4). The splitting of the valence band in the CdTe/HgTe/CdTe quantum well was recently revealed experimentally [28].

To take the inversion asymmetry of the structure into account the Hamiltonian (2.3) should be supplemented by the following term [29, 30]

$$
H_{\text{IA}} = \begin{pmatrix} 0 & 0 & 0 & e^{2i\theta}\Delta \\ 0 & 0 & -e^{2i\theta}\Delta & 0 \\ 0 & -e^{-2i\theta}\Delta & 0 & 0 \\ e^{-2i\theta}\Delta & 0 & 0 & 0 \end{pmatrix},
\tag{2.11}
$$

where θ is the angle between the edge of the sample and [010] crystallographic direction. The atomistic calculations [29] imply that Δ may be as large as the band gap $|M|$. For instance, for the $\text{Hg}_{0.3}\text{Cd}_{0.7}\text{Te}/\text{HgTe}/\text{Hg}_{0.3}\text{Cd}_{0.7}\text{Te}$ quantum well with the width $d = 7.0$ nm the inversion asymmetry parameter $\Delta \simeq 5$ meV whereas $|M| \simeq 10$ meV.

Under the rotation of the system around the z-axis on $\delta\theta$ degrees Δ in the upper 2×2 block of (2.11) transforms as $\Delta \to e^{2i\delta\theta}\Delta$ and in the lower block $-$ as $\Delta \to e^{-2i\delta\theta}\Delta$. The factors $e^{\pm 2i\delta\theta}$ in the transformation laws highlight the reduction of the in-plane rotational symmetry of the quantum well due to the inversion asymmetry.

Naturally, H_{IA} is time-reversal invariant. Hence, a pair of gapless edge states persists even in the presence of (2.11). Yet, the structure of these states is more sophisticated than (2.4):

$$
\psi_{\text{edge},\uparrow}(\boldsymbol{r}, k_y) = \left\{ \hat{\psi}_+ e^{-i|x|/\xi_\Delta} - \hat{\psi}_- e^{i|x|/\xi_\Delta - i\phi_\Delta} \right\} \frac{e^{-|x|/\xi}}{\sqrt{\xi}} e^{ik_y y - i\theta}\theta(-x),
\tag{2.12}
$$

$$\psi_{\text{edge},\downarrow}(\boldsymbol{r}, k_y) = \left\{ \hat{\psi}_+ e^{-i|x|/\xi_\Delta + i\phi_\Delta} + \hat{\psi}_- e^{i|x|/\xi_\Delta} \right\} \frac{e^{-|x|/\xi}}{\sqrt{\xi}} e^{ik_y y + i\theta} \theta(-x) \qquad (2.13)$$

where $\phi_\Delta = \arctan \Delta/|M|$, $\xi_\Delta = A/\Delta$, and the spinors $\hat{\psi}_\pm$ are defined by

$$\hat{\psi}_+ = \frac{1}{2} \left(e^{i\theta}, \, ie^{i\theta}, \, e^{-i\theta}, \, -ie^{-i\theta} \right)^T, \quad \hat{\psi}_- = \frac{1}{2} \left(-e^{i\theta}, \, -ie^{i\theta}, \, e^{-i\theta}, \, -ie^{-i\theta} \right)^T. \qquad (2.14)$$

The effective 2×2 Hamiltonian describing the states (2.12) and (2.13) reads

$$H_{\text{edge}}^{\text{e}} = -vk_y \sigma_z, \quad v = \frac{A}{\sqrt{1 + (\Delta/M)^2}}. \qquad (2.15)$$

It is similar to $H_{\text{edge}}^{\text{e}}$ in the absence of inversion asymmetry although the edge states velocity differs by the factor of $\sqrt{1 + (\Delta/M)^2}$. The electron-impurity interaction (2.7) may be readily projected onto the edge states subspace. This yields an exchange Hamiltonian of the form $H_{\text{edge}}^{\text{e-i}} = \mathcal{J}_{ij} S_i \sigma_j / 2\nu$ where neither of the dimensionless couplings $\mathcal{J}_{ij}$ $(i, j = x, y, z)$ equal zero in the general case. Thus, the helical edge and the magnetic impurity nearby may still be described by the Hamiltonian (2.8) albeit the matrix $\mathcal{J}$ does not have a simple form (2.9).

2.3.2 Kondo renormalization

When the typical energies of interest – defined by the maximum between the temperature T and the voltage V for the transport problems – are sufficiently low the Kondo-type renormalization of the coupling constants may become important by altering the structure of the matrix $\mathcal{J}$ significantly. One-loop renormalization group (RG) equations for the dimensionless coupling constants are given by [31]

$$\frac{d\mathcal{J}_{jk}}{d\zeta} = \frac{1}{2} \varepsilon_{jnm} \varepsilon_{kps} \mathcal{J}_{np} \mathcal{J}_{ms}. \qquad (2.16)$$

Here $\zeta = \ln |M|/E$ is the running RG logarithmic scale. Eqs. (2.16) are valid for the exchange matrix with arbitrary structure as long as $\mathcal{J} \ll 1$. To properly account for the renormalizations while determining the transport properties of the helical edge the RG system (2.16) has to be integrated from the energies of the order of the band gap, $E \sim |M|$, to the relevant energies $E \sim \max \{T, V\}$. In this section, we present the general solution of this problem for any initial coupling matrix $\mathcal{J}(\zeta = 0)$.

To begin with, we note that arbitrary matrix – even a non-diagonalizable one – may be subjected

to *singular-value decomposition*. Thus, at $\zeta = 0$ it is possible to represent[4]

$$\mathcal{J}(\zeta = 0) = \mathcal{R}_<\mathcal{L}\mathcal{R}_>, \quad \mathcal{L} = \text{diag}\left\{\lambda_1, \lambda_2, \lambda_3\right\}, \quad \mathcal{R}_{</>} \in SO(3). \qquad (2.17)$$

Next, we treat the matrices $\mathcal{R}_{</>}$ as ζ independent and, with the help of Eq. (2.16), derive the RG equations for the matrix $\mathcal{L}$. We find that in the course of the RG flow $\mathcal{L}$ preserves the diagonal form with the components satisfying

$$\frac{d\lambda_1}{d\zeta} = \lambda_2\lambda_3, \quad \frac{d\lambda_2}{d\zeta} = \lambda_1\lambda_3, \quad \frac{d\lambda_3}{d\zeta} = \lambda_1\lambda_2. \qquad (2.18)$$

In what follows we assume that at $\zeta = 0$ $|\lambda_1| \geq |\lambda_2| \geq |\lambda_3|$ and $\lambda_{1,2} \geq 0$. The fulfilment of these conditions may be always achieved with a proper redefinition of $\mathcal{R}_{</>}$ matrices. Notice that the system of Eqs. (2.18) conserves $\lambda_1^2 - \lambda_2^2 = A_1$ and $\lambda_2^2 - \lambda_3^2 = A_2$. With the help of these integrals we examine the solutions of (2.18) in all possible cases.

- If at $\zeta = 0$ at least two out of three λ_is nullify then $\lambda_{1,2,3}$ does not change with the RG scale ζ. In the following, we assume that this is not the case and at least two of λ_is are non-zero initially.

- If at $\zeta = 0$ $\lambda_1 \geq \lambda_2 \geq \lambda_3 \geq 0$ then the RG dynamics is trivial: λ_1, λ_2, and λ_3 flow to the manifold $\lambda_1 = \lambda_2 = \lambda_3 > 0$ blowing up to infinity at finite $\zeta = \zeta_K$. The RG scale ζ_K defines the Kondo temperature $T_K = |M|e^{-\zeta_K}$. In the described regime the explicit expression for ζ_K is

$$\zeta_K = \int_{\lambda_2(\zeta=0)}^{+\infty} \frac{d\lambda_2}{\sqrt{\lambda_2^2 + A_1}\sqrt{\lambda_2^2 - A_2}}. \qquad (2.19)$$

- If at $\zeta = 0$ $\lambda_3 < 0$, $\lambda_1 \geq \lambda_2 > 0$, and $\lambda_2 > -\lambda_3$ then in the course of RG flow λ_1 and λ_2 at first decrease while λ_3 increases. At some ζ λ_3 reaches 0. When this happens, $\lambda_2 = \sqrt{A_2}$ and $\lambda_1 = \sqrt{A_1 + A_2}$. After that the previously considered case reproduces: $\lambda_{1,2,3}$ grow tending to $\lambda_1 = \lambda_2 = \lambda_3 > 0$ manifold and diverging at

$$\zeta_K = \int_{\lambda_3(\zeta=0)}^{+\infty} \frac{d\lambda_3}{\sqrt{\lambda_3^2 + A_2}\sqrt{\lambda_3^2 + A_1 + A_2}}. \qquad (2.20)$$

- The least trivial dynamics takes place when at $\zeta = 0$ $\lambda_3 < 0$, $\lambda_1 \geq \lambda_2 > 0$, and $\lambda_2 = -\lambda_3 = \lambda$. In this scenario the relation $\lambda_2 = -\lambda_3$ is preserved in the course of the RG flow. The

---

[4]In the regular definition of singular-value decomposition $\mathcal{R}_{</>} \in O(3)$ and $\lambda_{1,2,3} > 0$. We take a different definition. We assume that some of $\lambda_{1,2,3}$ may be negative while fixing $\det \mathcal{R}_{</>} = 1$.

absolute value $|\lambda_{2,3}|$ monotonously drops to zero as ζ changes from 0 to $+\infty$. At the same time, λ_1 decreases reaching $\sqrt{A_1}$ asymptotically. If initially $\lambda_1 = \lambda_2$ then all λ_is fall to zero synchronously. This is a ferromagnetic Kondo effect. To reach it, a fine tuning of parameters is required.

To conclude this section, we mention that the the four-component form of the $\mathcal{J}$ matrix (2.9) is not preserved by the RG flow. At finite ζ $\mathcal{J}$ takes the five component form with $\mathcal{J}_{zx} \neq 0$ and $\mathcal{J}_{xx} \neq \mathcal{J}_{yy}$.

2.3.3 Other systems

The Hamiltonian (2.8) is, in principle, applicable to a wide range of problems. In particular, it is capable of describing magnetic impurities in other types of 2D topological insulators, e.g. InAs/GaSb heterostructures or WTe$_2$ monolayers. While the exchange matrix might have a form that differs from (2.9) the general structure of the helical edge Hamiltonian is the same as (2.8). Another prominent example which may be analysed with the help of (2.8) is a charge puddle in the topological insulator. Charge puddles are the conducting islands in the semiconducting heterostructures which are inherently present in 2D topological insulators due to the interplay between the potential disorder and small band gap. As it was shown in [18] the behavior of such islands in the odd valley regime of the Coulomb blockade is similar to those of spin-1/2 quantum magnetic impurities. Hence, the backscattering of the edge electrons by them may be described by the Hamiltonian (2.8) albeit the exchange matrix $\mathcal{J}$ is substantially different from (2.9). According to [18], it is *almost* isotropic:

$$\mathcal{J}_{ij} = \mathcal{J}_0 \delta_{ij} + \Delta \mathcal{J}_{ij}, \quad |\Delta \mathcal{J}_{ij}| \ll \mathcal{J}_0. \tag{2.21}$$

Despite being small, the anisotropic admixture is very important: if it was not for $\Delta \mathcal{J}_{ij}$ there would be no backscattering in the steady state regime.

Notice, that up until this point we have only been discussing the edge states, their exchange interaction with the magnetic impurity, and the respective contributions to the total Hamiltonian of the helical edge. At the same time, the impurity might have a non-trivial Hamiltonian H_{imp} of its own. In particular, if a spin of the impurity is larger than $1/2$ then the local magnetic anisotropy described by $H_{\text{imp}} = \mathcal{D}_{qp} S_q S_p$ ($\mathcal{D}_{qp}$ is a real symmetric matrix) is present. This anisotropy might have a profound influence on the quantum dynamics of the impurity and, consequently, on the transport properties of the edge of the topological insulator. We consider such effect in details in Chapter 4. However, at first we develop a theory of helical edge conductance in the case of

negligible anisotropy, $H_{\text{imp}} = 0$, and present it in Chapter 3. The range of applicability of this approximation is thoroughly discussed in Chapter 4.

To conclude the present chapter, we note that in the following, it will be convenient to work with a second-quantized version of the effective Hamiltonian (2.8). It is given by

$$H_{\text{edge}} = H_{\text{edge}}^{\text{e}} + H_{\text{edge}}^{\text{e}-\text{i}}, \tag{2.22}$$

$$H_{\text{edge}}^{\text{e}} = iv \int dy \Psi^\dagger(y) \sigma_z \partial_y \Psi(y), \quad H_{\text{edge}}^{\text{e}-\text{i}} = \frac{1}{\nu} \mathcal{J}_{ij} S_i s_j(y_0),$$

where $\Psi(y) = (\Psi_\uparrow(y), \Psi_\downarrow(y))^T$ is an annihilation operator of the edge electrons, $\Psi^\dagger(y)$ is its hermitian conjugate, and the edge electrons (pseudo-)spin density $s_j(y)$ equals

$$s_j(y) = \frac{1}{2} \Psi^\dagger(y) \sigma_j \Psi(y). \tag{2.23}$$

Chapter 3

Backscattering current mediated by the presence of a magnetic impurity

In this chapter we describe the transport along the helical edge in the presence of a magnetic impurity assuming that the local anisotropy is negligible. Formally, it means that in the total Hamiltonian

$$H_{\text{tot}} = H_{\text{edge}} + H_{\text{imp}}, \tag{3.1}$$

where H_{edge} is given by (2.22), we take the impurity Hamiltonian H_{imp} to be zero.

In section 3.1 we discuss the way in which a finite voltage V applied to the edge of the topological insulator may be taken into account within the framework of the model (2.22). In section 3.2 we reduce the problem of determining the backscattering current I_{bs} to the evaluation of certain impurity averages. To calculate these averages we derive the master equation for the impurity density matrix ρ_S. Next, in section 3.3 we employ the resultant equations to describe the correction to *the linear* conductance. Section 3.4 is devoted to the limit of sufficiently large voltages $V \gg \mathcal{J}T$. In section 3.5 we find the *exact* expression for the backscattering current due to a spin-1/2 magnetic impurity. Finally, in section 3.6 we present the numeric results for the correction to the conductance due to the impurities with $S \geq 1/2$.

The chapter is largely based on the recent article [23] prepared by the author of this thesis in collaboration with Pavel Kurilovich, Igor Burmistrov, and Moshe Goldstein.

3.1   Introduction

We suppose that a finite voltage $V > 0$ is applied to the edge of a two-dimensional topological insulator. We do not make any limiting assumptions about the relative magnitude of V and tem-

perature T: our goal is to describe the behavior of the backscattering mediated contribution to the current I_{bs} in the whole range of voltages covering both $V \lesssim T$ and $V \gtrsim T$.

To account for the applied voltage within the model (2.22) we assume that two leads (reservoirs) are attached to the edge of the topological insulator at $y = \pm L$ as depicted in Fig. 3.1. The chemical potential of the lead at $y = +L$ is shifted by V with respect to the chemical potential of the lead at $y = -L$. This property translates on the distribution functions of the edge electrons escaping from the respective reservoirs. Therefore, if it was not for the magnetic impurity the system would stay in a stationary non-equilibrium state with uneven populations of two helical branches described by the density matrix

$$\rho_e^0 = \frac{\exp\left(-\left(H_{edge}^e - V\Sigma_z - \mu N\right)/T\right)}{\mathrm{tr}_e\left\{\exp\left(-\left(H_{edge}^e - V\Sigma_z - \mu N\right)/T\right)\right\}}. \tag{3.2}$$

In this expression the trace $\mathrm{tr}_e\{...\}$ is taken over the edge states degrees of freedom, the Hamiltonian H_{edge}^e is defined in Eq. (2.22), $N = \int dy \left(\Psi_\uparrow^\dagger(y)\Psi_\uparrow(y) + \Psi_\downarrow^\dagger(y)\Psi_\downarrow(y)\right)$ is the number operator of the edge electrons, μ is the chemical potential, and

$$\Sigma_z = \int dy s_z(y) = \frac{1}{2}\int dy \left(\Psi_\uparrow^\dagger(y)\Psi_\uparrow(y) - \Psi_\downarrow^\dagger(y)\Psi_\downarrow(y)\right) \tag{3.3}$$

is the edge electrons overall spin z-projection. Notice, that, up to the factor $1/2$, Σ_z equals the difference between the number of electrons with spin up (and, hence, propagating in the direction opposite to y-axis) and spin down (propagating along y-axis). The density matrix (3.2) describes the ballistic current $I_0 = G_0 V$ flowing along the helical edge ($G_0 = e^2/h = (2\pi)^{-1}$ in the units $k_B, \hbar, |e| = 1$). The magnetic impurity located at $y = 0$ scatters some of the incident electrons back thus reducing the magnitude of the current from its ballistic value I_0 to $I_0 + I_{bs}$ (I_{bs} is negative). In the next section, we develop a formalism capable of describing the backscattering current I_{bs} at
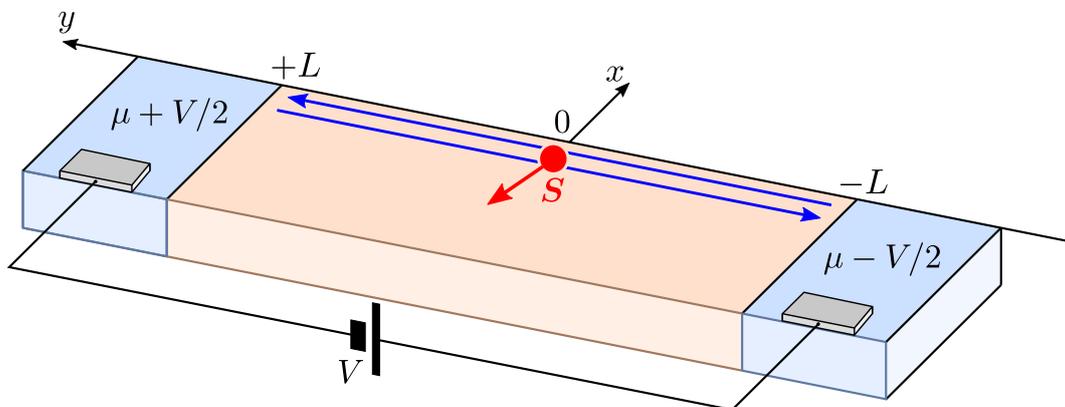

Figure 3.1: Sketch of the topological insulator with the voltage V applied to its helical edge. The voltage shifts the chemical potential of the leads: at $y = -L$ the chemical potential equals $\mu - V/2$ while at $y = +L$ the chemical potential is $\mu + V/2$. The magnetic impurity is located at $y = 0$.

arbitrary voltage.

3.2 Backscattering current and master equation

In this section we establish the expression for the backscattering current I_{bs} induced by the presence of a magnetic impurity near the helical edge. To this end, we note that, due to the spin-momentum locking, each backscattering event is associated with a change of the total z-projection of the edge electrons spin Σ_z by unity. Therefore, one determines

$$I_{\text{bs}} = \left\langle \frac{d\Sigma_z}{dt} \right\rangle = \frac{1}{\nu}\varepsilon_{zpl}\mathcal{J}_{mp}\langle S_m s_l(0)\rangle, \qquad (3.4)$$

The averaging $\langle ... \rangle = \text{tr}\{...\rho\}$ is carried out with respect to the *overall* density matrix ρ incorporating both the degrees of freedom of the magnetic impurity and of the edge electrons. Since the considered problem involves one impurity only in the following we suppress the spatial argument of the edge electrons spin density and use s_l instead of $s_l(0)$.

Unfortunately, the expression (3.4) by itself is not very handy to work with as it contains the operators related to the impurity and the operators related to the edge electrons simultaneously. However, there is a way to overcome this shortage and express the backscattering current I_{bs} in terms of the impurity spin averages (such as $\langle S_k \rangle$ and $\langle \{S_m, S_n\} \rangle$, $k, m, n = x, y, z$) *only* with the help of the perturbation theory in $\mathcal{J} \ll 1$. Since we are interested in the correction to *the dc conductance* these averages are to be evaluated over reduced density matrix of the magnetic impurity, $\rho_S = \text{tr}_e\rho$, *in the steady state regime*. Below, we first derive the equation for the evolution of ρ_S which allows one to find the steady state density matrix $\rho_S^{(\text{st})}$ and then establish the explicit relation between I_{bs} and the impurity averages.

3.2.1 Master equation

We begin by deriving the master equation which governs the evolution of the reduced density matrix of the magnetic impurity $\rho_S = \text{tr}_e\rho$. To this end, we follow the standard approach developed in a theory of open quantum systems (for a review, see [32]). First, we consider the full density matrix ρ describing both the edge electrons and the magnetic impurity. In the absence of H_{imp} its time dependence is determined by the Liouville equation $d\rho/dt = -i\left[H_{\text{edge}}^{\text{e}} + H_{\text{edge}}^{\text{e}-\text{i}}, \rho\right]$. A key feature of this equation is that at finite voltage V the electron-impurity interaction $H_{\text{edge}}^{\text{e}-\text{i}} = \mathcal{J}_{ij}S_i s_j/\nu$ acquires a non-vanishing mean-field expectation $H_{\text{mf}}^{\text{e}-\text{i}}$ [18, 20]. Indeed, averaging $H_{\text{edge}}^{\text{e}-\text{i}}$ over the

density matrix (3.2) one finds

$$H_{\text{mf}}^{\text{e}-\text{i}} = \text{tr}_{\text{e}} \left\{ H_{\text{edge}}^{\text{e}-\text{i}} \rho_{\text{e}}^0 \right\} = \mathcal{J}_{iz} S_i \frac{V}{2}. \tag{3.5}$$

Here we used the fact that at non-zero voltage the helical edge is spin-polarized along the z direction, i.e. $\langle s_j \rangle_0 = \text{tr}_{\text{e}} \left\{ s_j \rho_{\text{e}}^0 \right\} = \delta_{jz} \nu V / 2$. Thus, for the evolution of ρ we obtain

$$\frac{d\rho}{dt} = -i \left[H_{\text{mf}}^{\text{e}-\text{i}}, \rho \right] - i \left[H_{\text{edge}}^{\text{e}} + : H_{\text{edge}}^{\text{e}-\text{i}} :, \rho \right], \tag{3.6}$$

where we defined

$$: H_{\text{edge}}^{\text{e}-\text{i}} := \frac{1}{\nu} \mathcal{J}_{ij} S_i : s_j :, \quad : s_j := s_j - \langle s_j \rangle_0. \tag{3.7}$$

Remarkably, the mean-field interaction $H_{\text{mf}}^{\text{e}-\text{i}}$ operates as an effective magnetic field acting on the impurity spin. Hence, even though we have started with $H_{\text{imp}} = 0$, the finite voltage results in a Zeeman-type splitting of the impurity levels.

In the equation (3.6) it is convenient to switch to the interaction representation. To do that, we introduce

$$\rho^I(t) = \exp \left\{ -i \left(H_{\text{mf}}^{\text{e}-\text{i}} + H_{\text{edge}}^{\text{e}} \right) t \right\} \rho(t) \exp \left\{ i \left(H_{\text{mf}}^{\text{e}-\text{i}} + H_{\text{edge}}^{\text{e}} \right) t \right\}, \tag{3.8}$$

$$: H_{\text{edge}}^{\text{e}-\text{i},I}(t) := \exp \left\{ i \left(H_{\text{mf}}^{\text{e}-\text{i}} + H_{\text{edge}}^{\text{e}} \right) t \right\} : H_{\text{edge}}^{\text{e}-\text{i}} : \exp \left\{ -i \left(H_{\text{mf}}^{\text{e}-\text{i}} + H_{\text{edge}}^{\text{e}} \right) t \right\}. \tag{3.9}$$

Next, we solve (3.6) recursively by substituting its formal solution back into itself. As a result, we get

$$\frac{d\rho^I(t)}{dt} = -\int_{-\infty}^{t} dt' \left[: H_{\text{edge}}^{\text{e}-\text{i},I}(t) : \left[: H_{\text{edge}}^{\text{e}-\text{i},I}(t') :, \rho^I(t') \right] \right]. \tag{3.10}$$

Deriving Eq. (3.10) we assumed that the exchange interaction between the edge electrons and the impurity adiabatically switches on at $t = -\infty$ and, hence, $\rho(-\infty) = \rho^I(-\infty) = \rho_0^{\text{e}} \otimes \rho_S^{\text{(eq)}}$, where ρ_0^{e} is defined in Eq. (3.2), $\otimes$ sign denotes the tensor product of the operators acting in the edge electrons subspace and in the impurity subspace, $\rho_S^{\text{(eq)}} = I_{(2S+1)\times(2S+1)}/(2S+1)$, and $I_{(2S+1)\times(2S+1)}$ is a unity matrix of size $2S + 1$. We notice that the right hand side of Eq. (3.10) is already of the second order in $\mathcal{J}$. Therefore, *the Born approximation* may be employed to simplify it [32]: one can replace $\rho^I(t')$ with $\rho_0^{\text{e}} \otimes \rho_S^I(t')$, where $\rho_S^I = \text{tr}_{\text{e}} \rho^I$ is a reduced density matrix of the magnetic impurity in the interaction representation. The corrections to this approximation are of the higher orders in the dimensionless coupling constants $\mathcal{J}_{ij}$ and, hence, may be disregarded. With that in mind, we take the partial trace of Eq. (3.10) over the edge electrons degrees of freedom

and obtain

$$\frac{d\rho_S^I(t)}{dt} = \mathcal{J}_{mi}\mathcal{J}_{nj}\int_{-\infty}^{t}dt'\left\{\left[S_m^I(t')\rho_S^I(t'), S_n^I(t)\right]K_V^{ij}(t-t') + \text{h.c.}\right\}, \qquad (3.11)$$

where h.c. denotes the hermitian conjugate, $S_{x,y,z}^I(t) = \exp\left\{iH_{\text{mf}}^{\text{e}-\text{i}}t\right\}S_{x,y,z}\exp\left\{-iH_{\text{mf}}^{\text{e}-\text{i}}t\right\}$, and the irreducible spin-spin correlation function K_V^{ij} is defined by

$$K_V^{ij}(\tau) = \frac{1}{\nu^2}\text{tr}_{\text{e}}\left\{: s_j^I(\tau) :: s_i^I(0) : \rho_0^{\text{e}}\right\}. \qquad (3.12)$$

The lower subscript V in the correlator $K_V^{ij}(\tau)$ underscores that the latter is evaluated at finite voltage V. We note that the matrix elements of $K_V(\tau)$ decay on a time-scale controlled either by the inverse voltage or the inverse temperature. At the same time, Eq. (3.11) implies that $\rho_S^I(t)$ typically changes on a much larger time-scale which has additional greatness of $\mathcal{J}^{-2}$. Thus, $\rho_S^I(t')$ in the right hand side of Eq. (3.11) may be safely transformed into $\rho_S^I(t)$. As a result of such transformation, Eq. (3.11) acquires *the Markovian form* in which the evolution of the impurity density matrix at any given time t is independent of the previous history and is defined by the present value of $\rho_S^I(t)$ only:

$$\frac{d\rho_S^I(t)}{dt} = \mathcal{J}_{mi}\mathcal{J}_{nj}\int_{-\infty}^{t}dt'\left\{\left[S_m^I(t')\rho_S^I(t), S_n^I(t)\right]K_V^{ij}(t-t') + \text{h.c.}\right\}. \qquad (3.13)$$

In this expression it is convenient to represent the impurity spin operators as

$$S_{x,y,z} = \sum_{\alpha\beta}\mathcal{S}_{x,y,z}^{\alpha\beta}, \quad \mathcal{S}_{x,y,z}^{\alpha\beta} = |\psi_S^\alpha\rangle S_{x,y,z}^{\alpha\beta}\langle\psi_S^\beta|, \quad S_{x,y,z}^{\alpha\beta} = \langle\psi_S^\alpha|S_{x,y,z}|\psi_S^\beta\rangle, \qquad (3.14)$$

where $|\psi_S^\alpha\rangle$ is the α-th eigenstate of the magnetic impurity Hamiltonian $H_{\text{mf}}^{\text{e}-\text{i}}$ corresponding to the energy E_S^α. Since $H_{\text{mf}}^{\text{e}-\text{i}} = \mathcal{J}_{iz}S_iV/2$ has a form of a Zeeman field, its eigenstates may be characterized by the projection $\alpha = S, S-1, ..., -S$ of the impurity spin on the direction $\boldsymbol{n} = (\mathcal{J}_{xz}, \mathcal{J}_{yz}, \mathcal{J}_{zz})/\sqrt{(\mathcal{J}^T\mathcal{J})_{zz}}$: $|\psi_S^\alpha\rangle = |S_{\boldsymbol{n}} = \alpha\rangle$ and has energy $E_S^\alpha = \alpha\sqrt{(\mathcal{J}^T\mathcal{J})_{zz}}V/2$. Substituting Eq. (3.14) into Eq. (3.13) and then integrating the latter over t' we obtain *the Bloch-Redfield master equation* for the reduced density matrix of the magnetic impurity:

$$\frac{d\rho_S^I(t)}{dt} = \mathcal{J}_{mi}\mathcal{J}_{nj}\sum_{\alpha\beta\gamma\delta}\left\{\left[\left(\mathcal{S}_m^{\alpha\beta}\right)^I(t)\rho_S^I(t), \left(\mathcal{S}_n^{\gamma\delta}\right)^I(t)\right]K_V^{ij}(\omega_{\alpha\beta}) + \text{h.c.}\right\}, \qquad (3.15)$$

where $\omega_{\alpha\beta} = E_S^\beta - E_S^\alpha$ and $K_V^{ij}(\omega) = \int_0^{+\infty}d\tau e^{i(\omega+i0)\tau}K_V^{ij}(\tau)$. Next, we divide the spin-spin correlator into a Hermitian and an antihermitian parts, $K_V^{ij} = \mathcal{K}_V^{ij}/2 + i\kappa_V^{ij}$, where the Hermitian

matrices $\mathcal{K}_V$ and κ_V are given by

$$\mathcal{K}_V^{ij}(\omega) = \frac{\pi}{2} \sum_{\sigma_1 \sigma_2} \int d\xi \sigma_j^{\sigma_1 \sigma_2} \sigma_i^{\sigma_2 \sigma_1} n_F(\xi - \sigma_1 V/2)(1 - n_F(\xi + \omega - \sigma_2 V/2)), \tag{3.16}$$

$$\kappa_V^{ij}(\omega) = \frac{1}{4} \sum_{\sigma_1 \sigma_2} \text{v.p.} \int d\xi_1 d\xi_2 \sigma_j^{\sigma_1 \sigma_2} \sigma_i^{\sigma_2 \sigma_1} \frac{n_F(\xi_1 - \sigma_1 V/2)(1 - n_F(\xi_2 - \sigma_2 V/2))}{\omega + \xi_1 - \xi_2}. \tag{3.17}$$

Here $\sigma_1, \sigma_2 = \pm 1$, $n_F(\xi) = (\exp\{(\xi - \mu)/T\} + 1)^{-1}$ is the Fermi distribution function, and v.p. denotes the principal value of the integral.

Notice that the integrals over energy featured in the matrix elements of κ_V diverge in the ultraviolet limit. These divergences are due to the renormalizations of the magnetic impurity Hamiltonian and, therefore, describe the Lamb shift of the impurity energy levels [32]. For now, we disregard this effect and discuss it in details in section 3.2.2.

The integrals for $\mathcal{K}_V^{ij}(\omega)$ may be readily evaluated:

$$\mathcal{K}_V(\omega) = \mathcal{K}_V^+(\omega) + \mathcal{K}_V^-(\omega), \quad \mathcal{K}_V^\pm(\omega) = \frac{\pi}{2} \begin{pmatrix} f(\omega \pm V) & \mp i f(\omega \pm V) & 0 \\ \pm i f(\omega \pm V) & f(\omega \pm V) & 0 \\ 0 & 0 & f(\omega) \end{pmatrix}, \tag{3.18}$$

where $f(\omega) = \omega/(1 - \exp\{-\omega/T\})$. We notice that typical frequencies $\omega_{\alpha\beta}$ at which the spin-spin correlator $\mathcal{K}_V$ is evaluated in the master equation are of the order of the impurity level spacing $\mathcal{J}V \ll V$. Thus, it is possible to replace $\mathcal{K}_V(\omega_{\alpha\beta})$ in Eq. (3.15) by $\mathcal{K}_V^0 \equiv \mathcal{K}_V(0)$. The accuracy of such approximation is controlled by a small parameter $\mathcal{J} \ll 1$. As a result, we find

$$\frac{d\rho_S}{dt} = -i \left[\mathcal{J}_{kz} S_k V/2, \rho_S \right] + \eta_{mn} \left(S_m \rho_S S_n - \frac{1}{2} \{ \rho_S, S_n S_m \} \right), \quad \eta = \mathcal{J} \mathcal{K}_V^0 \mathcal{J}^T. \tag{3.19}$$

To derive Eq. (3.19) we switched back from the interaction representation to the Schrödiner representation in Eq. (3.15) and carried out the summation over the eigenstates explicitly. We mention that

$$\mathcal{K}_V^0 = \pi T \begin{pmatrix} \frac{V}{2T} \coth \frac{V}{2T} & -i \frac{V}{2T} & 0 \\ i \frac{V}{2T} & \frac{V}{2T} \coth \frac{V}{2T} & 0 \\ 0 & 0 & 1 \end{pmatrix}. \tag{3.20}$$

The first term in Eq. (3.19) describes the Liouvillian dynamics of the density matrix ρ_S which is associated with the rotation of the magnetic impurity spin in the effective Zeeman field $H_{\text{mf}}^{\text{e}-\text{i}}$. The second term describes the Korringa-type relaxation [21, 33] and decoherence of ρ_S. It has the Lindblad form [32]. Therefore, the normalization $\text{tr}_S \rho_S = 1$ ($\text{tr}_S \{...\}$ is a partial trace over the

impurity degrees of freedom) and the positive semidefiniteness of ρ_S are automatically ensured in the evolution described by Eq. (3.19), as it should be.

3.2.2 Renormalizations

While deriving Eq. (3.19) we encountered a group of divergent terms that originate from the anti-hermitian part κ_V of the the spin-spin correlation function K_V. In this section we discuss the origin of these divergences. To begin with, we notice that some elements of κ_V equal zero identically due to the structure of the spin summations in Eq. (3.17): $\kappa_V^{xz/zx} = \kappa_V^{zy/yz} = 0$. Next, we find that the integral over energies diverge linearly for the diagonal elements of κ_V:

$$\kappa_V^{xx} = \kappa_V^{yy} = \kappa_V^{zz} \sim - \int d\xi = -|M|. \tag{3.21}$$

Here we have taken into the account the fact that the edge states are defined only in a finite interval of energies of the order of the band gap $|M|$ and introduced a corresponding ultraviolet cut-off in the ξ-integral. These diagonal components produce the correction to the master equation (3.19) of a Liouvillian form: $-i \left[H_{\text{anis}}^{\text{edge}}, \rho_S \right]$, where

$$H_{\text{anis}}^{\text{edge}} = -\Lambda_{\text{edge}} |M| \left(\mathcal{J} \mathcal{J}^T \right)_{qp} S_q S_p, \quad \Lambda_{\text{edge}} \sim 1. \tag{3.22}$$

Together with $H_{\text{mf}}^{\text{e}-\text{i}}$ the contribution $H_{\text{anis}}^{\text{edge}}$ plays the role of a total Hamiltonian of the impurity. By its structure, $H_{\text{anis}}^{\text{edge}}$ is nothing but a local magnetic anisotropy. Chapter 4 is solely devoted to the discussion of the influence of the anisotropy alike that on the helical edge transport whereas in the remainder of this Chapter we disregard its effects. A particular scenario in which such a neglect is well-justified is when the voltage is sufficiently large, $V \gg \mathcal{J}^2 |M|$, so that the mean-field interaction $H_{\text{mf}}^{\text{e}-\text{i}}$ dominates over $H_{\text{anis}}^{\text{edge}}$ in the Liouvillian part of the master equation.

We note that the interaction with the edge states is not the only source of the local anisotropy. For instance, a similar contribution $H_{\text{anis}}^{\text{bulk}}$ arises due to the interaction between the impurity and the bulk states in the topological insulator. We will show in Chapter 4 that typically $H_{\text{anis}}^{\text{bulk}} \gg H_{\text{anis}}^{\text{edge}}$. Therefore, $H_{\text{anis}}^{\text{edge}}$ acts as a renormalization of $H_{\text{anis}}^{\text{bulk}}$.

Next, we consider the off-diagonal elements κ_V^{xy} and κ_V^{yx} which diverge logarithmically. They can be estimated as

$$\kappa_V^{xy} = -\kappa_V^{yx} = iV \ln \left(|M| / \max \{T, V\} \right) / 2. \tag{3.23}$$

Here as an infrared cut-off we used the typical energy of the edge electrons, i.e. $\max \{T, V\}$, and

as an ultraviolet cut-off – the band gap $|M|$. The contributions corresponding to κ_V^{xy}, κ_V^{yx} produce the correction to the master equation of the form $-i\left[\delta H_{\mathrm{mf}}^{\mathrm{e-i}}, \rho_S\right]$, where

$$\delta H_{\mathrm{mf}}^{\mathrm{e-i}} = V \varepsilon_{kmn} \mathcal{J}_{mx} \mathcal{J}_{nx} \ln\left(|M|/\max\{T, V\}\right)/2. \tag{3.24}$$

Remarkably, the structure of $\delta H_{\mathrm{mf}}^{\mathrm{e-i}}$ is similar to those of the mean-field interaction $H_{\mathrm{mf}}^{\mathrm{e-i}}$. Hence, $\delta H_{\mathrm{mf}}^{\mathrm{e-i}}$ may be treated as a renormalization of the latter,

$$H_{\mathrm{mf}}^{\mathrm{e-i}} + \delta H_{\mathrm{mf}}^{\mathrm{e-i}} = \frac{V}{2} S_k \left(\mathcal{J}_{kz} + \varepsilon_{kmn} \mathcal{J}_{mx} \mathcal{J}_{nx} \ln\left(|M|/\max\{T, V\}\right)\right). \tag{3.25}$$

From this expression, we establish that $\delta H_{\mathrm{mf}}^{\mathrm{e-i}}$ emerges due to the Kondo renormalization of the coupling constants $\mathcal{J}_{kz}$ (see Eq. (2.16)). In what follows, we assume that $\max\{T, V\} \gg T_{\mathrm{K}}$ and, hence, do not discuss the Kondo corrections to the results presented below in details.

Having considered the renormalizations which arise due to the antihermitian part κ_V of the spin-spin correlator we now return to the master equation (3.19) and employ it to derive the equation for the evolution of the impurity spin.

3.2.3 Bloch equation

A particularly useful consequence of Eq. (3.19) is a Bloch-type equation for the evolution of the average impurity spin $\langle \boldsymbol{S} \rangle$:

$$\frac{d\langle S_l \rangle}{dt} = \frac{\pi T}{2} \left(\frac{V}{2T} \varepsilon_{zpq} \varepsilon_{lkm} \mathcal{J}_{kp} \mathcal{J}_{nq} \langle\{S_m, S_n\}\rangle - \Gamma_{lk} \langle S_k \rangle\right), \tag{3.26}$$

where we introduced the matrix

$$\Gamma_{lk} = \frac{1}{\pi T} \left(\delta_{lk} \mathrm{tr}\eta - \frac{\eta_{lk} + \eta_{kl}}{2} + V \varepsilon_{lkj} \mathcal{J}_{jz}\right). \tag{3.27}$$

Notice that the system of equations (3.26) for the vector $\langle \boldsymbol{S} \rangle$ is not closed in a sense that the evolution of $\langle \boldsymbol{S} \rangle$ is determined not only by $\langle \boldsymbol{S} \rangle$ but also by the higher order expectations $\langle\{S_m, S_n\}\rangle$ $(m, n = x, y, z)$. In the general case, the latter averages cannot be expressed in terms of the components of $\langle \boldsymbol{S} \rangle$ and, therefore, the knowledge of the impurity density matrix ρ_S is required to find $\langle \boldsymbol{S} \rangle$. Despite that, Eq. (3.26) will be very helpful in the analysis of the case $V \ll T$ for $S > 1/2$ and also at any voltage for the investigation of $S = 1/2$.

3.2.4 Backscattering current

Now, we employ the machinery similar to those we used to derive the master equation in order to obtain the expression for the backscattering current I_{bs} in terms of the steady state impurity spin averages. First, we rewrite the expression (3.4) in the interaction representation as

$$I_{\text{bs}} = -\frac{i}{\nu^2} \varepsilon_{zpl} \mathcal{J}_{mp} \mathcal{J}_{nq} \int_{-\infty}^{t} dt' \text{tr} \left\{ S_m^I(t) : s_l^I(t) : \left[S_n^I(t') : s_q^I(t') :, \rho^I(t') \right] \right\}, \qquad (3.28)$$

where t is a given moment in time at which the impurity density matrix already reached its stationary state $\rho_S^{(\text{st})}$. Then we perform the Markov-Born approximation by changing $\rho^I(t')$ in the right hand side of Eq. (3.28) to $\rho_0^{\text{e}} \otimes \rho_{S,I}^{(\text{st})}(t)$, where $\rho_{S,I}^{(\text{st})}(t)$ is the stationary density matrix in the interaction representation[1]. After that, we carry out integration over t' and find

$$I_{\text{bs}} = \frac{1}{2} \varepsilon_{zpl} \mathcal{J}_{mp} \mathcal{J}_{nq} \left(-i \langle S_m S_n \rangle \left(\mathcal{K}_V^0 \right)_{ql} + \text{c.c} \right). \qquad (3.29)$$

The averages in this expression are evaluated with respect to $\rho_S^{(\text{st})}$: $\langle ... \rangle = \text{tr}_S \left\{ ... \rho_S^{(\text{st})} \right\}$. Substituting into this equation the explicit form of $\mathcal{K}_V^0$ we finally obtain

$$I_{\text{bs}} = \frac{\pi^2}{2} \left(\mathcal{X}_k \langle S_k \rangle \coth \frac{V}{2T} - \sum_{q=x,y} \mathcal{J}_{mq} \mathcal{J}_{nq} \langle \{ S_m, S_n \} \rangle \right) G_0 V. \qquad (3.30)$$

Here we introduced the vector $\mathcal{X}_k = 2 \varepsilon_{kmn} \mathcal{J}_{mx} \mathcal{J}_{ny}$.

A pair of Eqs. (3.30) and (3.19) in principle allows us to determine the backscattering current for any given parameters of the problem as long as the condition $\mathcal{J} \ll 1$ is fulfilled. However, the analytic solution which would be valid for arbitrary impurity spin S, voltage V, and temperature T is hindered. For this reason, in the following, we consider the limiting cases in which it possible to derive the closed-form expressions for I_{bs}.

To begin with, we notice that the Lindblad term in the master equation (3.19) is associated with a rate $\tau_K^{-1} \sim \mathcal{J}^2 \max \{ T, V \}$, where τ_K is a Korringa-type relaxation time. The Liovillian term which originates from the mean-field interaction $H_{\text{mf}}^{\text{e}-\text{i}}$ is of the order of $\mathcal{J} V$. Hence, for $V \ll \mathcal{J} T$ the energy levels of the magnetic impurity are strongly broadened by the relaxation and $-i \left[H_{\text{mf}}^{\text{e}-\text{i}}, \rho_S \right]$ may be completely disregarded in Eq. (3.19). If, on the contrary, $V \gg \mathcal{J} T$ then the smearing of the energy levels $\sim \tau_K^{-1}$ is much smaller than the level spacing $\sim \mathcal{J} V$.

The behavior of the backscattering current in the low voltage limit $V \ll \mathcal{J} T$ differs drastically from those in the limit of well-separated energy levels $V \gg \mathcal{J} T$. Thus, in the next sections we

---

[1]Notice, that the stationary density matrix may still depend on time in the interaction representation .

separately describe the regimes $V \ll \mathcal{J}T$ (section 3.3) and $V \gg \mathcal{J}T$ (section 3.4).

3.3 Transport at low voltages

The goal of this section is to analyse the behavior of the backscattering current in the regime of low voltages $V \ll \mathcal{J}T$. We note that the inequality $V \ll \mathcal{J}T$ immediately implies $V \ll T$ because the dimensionless couplings $\mathcal{J}_{ij}$ are assumed to be small. The fulfilment of $V \ll T$ guarantees that the density matrix of the magnetic impurity is close to equipartitioning, $\rho_S \simeq \rho_S^{(\mathrm{eq})} = I_{(2S+1)\times(2S+1)}/(2S+1)$. Therefore, with the required accuracy the anticommutators $\langle \{S_m, S_n\} \rangle$ entering Eqs. (3.30) and (3.26) may be safely substituted by $2\delta_{mn}S(S+1)/3$. As a result, Eq. (3.26) for the dynamics of the average spin becomes closed, i.e. in the considered limit the evolution of $\langle \boldsymbol{S} \rangle$ is determined by $\langle \boldsymbol{S} \rangle$ only. Furthermore, the condition $V \ll \mathcal{J}T$ allows one to disregard the mean-field term $V\varepsilon_{lkj}\mathcal{J}_{jz}$ in the matrix Γ (see Eq. (3.27)) and evaluate the latter at zero voltage. Under such approximations Eq. (3.26) may be trivially solved for the steady state value $\langle S_k \rangle$:

$$\langle S_k \rangle = \frac{S(S+1)}{3}\frac{V}{T}\left(\Gamma_0^{-1}\right)_{kl}\mathcal{X}_l, \tag{3.31}$$

where $\Gamma_0 = \Gamma|_{V=0} = \mathrm{tr}\left(\mathcal{J}\mathcal{J}^T\right) - \mathcal{J}\mathcal{J}^T$. Substituting this result into Eq. (3.30) we establish

$$I_{\mathrm{bs}} = \frac{\pi^2 S(S+1)}{3}\left(\mathcal{X}^T\Gamma_0^{-1}\mathcal{X} - g\right)G_0 V, \tag{3.32}$$

where $g = \sum_{q=x,y}\mathcal{J}_{mq}\mathcal{J}_{mq} = \left(\mathcal{J}^T\mathcal{J}\right)_{xx} + \left(\mathcal{J}^T\mathcal{J}\right)_{yy}$ and $\mathcal{X}^T\Gamma_0^{-1}\mathcal{X} \equiv \mathcal{X}_k\left(\Gamma_0^{-1}\right)_{kl}\mathcal{X}_l$. Interestingly, the correction to the ballistic conductance based on Eq. (3.32), $\Delta G = I_{\mathrm{bs}}/V$, does not depend on voltage. Thus, the limit $V \ll \mathcal{J}T$ corresponds to *the linear* backscattering regime.

The expression (3.32) illustrates several features of the model (3.1) with $H_{\mathrm{imp}} = 0$ which are valid at any voltage V.

- First of all, Eq. (3.32) is invariant under the *left* rotations of the exchange coupling matrix, i.e. $\mathcal{J} \to \mathcal{U}\mathcal{J}$ with arbitrary $\mathcal{U} \in SO(3)$. This property is a consequence of a symmetry of the model (3.1) with respect to redefinitions of the impurity spin operators $S_i \to S_k\mathcal{U}_{ki}$ which is present when $H_{\mathrm{imp}} = 0$.

- Next, the backscattering current vanishes for the interaction matrix of the form $\mathcal{J}^{(\mathrm{iso})} = \mathrm{diag}\{\mathcal{J}_\perp, \mathcal{J}_\perp, \mathcal{J}_z\}$. The reason behind this nullification is that the respective exchange Hamiltonian

$$H_{\mathrm{edge}}^{\mathrm{e-i}} = \frac{1}{\nu}\left(\frac{\mathcal{J}_\perp}{2}(S_+s_- + S_-s_+) + \mathcal{J}_z S_z s_z\right) \tag{3.33}$$

conserves the z-projection of total angular momentum $S_z + \Sigma_z$. Indeed, using the facts that $\langle S_z \rangle$ is constant when the system is in the steady state and that $I_{\text{bs}} = \langle d\Sigma_z/dt \rangle$ one concludes

$$I_{\text{bs}} = \left\langle \frac{d\Sigma_z}{dt} \right\rangle = \left\langle \frac{d}{dt}(S_z + \Sigma_z) \right\rangle = 0.$$

A symmetry with respect to left rotations of $\mathcal{J}$ implies that the backscattering is also absent in the stationary state for any exchange matrix of the form $\mathcal{U}\mathcal{J}^{(\text{iso})}$, where $\mathcal{U}$ is an arbitrary $SO(3)$ matrix.

We stress that in the general case the local anisotropy $H_{\text{imp}} = \mathcal{D}_{qp}S_qS_p$ breaks both of these properties.

For illustrative purposes, we mention that for the four-component $\mathcal{J}$-matrix (2.9) the backscattering current reads

$$I_{\text{bs}} = -\frac{4S(S+1)}{3M^2\xi^4}e^{-4|x_0|/\xi}\frac{J_m^2 J_0^2}{J_m^2 + J_z^2 + 2J_0^2}G_0 V. \tag{3.34}$$

Notice that *both* the angular momentum conserving processes (controlled by J_m) and the angular momentum non-conserving processes (controlled by J_0) are required to guarantee a non-zero backscattering. Indeed, in the absence of J_0 the matrix (2.9) has the form $\mathcal{J}^{(\text{iso})}$ which implies $I_{\text{bs}} = 0$. At the same time, J_0-related processes do not flip the edge electrons spin and, hence, are incapable of reflecting the electrons back by themselves. Thus, $I_{\text{bs}} = 0$ if $J_m = 0$ as well. A qualitative time-resolved picture of the backscattering process for the matrix $\mathcal{J}$ of the form (2.9) is presented in Fig. 3.2. It emphasizes that a simultaneous presence of J_m and J_0 is required to guarantee $I_{\text{bs}} \neq 0$.
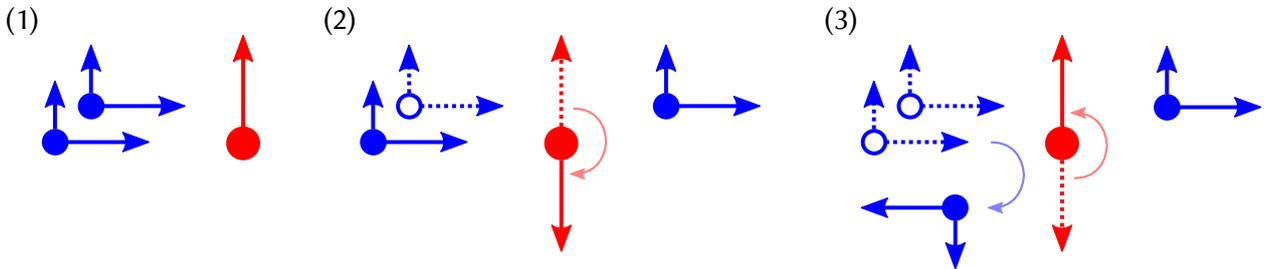
Figure 3.2: Qualitative picture of the backscattering current in the steady state. (1) The impurity is in the stationary state (depicted as spin up). There are electrons incident on the impurity. (2) One electron interacted with the impurity by a J_0-related process: it flipped the impurity spin but did not change its own. (3) Another electron interacted with the impurity by a J_m-related process. The total angular momentum z-projection $S_z + \Sigma_z$ was conserved. As a result of the cycle (1) $\rightarrow$ (2) $\rightarrow$ (3) one electron was backscattered while the impurity returned to its initial state. The repetition of such cycle allows for the non-zero I_{bs} in the stationary state.

We mention that for the weakly anisotropic exchange matrix $\mathcal{J}_{ij} = \mathcal{J}_0 \delta_{ij} + \Delta \mathcal{J}_{ij}$, $|\Delta \mathcal{J}_{ij}| \ll \mathcal{J}_0$ the formula (3.32) reproduces the result presented in [18].

According to section 2.3 for manganese impurities in the topological insulator based on the CdTe/HgTe/CdTe quantum well $\mathcal{J} \sim 10^{-4} \div 10^{-3}$. Hence, the relative backscattering correction to the ballistic conductance *due to a single magnetic impurity* may be estimated as $|\Delta G/G_0| \sim 10^{-6} \div 10^{-4} \ll 1$.

Eq. (3.32) may be equivalently represented in terms of the parameters $\lambda_{1,2,3}$ and the matrix $\mathcal{R}_>$ (see section 2.3.2) as

$$I_{\text{bs}} = -\frac{\pi^2 S(S+1)}{3} \left[\mathcal{R}_>^{-1} \mathcal{I} \mathcal{R}_> \right]_{zz} G_0 V,$$

$$\mathcal{I} = \text{diag} \left\{ \frac{(\lambda_2^2 - \lambda_3^2)^2}{\lambda_2^2 + \lambda_3^2}, \frac{(\lambda_3^2 - \lambda_1^2)^2}{\lambda_3^2 + \lambda_1^2}, \frac{(\lambda_1^2 - \lambda_2^2)^2}{\lambda_1^2 + \lambda_2^2} \right\}. \tag{3.35}$$

The structure of the expression (3.35) is quite remarkable.

- Firstly, all of the entries of the $\mathcal{I}$ matrix are non-negative. Thus, the backscattering correction to the linear conductance (3.35) is always *non-positive*.

- Secondly, the expressions in the numerators of $\mathcal{I}$, i.e. $(\lambda_2^2 - \lambda_3^2)^2$, $(\lambda_3^2 - \lambda_1^2)^2$, and $(\lambda_1^2 - \lambda_2^2)^2$, are invariant under the one-loop RG flow (2.16). At the same time, the denominators $\lambda_2^2 + \lambda_3^2$, $\lambda_3^2 + \lambda_1^2$, and $\lambda_1^2 + \lambda_2^2$ diverge as T approaches the Kondo temperature T_{K}. Therefore, the correction to the linear conductance due to the backscattering vanishes at $T = T_{\text{K}}$.

To conclude this section, we mention that the correction to the linear conductance, i.e. $\Delta G = (I_{\text{bs}}/V)|_{V \ll \mathcal{J}T}$, depends on temperature due to the renormalization of the coupling constants only (see 2.3.2). Thus, ΔG is almost temperature independent for $T \gg T_{\text{K}}$ and $\mathcal{J} \ll 1$. As was discussed in Chapter 1 a weak dependence of the linear conductance on temperature is a required element for a successful theory of the helical edge transport.

3.4   Limit of well-separated energy levels of the impurity

In the present section we discuss the transport along the helical edge assuming that the broadening of the energy levels of the magnetic impurity $\sim \mathcal{J}^2 \max\{T, V\}$ is greatly exceeded by the Zeeman splitting $\sim \mathcal{J}V$, i.e. $V \gg \mathcal{J}T$. In this regime the master equation (3.19) may be significantly

simplified. To see that, we first switch to the interaction representation in Eq. (3.19):

$$\frac{d\rho_S^I(t)}{dt} = \eta_{mn}\left(\sum_{\alpha\beta\gamma\delta} e^{-i(\omega_{\alpha\beta}+\omega_{\gamma\delta})t}\mathcal{S}_m^{\alpha\beta}\rho_S^I\mathcal{S}_n^{\gamma\delta} - \frac{1}{2}\sum_{\alpha\beta\gamma} e^{-i\omega_{\alpha\gamma}t}\left\{\rho_S^I, \mathcal{S}_n^{\alpha\beta}\mathcal{S}_m^{\beta\gamma}\right\}\right). \tag{3.36}$$

We remind that $\mathcal{S}_{x,y,z}^{\alpha\beta} = \sum_{\alpha\beta}|\psi_S^\alpha\rangle S_{x,y,z}^{\alpha\beta}\langle\psi_S^\beta|$, where $S_{x,y,z}^{\alpha\beta} = \langle\psi_S^\alpha|S_{x,y,z}|\psi_S^\beta\rangle$, and $|\psi_S^\alpha\rangle$ is the α-th eigenstate of the impurity Hamiltonian $H_{\mathrm{mf}}^{\mathrm{e-i}}$ which corresponds E_S^α. The transition frequencies are defined as $\omega_{\alpha\beta} = E_S^\beta - E_S^\alpha$. Next, we apply the *rotating wave approximation* [32, 34]. To this end, we average Eq. (3.36) over the time interval Δt which satisfies $\Delta t \ll \tau_K \sim (\mathcal{J}^2 \max\{T, V\})^{-1}$ on the one hand and $\Delta t \gg (\min_{\alpha\neq\beta}|\omega_{\alpha\beta}|)^{-1} \sim (\mathcal{J}V)^{-1}$ on the other hand. The fulfilment of the condition $V \gg \mathcal{J}T$ guarantees the scale separation required to perform such a procedure. Then, to the leading order in a small parameter $\mathcal{J}\max\{T, V\}/V$ we find

$$\frac{d\rho_S^I}{dt} = \eta_{mn}\left(\sum_{\alpha\beta\gamma\delta} \mathcal{S}_m^{\alpha\beta}\rho_S^I\mathcal{S}_n^{\gamma\delta}\delta_{\omega_{\alpha\beta},\omega_{\delta\gamma}} - \frac{1}{2}\sum_{\alpha\beta}\left\{\rho_S^I, \mathcal{S}_n^{\alpha\beta}\mathcal{S}_m^{\beta\alpha}\right\}\right). \tag{3.37}$$

Deriving (3.37) we explicitly employed the non-degenerate character of the Hamiltonian $H_{\mathrm{mf}}^{\mathrm{e-i}}$. At this step, it is convenient to divide the density matrix into its diagonal and off-diagonal parts:

$$\rho_S^I(t) = \sum_\alpha p_\alpha(t)|\psi_S^\alpha\rangle\langle\psi_S^\alpha| + \sum_{\alpha\neq\beta}\pi_{\alpha\beta}(t)|\psi_S^\alpha\rangle\langle\psi_S^\beta|. \tag{3.38}$$

A remarkable feature of Eq. (3.37) is that the evolution of the diagonal components p_α is fully decoupled from the evolution of the off-diagonal components $\pi_{\alpha\beta}$. For p_α we obtain

$$\frac{dp_\alpha}{dt} = \sum_\beta \mathcal{W}_{\alpha\beta}p_\beta, \quad \mathcal{W}_{\alpha\beta} = w_{\alpha\leftarrow\beta} - \delta_{\alpha\beta}\sum_{\beta'}w_{\beta'\leftarrow\alpha}, \quad w_{\alpha\leftarrow\beta} = \eta_{mn}S_m^{\alpha\beta}S_n^{\beta\alpha} \tag{3.39}$$

This is a *classical* Markov equation for the populations of the energy levels in which the transition rates are given by $w_{\alpha\leftarrow\beta}$. Noticeably, in the considered regime $V \gg \mathcal{J}T$ the off-diagonal components of the density matrix decay to zero at the time scale τ_K. Thus, the steady state density matrix of the magnetic impurity has the form

$$\rho_S^{(\mathrm{st})} = \sum_\alpha p_\alpha^{(\mathrm{st})}|\psi_S^\alpha\rangle\langle\psi_S^\alpha|, \tag{3.40}$$

where $p_\alpha^{(\mathrm{st})}$ is a stationary solution of Eq. (3.39). We note that $\rho_S^{(\mathrm{st})}$ commutes with the impurity Hamiltonian $H_{\mathrm{mf}}^{\mathrm{e-i}}$ and, hence, there is no difference between $\rho_{S,I}^{(\mathrm{st})}$ and $\rho_S^{(\mathrm{st})}$ in this case.

In order to obtain an explicit expression for $p_\alpha^{(\mathrm{st})}$ it is convenient to rotate the impurity spin

operator $S_i = \widetilde{S}_k \mathcal{U}_{ki}$, $\mathcal{U} \in SO(3)$, so that the transformed exchange matrix $\widetilde{\mathcal{J}} = \mathcal{U}\mathcal{J}$ has no $\widetilde{\mathcal{J}}_{xz}$ and $\widetilde{\mathcal{J}}_{yz}$ components while $\widetilde{\mathcal{J}}_{zz} > 0$. After the transformation, the effective Zeeman field is directed along the z-axis, i.e. $H_{\text{mf}}^{\text{e}-\text{i}} = \widetilde{\mathcal{J}}_{zz}\widetilde{S}_z V/2$. Therefore, the eigenstates of $H_{\text{mf}}^{\text{e}-\text{i}}$ may be characterized by the value of $\widetilde{S}_z$: $|\psi_S^\alpha\rangle = |\widetilde{S}_z = \alpha\rangle$, $\alpha = S, S-1, ..., -S$.

Next, we evaluate the transition rates $w_{\alpha \leftarrow \beta}$ and find that in the basis[2] $|S\rangle$, $|S-1\rangle$,..., $|-S\rangle$ the matrix $\mathcal{W}_{\alpha\beta}$ has a *tridiagonal* structure with the matrix elements given by

$$\mathcal{W}_{\alpha,\alpha\mp1} = \widetilde{\eta}_\pm \left(S(S+1) - \alpha(\alpha \mp 1)\right)/4, \tag{3.41}$$

$$\mathcal{W}_{\alpha,\alpha} = -W_{\alpha-1,\alpha} - W_{\alpha+1,\alpha}. \tag{3.42}$$

Here $\widetilde{\eta}_\pm = (\widetilde{\eta}_{xx} \pm i\widetilde{\eta}_{xy}) \mp i(\widetilde{\eta}_{yx} \pm i\widetilde{\eta}_{yy})$, $\widetilde{\eta}_{mn} = \pi T \left(\widetilde{\mathcal{J}}\mathcal{K}_V^0 \widetilde{\mathcal{J}}^T\right)_{mn}$. From Eqs. (3.41) and (3.42) one readily finds

$$p_\alpha^{(\text{st})} = \frac{1}{\mathcal{Z}} \left(\frac{\widetilde{\eta}_+}{\widetilde{\eta}_-}\right)^\alpha, \quad \alpha = S, S-1, ..., -S, \tag{3.43}$$

where the partition function $\mathcal{Z} = \sum_{\alpha=-S}^S (\widetilde{\eta}_+/\widetilde{\eta}_-)^\alpha$ ensures that $\text{tr}_S \rho_S^{(\text{st})} = 1$. Intriguingly, the steady state density matrix $\rho_S^{(\text{st})}$ has a Gibbs structure. It may be equivalently rewritten in a basis independent form as

$$\rho_S^{(\text{st})} = \frac{1}{\mathcal{Z}} \exp\left\{-H_{\text{mf}}^{\text{e}-\text{i}}/T_{\text{eff}}\right\}, \tag{3.44}$$

where *the effective temperature* T_{eff} is defined by

$$T_{\text{eff}} = -\frac{V}{4}\widetilde{\mathcal{J}}_{zz} \left[\text{arccoth}\left(\frac{\widetilde{\mathcal{J}}_{zz}\left(\widetilde{\Gamma}_0\right)_{zz}}{2\left(\det\mathcal{J}\right)}\coth\frac{V}{2T}\right)\right]^{-1}. \tag{3.45}$$

Here $\widetilde{\Gamma}_0 = \text{tr}\widetilde{\mathcal{J}}\widetilde{\mathcal{J}}^T - \widetilde{\mathcal{J}}\widetilde{\mathcal{J}}^T$. The determinant $\det\mathcal{J}$ does not feature a tilde sign due to its invariance under $\mathcal{J} \to \mathcal{U}\mathcal{J}$. The effective temperature (3.45) may be alternatively expressed in terms of the initial exchange matrix $\mathcal{J} = \mathcal{U}^T \widetilde{\mathcal{J}}$ as

$$T_{\text{eff}} = -\frac{V}{4}\sqrt{(\mathcal{J}^T\mathcal{J})_{zz}} \left[\text{arccoth}\frac{(\mathcal{J}^T\Gamma_0\mathcal{J})_{zz}\coth\frac{V}{2T}}{2\left(\det\mathcal{J}\right)\sqrt{(\mathcal{J}^T\mathcal{J})_{zz}}}\right]^{-1}. \tag{3.46}$$

The representation (3.46) is invariant with respect to the left rotations of the $\mathcal{J}$ matrix. It is worth mentioning that T_{eff} is not a sign-fixed quantity. It is either positive or negative depending on the structure of the matrix $\mathcal{J}$. This feature is a consequence of the non-equilibrium character of the considered problem. Interestingly, for $V \gg T$ both the mean-field interaction $H_{\text{mf}}^{\text{e}-\text{i}}$ and the

---

[2]Hereinafter, we use a shorthand notation $|\alpha\rangle \equiv |S_{\boldsymbol{n}} = \alpha\rangle$ for the states once the quantization axis $\boldsymbol{n}$ is specified.

effective temperature are proportional to voltage. As a result, the Gibbs factor $p_{\alpha+1}^{(\text{st})}/p_{\alpha}^{(\text{st})}$ ($\alpha = S - 1, S - 2, ..., -S$) tends to a finite value in the limit $V \gg T$. Therefore, the impurity is never fully polarized in case the matrix $\mathcal{J}$ has a general form. A particular exception from this rule is the isotropic $\mathcal{J}$-matrix, $\mathcal{J}^{(\text{iso})} = \text{diag}\{\mathcal{J}_\perp, \ \mathcal{J}_\perp, \ \mathcal{J}_z\}$, for which (we assume $\mathcal{J}_z > 0$)

$$\rho_S^{(\text{st})} = \frac{1}{\mathcal{Z}} \exp\left\{ \frac{V}{T} S_z \right\}. \tag{3.47}$$

In the limit $V \gg T$ only the state with $S_z = S$ is occupied.

At arbitrary voltage $V \gg \mathcal{J}T$ the steady state density matrix (3.44) allows one to evaluate the averages $\langle S_k \rangle$ and $\langle \{S_m, S_n\} \rangle$ entering Eq. (3.30) and thus find the backscattering current. It is enlightening to follow this procedure in order to consider the helical edge transport in the regime $\mathcal{J}T \ll V \ll T$. Expanding the expression for $\rho_S^{(\text{st})}$ to the first order in V/T we find

$$\langle S_k \rangle \simeq \frac{2S(S+1)}{3} \frac{V}{T} \frac{\mathcal{J}_{kz} \det \mathcal{J}}{(\mathcal{J}^T \Gamma_0 \mathcal{J})_{zz}}. \tag{3.48}$$

To the zero order in V/T the density matrix $\rho_S^{(\text{st})} \simeq \rho_S^{(\text{eq})} = I_{(2S+1)\times(2S+1)}/(2S+1)$. Therefore, $\langle \{S_m, S_n\} \rangle \simeq 2\delta_{mn} S(S+1)/3$. Then, with the help of Eq. (3.30) for the backscattering current we establish

$$I_{\text{bs}} = \frac{\pi^2 S(S+1)}{3} \left(\frac{4(\det \mathcal{J})^2}{(\mathcal{J}^T \Gamma_0 \mathcal{J})_{zz}} - g \right) G_0 V. \tag{3.49}$$

Here we used the relation $J_{kz}\mathcal{X}_k = 2\det \mathcal{J}$. We recall that $g = \left(\mathcal{J}^T \mathcal{J}\right)_{xx} + \left(\mathcal{J}^T \mathcal{J}\right)_{yy}$.

Interestingly, the correction to the conductance, $\Delta G = I_{\text{bs}}/V$ in the regime $\mathcal{J}T \ll V \ll T$ is substantially different from ΔG in the linear regime (see Eq. (3.32)). For instance, for the four-component matrix (2.9) I_{bs} based on Eq. (3.49) acquires the form

$$I_{\text{bs}} = -\frac{4S(S+1)}{3M^2\xi^4} e^{-4|x_0|/\xi} \frac{J_m^2 J_0^2}{J_z^2 + 2J_0^2} G_0 V. \tag{3.50}$$

which lacks J_m^2 in the denominator as compared to the corresponding linear result (3.34). Thus, as a function of voltage ΔG exhibits a crossover at $V \sim \mathcal{J}T$ between the expression (3.49) valid for $\mathcal{J}T \ll V \ll T$ and the expression (3.32) applicable in the linear regime $V \ll \mathcal{J}T$. For $V \ll T$ the interpolation between the two limits may be described by

$$I_{\text{bs}} = \frac{\pi^2 S(S+1)}{3} \left(\mathcal{X}^T \Gamma^{-1} \mathcal{X} - g \right) G_0 V, \quad \Gamma_{lk} \simeq (\Gamma_0)_{lk} + \frac{V}{\pi T} \varepsilon_{lkj} \mathcal{J}_{jz}. \tag{3.51}$$

This formula follows from Eqs. (3.26), (3.30), and the fact that for $V \ll T$ the density matrix

is close to equipartitioning. We mention that the impurity spin S enters the expression for the backscattering current (3.51) as a factor $S(S + 1)$ only. This is not the case for $V \gtrsim T$.

Given the expression (3.46) for the effective temperature one may expect that after the crossover at $V \sim \mathcal{J}T$ the correction to the conductance ΔG gradually changes and saturates at $V \sim T$. Intriguingly, while this is indeed the case for the impurities with $S > 1/2$, for the spin-1/2 impurity the saturation happens much earlier: already at $V \sim \mathcal{J}T$. We discuss this peculiarity in the following section.

3.5   Backscattering current due to a spin-1/2 impurity

For a spin-1/2 magnetic impurity it is possible to establish an analytic expression for the backscattering current valid at arbitrary voltages. A simplification in comparison with higher spin impurities comes from the *exact* relation $\{S_m, S_n\} = \delta_{mn}/2$ specific to $S = 1/2$. With its help from Eqs. (3.26) and (3.30) we find

$$I_{\mathrm{bs}} = \frac{\pi^2}{4} \left(\mathcal{X}^T \Gamma^{-1} \mathcal{X} \frac{V}{2T} \coth \frac{V}{2T} - g \right) G_0 V. \tag{3.52}$$

We mention that in the limit $V \gg \mathcal{J}T$ the inverse Γ-matrix may be evaluated explicitly as

$$\left(\Gamma^{-1} \right)_{kl} = \frac{\mathcal{J}_{kz} \mathcal{J}_{lz}}{(\mathcal{J}^T \Gamma_0 \mathcal{J})_{zz}} \left(\frac{V}{2T} \coth \frac{V}{2T} \right)^{-1}. \tag{3.53}$$

Hence, for $V \gg \mathcal{J}T$ the backscattering current is given by

$$I_{\mathrm{bs}} = \frac{\pi^2}{4} \left(\frac{4 \left(\det \mathcal{J} \right)^2}{(\mathcal{J}^T \Gamma_0 \mathcal{J})_{zz}} - g \right) G_0 V. \tag{3.54}$$

Remarkably, this expression is voltage independent. Thus, for $S = 1/2$ the saturation of ΔG happens at $V \sim \mathcal{J}T$ and not at $V \sim T$. This is not the case for higher spins. If $S > 1/2$ ΔG is constant only as long as $V \gtrsim T$.

3.6   Numeric solution

In the previous sections of this Chapter we studied the correction to the ballistic conductance due to the magnetic impurity in the regimes $V \ll \mathcal{J}T$ and $V \gg \mathcal{J}T$ analytically. Concluding this chapter we compare the corresponding asymptotic expressions with the exact results obtained with
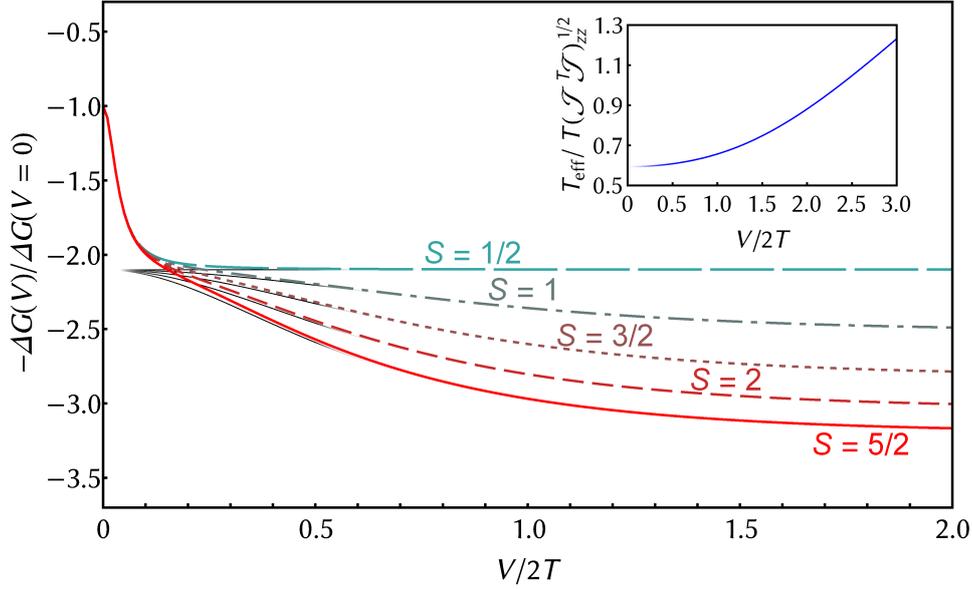
Figure 3.3: The correction to the ballistic conductance $\Delta G = I_{bs}/V$ as a function of $V/2T$ for the magnetic impurities with different spins. $\Delta G(V)$ is measured in units of $-\Delta G(V=0)$. The non-zero dimensionless couplings are $\mathcal{J}_{xx} = \mathcal{J}_{yy} = 10^{-2}$, $\mathcal{J}_{xz} = 0.8\mathcal{J}_{xx}$, $\mathcal{J}_{zx} = 0.3\mathcal{J}_{xx}$, $\mathcal{J}_{zz} = 0.9\mathcal{J}_{xx}$. Black solid fading lines depict approximate ($V \gg \mathcal{J}T$) conductance curves based on Eqs. (3.30) and (3.44). The inset presents the effective temperature T_{eff} as a function of $V/2T$. With slight changes, the image is adapted from [23].

the help of numeric methods.

In Fig. 3.3 we present the correction to the conductance $\Delta G(V)$, which is based on the numeric solutions of Eqs. (3.19) and (3.30), for the impurities with $S = 1/2, 1, 3/2, 2$, and $5/2$. The choice of the exchange matrix $\mathcal{J}$ is specified in the caption. For each impurity spin $\Delta G(V)$ is measured in the units of $-\Delta G(V=0)$. Thus, all of the curves presented in Fig. 3.3 depart from -1.

All of the main features discussed in the present Chapter are vividly illustrated in Fig. 3.3. To begin with, there is a sharp crossover at $V \sim \mathcal{J}T$ which is connected with the transition between the linear regime $V \ll \mathcal{J}T$ (see Eq. (3.32)) and the regime $\mathcal{J}T \ll V \ll T$ (see Eq. (3.49)). Next, the curves for the impurities with different spins coincide when $V \ll T$. The reason behind this feature is that for $V \ll T$ the impurity spin S enters the expression for the backscattering current as a multiplier $S(S+1)$ only (see Eq. (3.51)). Black fading curves depict the correction to the conductance calculated with the help of the Gibbs density matrix (3.44). These curves match with the numeric results as soon as the condition $V \gg \mathcal{J}T$ is fulfilled. In agreement with section 3.5, the correction to the conductance saturates at $V \sim \mathcal{J}T$ for $S = 1/2$. For $S > 1/2$ the saturation happens at $V \sim T$.

Chapter 4

Influence of local magnetic anisotropy of the impurity on the helical edge transport

In the previous chapter, we have considered the transport along the helical edge assuming that the impurity Hamiltonian $H_{\text{imp}} = 0$. At the same time, already on the level of the master equation we have seen that the interaction between the edge electrons in the topological insulator and the impurity induces the local magnetic anisotropy of the latter (see section 3.2.2): $H_{\text{anis}}^{\text{edge}} = -\Lambda_{\text{edge}} |M| \left(\mathcal{J} \mathcal{J}^T \right)_{qp} S_q S_p$, $\Lambda_{\text{edge}} \sim 1$. Therefore, it is important to i) identify other possible sources of local anisotropy, ii) determine the conditions under which the local anisotropy may be neglected, iii) understand what is the influence of the anisotropy on the transport properties of the edge of the topological insulator once it cannot be disregarded. In the present chapter we address these questions in details.

In section 4.1 we consider in details the local anisotropy generated by the indirect exchange interaction of the magnetic impurity with itself. Here we focus on the topological insulators based on the CdTe/HgTe/CdTe quantum wells although qualitatively the obtained results are applicable to other structures as well. In section 4.2 we derive the master equation and the equation for the backscattering current taking the anisotropy into account. Section 4.3 is devoted to the helical edge transport in the presence of the impurity with *uniaxial* anisotropy. Finally, in section 4.4 the case of non-uniaxial anisotropy is discussed.

4.1   Local magnetic anisotropy

The local anisotropy of a spin S magnetic impurity embedded into the topological insulator originates from a number of sources. In section 3.2.2 we already identified one of them: the anisotropy

is generated by the exchange interaction between the impurity and the edge electrons. The exchange between the magnetic impurity and the bulk electrons results in a contribution to the local anisotropy in the same way [27]. In addition to that, the crystalline field induces the quadrupolar splitting of the impurity energy levels [35]. Furthermore, strains in the heterostructure might produce the anisotropy as well although we do not discuss this mechanism in details in the present thesis.

To account for these effects, in the following sections we use a phenomenological impurity Hamiltonian $H_{\text{imp}} = \mathcal{D}_{qp} S_q S_p$ without referring to any specific origin of the anisotropy emergence. However, in order to understand whether the presented considerations are relevant in realistic experimental conditions as well as to reveal possible matrix structure of $\mathcal{D}_{qp}$ we first discuss different sources of the local anisotropy in a more detail. Below, we assume that the considered topological insulator is based on the CdTe/HgTe/CdTe quantum well. Yet, on a qualitative level, the results presented in this section are valid for the other 2D topological insulators as well.

Let us first consider the local anisotropy generated by the interaction between the magnetic impurity and the electrons in the quantum well. This contribution to the total anisotropy may be viewed as the one produced by the indirect exchange interaction of the impurity with itself (see [27]). In order to evaluate it, we represent the exchange Hamiltonian (2.7) as a sum over the impurity spin components: $H^{\text{e}-\text{i}} = \check{J}_q S_q \delta(\boldsymbol{r} - \boldsymbol{r}_0)$. Here $\check{J}_{x,y,z}$ are 4×4 matrices operating in the basis of spatially quantized states $|E_1, +\rangle, |H_1, +\rangle, |E_1, -\rangle, |H_1, -\rangle$ and $\boldsymbol{r}_0 = (x_0, \ y_0)^T$ is an in-plane radius vector of the impurity. Then, with the help of Matsubara diagram technique to the second order in $\check{J}$ we find

$$H_{\text{imp}} = \mathcal{D}_{qp} S_q S_p, \quad \mathcal{D}_{qp} = \frac{1}{2} \int \frac{d\epsilon}{2\pi} \text{tr}_{\text{qw}} \left\{ \mathcal{G}(i\epsilon, \boldsymbol{r}_0, \boldsymbol{r}_0) \check{J}_q \mathcal{G}(i\epsilon, \boldsymbol{r}_0, \boldsymbol{r}_0) \check{J}_p \right\}, \tag{4.1}$$

where $\text{tr}_{\text{qw}} \{...\}$ is a trace over the matrix indexes in $|E_1, \pm\rangle, |H_1, \pm\rangle$ space and $\mathcal{G}(i\epsilon, \boldsymbol{r}_1, \boldsymbol{r}_2)$ is the Matsubara Green's function. For the estimate, we assumed that $T = 0$. In the expression (4.1), it is convenient to represent each Green's function as a sum over the edge and bulk states. To do that, we use the identity

$$\mathcal{G} = \mathcal{G}_{\text{edge}} + \mathcal{G}_{\text{bulk}}, \quad \mathcal{G}_{\text{edge}}(i\epsilon, \boldsymbol{r}_1, \boldsymbol{r}_2) = \sum_{s=\uparrow/\downarrow} \sum_{k_y} \frac{\psi_{\text{edge},s}(\boldsymbol{r}_1, k_y) \psi_{\text{edge},s}^{\dagger}(\boldsymbol{r}_2, k_y)}{i\epsilon - E_{\text{edge},s}(k_y) + \mu}, \tag{4.2}$$

$$\mathcal{G}_{\text{bulk}}(i\epsilon, \boldsymbol{r}_1, \boldsymbol{r}_2) = \sum_{b=\pm} \sum_{s=\uparrow/\downarrow} \sum_{\boldsymbol{k}} \frac{\psi_{\text{bulk},s}^{b}(\boldsymbol{r}_1, \boldsymbol{k}) \psi_{\text{bulk},s}^{b,\dagger}(\boldsymbol{r}_2, \boldsymbol{k})}{i\epsilon - E_{\text{bulk},s}^{b}(\boldsymbol{k}) + \mu}.$$

The wave functions of the edge and bulk states within the model (2.3) are presented in Eqs. (2.4) and

(2.6) correspondingly. We recall that $E_{\text{edge},\uparrow/\downarrow}(k_y) = \mp A k_y$ and $E_{\text{bulk},\uparrow}^{\pm}(\boldsymbol{k}) = E_{\text{bulk},\downarrow}^{\pm}(\boldsymbol{k}) = \pm\mathcal{E}(k)$, where $\mathcal{E}(k) = \sqrt{M^2 + A^2 k^2}$. The representation (4.2) hints that it is possible to divide the impurity Hamiltonian H_{imp} into *three* terms of different origin:

$$H_{\text{imp}} = H_{\text{anis}}^{\text{edge}} + H_{\text{anis}}^{\text{bulk}} + H_{\text{anis}}^{\text{int}}, \quad H_{\text{anis}}^{\text{edge (bulk, int)}} = \mathcal{D}_{qp}^{\text{edge (bulk, int)}} S_q S_p, \tag{4.3}$$

where

$$\mathcal{D}_{qp}^{\text{edge (bulk)}} = \frac{1}{2}\int \frac{d\epsilon}{2\pi}\text{tr}_{\text{qw}}\left\{\mathcal{G}^{\text{edge (bulk)}}(i\epsilon, \boldsymbol{r}_0, \boldsymbol{r}_0)\check{J}_q \mathcal{G}^{\text{edge (bulk)}}(i\epsilon, \boldsymbol{r}_0, \boldsymbol{r}_0)\check{J}_p\right\}, \tag{4.4}$$

$$\mathcal{D}_{qp}^{\text{int}} = \frac{1}{2}\int \frac{d\epsilon}{2\pi}\text{tr}_{\text{qw}}\left\{\mathcal{G}^{\text{bulk}}(i\epsilon, \boldsymbol{r}_0, \boldsymbol{r}_0)\check{J}_q \mathcal{G}^{\text{edge}}(i\epsilon, \boldsymbol{r}_0, \boldsymbol{r}_0)\check{J}_p\right\} + (q \leftrightarrow p). \tag{4.5}$$

Here $H_{\text{anis}}^{\text{edge (bulk)}}$ describes the local anisotropy generated by the interaction between the magnetic impurity and the edge (bulk) electrons. Interestingly, the last term in Eq. (4.3), $H_{\text{anis}}^{\text{int}}$, is determined by the edge and bulk states simultaneously. Hence, it is mediated by the interference between the two types of states.

Now, we discuss these contributions to the anisotropy in various scenarios. To begin with, we consider the case in which the magnetic impurity is located far away from the helical edge, $|x_0| \gg \xi = A/|M|$. In this regime, the edge and the interference terms in Eq. (4.3) are exponentially suppressed as compared with the bulk term $H_{\text{anis}}^{\text{bulk}} = \mathcal{D}_{qp}^{\text{bulk}} S_q S_p$. The latter may be estimated as (see [27])

$$\mathcal{D}_{qp}^{\text{bulk}} = -\Lambda_{\text{bulk}}^{\infty}|M|^3 \text{tr}_{\text{qw}}\left\{\check{J}_q \check{J}_p\right\}/A^4,$$

$$\Lambda_{\text{bulk}}^{\infty} \sim \frac{A^4}{|M|^3}\int \frac{d\epsilon}{2\pi}\frac{d^2\boldsymbol{k}_1}{(2\pi)^2}\frac{d^2\boldsymbol{k}_2}{(2\pi)^2}\frac{\epsilon^2}{(\epsilon^2 + \mathcal{E}(k_1)^2)(\epsilon^2 + \mathcal{E}(k_2)^2)}. \tag{4.6}$$

The integral for the dimensionless multiplier $\Lambda_{\text{bulk}}^{\infty}$ diverges in the ultraviolet limit. The divergence emerges as a consequence of the approximation that the electron-impurity interaction $H^{\text{e-i}}$ bears a local character. Realistically, the impurity potential has a finite range l_{imp} of the order of several lattice constants. For instance, for a Mn^{2+} impurity in CdTe we estimate $l_{\text{imp}} = a_B \varepsilon_{\text{CdTe}} m_{\text{CdTe}}/2m_{\text{e}} \simeq 3$ nm, where $\varepsilon_{\text{CdTe}} \simeq 10$ is the dielectric constant of CdTe, $m_{\text{CdTe}} \simeq 0.1 m_{\text{e}}$ is the electron band effective mass, m_{e} is the bare electron mass, and a_B is the Bohr radius[1]. The integral (4.6) should be regularized at high momenta $k_{\text{max}} \sim l_{\text{imp}}^{-1}$. As a result, we find

$$\Lambda_{\text{bulk}}^{\infty} \sim \left(\frac{\xi}{l_{\text{imp}}}\right)^3. \tag{4.7}$$

---

[1] For the reference, the lattice constant of CdTe is $a_{\text{CdTe}} \simeq 0.6$ nm.

We mention that for the CdTe/HgTe/CdTe quantum well with the width $d = 7.0\,\mathrm{nm}$ the length scale $\xi \simeq 40\,\mathrm{nm} \gg l_{\mathrm{imp}} \sim 1\,\mathrm{nm}$. Hence, in this realistic setting the ratio ξ/l_{imp} is large and $\Lambda^\infty_{\mathrm{bulk}} \gg 1$.

Next, we discuss the case of the impurity located very close to the edge, $|x_0| \ll \xi$. In this regime, bulk and edge states which are characterized by the same index $\uparrow / \downarrow$ have the same spinor structure (see Eqs. (2.4) and (2.6)). Therefore, the matrix form of $\mathcal{D}^{\mathrm{edge}}_{qp}$, $\mathcal{D}^{\mathrm{bulk}}_{qp}$, and $\mathcal{D}^{\mathrm{int}}_{qp}$ is the same:

$$\mathcal{D}^{\mathrm{bulk}}_{qp} = -\Lambda^0_{\mathrm{edge}}|M|^3\mathrm{tr}_{\mathrm{qw}}\left\{\mathcal{P}\check{J}_q\mathcal{P}\check{J}_p\right\}/A^4, \quad \mathcal{D}^{\mathrm{bulk}}_{qp} = -\Lambda^0_{\mathrm{edge}}|M|^3\mathrm{tr}_{\mathrm{qw}}\left\{\mathcal{P}\check{J}_q\mathcal{P}\check{J}_p\right\}/A^4$$

$$\mathcal{D}^{\mathrm{int}}_{qp} = -\Lambda^0_{\mathrm{int}}|M|^3\mathrm{tr}_{\mathrm{qw}}\left\{\mathcal{P}\check{J}_q\mathcal{P}\check{J}_p\right\}/A^4, \tag{4.8}$$

where the matrix $\mathcal{P}$ is defined by

$$\mathcal{P} = \begin{pmatrix} 1 & -i & 0 & 0 \\ i & 1 & 0 & 0 \\ 0 & 0 & 1 & i \\ 0 & 0 & -i & 1 \end{pmatrix}. \tag{4.9}$$

At the same time, the numeric factors $\Lambda^0_{\mathrm{edge}}$, $\Lambda^0_{\mathrm{bulk}}$, and Λ^0_{int} are parametrically different. Using the explicit structure of the bulk and edge states in the CdTe/HgTe/CdTe heterostructure we determine

$$\Lambda^0_{\mathrm{edge}} \sim \frac{A^2}{|M|}\int\frac{d\epsilon}{2\pi}\frac{dk_{y,1}}{2\pi}\frac{dk_{y,2}}{2\pi}\frac{\epsilon^2}{\left(\epsilon^2 + A^2k^2_{y,1}\right)\left(\epsilon^2 + A^2k^2_{y,2}\right)} \sim \frac{1}{|M|}\int d\epsilon \sim 1, \tag{4.10}$$

$$\Lambda^0_{\mathrm{int}} \sim \frac{A^3}{M^2}\int\frac{d\epsilon}{2\pi}\frac{d^2\boldsymbol{k}_1}{(2\pi)^2}\frac{dk_{y,2}}{2\pi}\frac{\epsilon^2}{\left(\epsilon^2 + \mathcal{E}(k_1)^2\right)\left(\epsilon^2 + A^2k^2_{y,2}\right)}\frac{A^2k^2_{x,1}}{\mathcal{E}(k_1)(\mathcal{E}(k_1) + Ak_{y,1})} \sim$$

$$\sim \frac{1}{|M|}\int d\epsilon \sim 1, \tag{4.11}$$

$$\Lambda^0_{\mathrm{bulk}} \sim \frac{A^4}{|M|^3}\int\frac{d\epsilon}{2\pi}\frac{d^2\boldsymbol{k}_1}{(2\pi)^2}\frac{d^2\boldsymbol{k}_2}{(2\pi)^2}\frac{\epsilon^2}{\left(\epsilon^2 + \mathcal{E}(k_1)^2\right)\left(\epsilon^2 + \mathcal{E}(k_2)^2\right)}\frac{1}{\mathcal{E}(k_1)\mathcal{E}(k_2)} \times$$

$$\times \frac{A^4k^2_{x,1}k^2_{x,2}}{(\mathcal{E}(k_1) + Ak_{y,1})(\mathcal{E}(k_2) + Ak_{y,2})} \sim \left(\frac{\xi}{l_{\mathrm{imp}}}\right)^3. \tag{4.12}$$

Deriving the estimates for $\Lambda^0_{\mathrm{edge}}$ and Λ^0_{int} we introduced an ultraviolet cut-off $\epsilon_{\max} \sim |M|$ in the integrals over energies. It accounts for the fact that the edge states are defined in a finite interval of energies of the order of the band gap only. Remarkably, the expressions (4.8) may be equivalently rewritten in terms of the dimensionless exchange coupling matrix $\mathcal{J}$ as

$$\mathcal{D}^{\mathrm{bulk\ (edge,\ int)}}_{qp} = -2\pi^2\Lambda^{\mathrm{bulk\ (edge,\ int)}}_0|M|\left(\mathcal{J}\mathcal{J}^T\right)_{qp}. \tag{4.13}$$

Comparing the resultant expression (4.13) with Eq. (3.22) we conclude the linearly divergent terms

which we encountered in the derivation of the master equation for the density matrix ρ_S precisely describe the anisotropy due to the interaction between the impurity and the edge electrons.

Notice that the bulk contribution $H_{\text{anis}}^{\text{bulk}}$ to the anisotropy has the same order of magnitude in cases $|x_0| \ll \xi$ and $|x_0| \gg \xi$. Hence, as the impurity gets displaced from the edge of the sample into the bulk the value of $\mathcal{D}_{qp}^{\text{bulk}}$ is roughly preserved, whereas its matrix structure smoothly changes from $\text{tr}_{\text{qw}} \left\{ \mathcal{P} \breve{J}_q \mathcal{P} \breve{J}_p \right\}$ to $\text{tr}_{\text{qw}} \left\{ \breve{J}_q \breve{J}_p \right\}$ on a length scale of ξ.

Interestingly, $H_{\text{anis}}^{\text{bulk}}$ typically transcends the contributions due to the interaction with the edge electrons or due to the interference: $H_{\text{anis}}^{\text{edge}}$ and $H_{\text{anis}}^{\text{int}}$ respectively.

We mention that the anisotropy $H_{\text{anis}}^{\text{bulk}}$ in the model (2.7) is uniaxial for the impurity located far away from the edge,

$$H_{\text{anis}}^{\text{bulk}} = -2\Lambda_{\text{bulk}}^{\infty} |M|^3 \left\{ J_1^2 + J_2^2 - J_m^2 - 2J_0^2 \right\} S_z^2 / A^4. \tag{4.14}$$

Here we omitted the constant energy shift. On the contrary, for the impurity located near the edge the bulk contribution to the anisotropy is non-uniaxial,

$$H_{\text{anis}}^{\text{bulk}} = -2\Lambda_{\text{bulk}}^{0} |M|^3 \left\{ ((J_1 + J_2)^2 - J_m^2) S_z^2 + 4J_0(J_1 + J_2) S_x S_z + 4J_0^2 S_x^2 \right\} / A^4. \tag{4.15}$$

Using the approximate values of $J_{0,1,2,m}$ (see [27]) we establish that in the CdTe/HgTe/CdTe quantum well with the width $d = 7.0$ nm the bulk contribution to the anisotropy may be estimated as $|\mathcal{D}_{qp}^{\text{bulk}}| \sim 0.1$ K for the manganese impurity. Another possible source of the local anisotropy – the quadrupolar splitting – is of the order of $\sim 10^{-3}$ K [35] and, hence, may be disregarded in comparison with $H_{\text{anis}}^{\text{bulk}}$. Thus, while in the following we will consider the effects of the anisotropy in a phenomenological model $H_{\text{imp}} = \mathcal{D}_{qp} S_q S_p$, we will keep in mind that $\mathcal{D}_{qp}$ mainly originates due to the interaction of the impurity with the bulk electrons.

To conclude this section, we note that the time-reversal symmetry which is present in the considered system implies that the Hermitian matrix $\mathcal{D}$ is real and, therefore, symmetric. The expressions (4.6) and (4.8) illustrate this observation. Importantly, the symmetry of the matrix $\mathcal{D}$ entails that for a spin-1/2 magnetic impurity the expression $\mathcal{D}_{qp} S_q S_p$ *always* reduces to a mere constant. Hence, the anisotropy is never relevant for the impurities with $S = 1/2$.

4.2 Master equation and backscattering current

In the presence of the anisotropic impurity with $H_{\text{imp}} = \mathcal{D}_{qp}S_qS_p$ the total Hamiltonian H_{tot} of the edge of the topological insulator has the form

$$H_{\text{tot}} = \mathcal{D}_{qp}S_qS_p + \mathcal{J}_{kz}S_k\frac{V}{2} + \frac{1}{\nu}\mathcal{J}_{ij}S_i : s_j : +iv\int dy\,\Psi^\dagger(y)\sigma_z\partial_y\Psi(y)dy. \qquad (4.16)$$

Here we divided the electron-impurity interaction $H_{\text{edge}}^{\text{e-i}} = \mathcal{J}_{ij}S_is_j/\nu$ into its mean-field part $H_{\text{mf}}^{\text{e-i}} = \mathcal{J}_{kz}S_kV/2$ and the fluctuations around it, $: H_{\text{edge}}^{\text{e-i}} := \mathcal{J}_{ij}S_i : s_j : /\nu$. We recall that the spin density fluctuation operator, which enters the expression for $: H_{\text{edge}}^{\text{e-i}} :$, is defined by $: s_j := s_j - \langle s_j\rangle_0$, where $\langle s_j\rangle_0 = \delta_{jz}\nu V/2$. The last term in Eq. (4.16), $H_{\text{edge}}^{\text{e}} = iv\int dy\,\Psi^\dagger(y)\sigma_z\partial_y\Psi(y)dy$, describes the kinematics of the edge electrons.

Notice that under the redefinition of the impurity spin operators $S_i \to S_k\mathcal{U}_{ki}$, where $\mathcal{U} \in SO(3)$, the anisotropy matrix $\mathcal{D}$ and the exchange interaction matrix $\mathcal{J}$ transform as

$$\mathcal{D} \to \mathcal{U}\mathcal{D}\mathcal{U}^T, \quad \mathcal{J} \to \mathcal{U}\mathcal{J}. \qquad (4.17)$$

Since $\mathcal{D}$ is a symmetric matrix it is always possible to choose a proper $\mathcal{U}$ so that $\mathcal{U}\mathcal{D}\mathcal{U}^T$ is diagonal and the transformed anisotropy Hamiltonian has the form $H_{\text{imp}} = \mathcal{D}_{xx}S_x^2 + \mathcal{D}_{yy}S_y^2 + \mathcal{D}_{zz}S_z^2$. Up to the constant energy shift the latter expression equals

$$H_{\text{imp}} = \mathcal{D}_xS_x^2 + \mathcal{D}_zS_z^2, \qquad (4.18)$$

where we defined $\mathcal{D}_x = \mathcal{D}_{xx} - \mathcal{D}_{yy}$ and $\mathcal{D}_z = \mathcal{D}_{zz} - \mathcal{D}_{yy}$. Hence, throughout the Chapter we will use the Hamiltonian (4.18) with $|\mathcal{D}_z| \geq |\mathcal{D}_x|$ instead of $H_{\text{imp}} = \mathcal{D}_{qp}S_qS_p$. As long as we assume that the exchange matrix $\mathcal{J}$ has an arbitrary form such substitution does not diminish the generality of our considerations.

Next, we notice that the first two terms in Eq. (4.16) describe the degrees of freedom related to the impurity only. Therefore, it reasonable to combine them in a *total* Hamiltonian of the magnetic impurity

$$H_{\text{imp}}^{\text{tot}} = H_{\text{imp}} + H_{\text{mf}}^{\text{e-i}} = \mathcal{D}_xS_x^2 + \mathcal{D}_zS_z^2 + \mathcal{J}_{kz}S_k\frac{V}{2}. \qquad (4.19)$$

We denote the eigenstates of $H_{\text{imp}}^{\text{tot}}$ and the corresponding energies as $|\psi_S^\alpha\rangle$ and E_S^α respectively. The index α can have $2S + 1$ distinct values.

To evaluate the backscattering current at arbitrary voltage and temperature we follow the methodology developed in Chapter 3. First, we derive the master equation for the reduced density matrix

of the magnetic impurity ρ_S. To this end, in the Liouville equation $d\rho/dt = -i[H_{\text{tot}}, \rho]$ we switch to the interaction representation by introducing

$$\rho^I(t) = \exp\left\{-i(H_{\text{imp}}^{\text{tot}} + H_{\text{edge}}^{\text{e}})t\right\} \rho(t) \exp\left\{i(H_{\text{imp}}^{\text{tot}} + H_{\text{edge}}^{\text{e}})t\right\}. \tag{4.20}$$

Then we take the partial trace over the edge electrons. As a result, we reproduce the Bloch-Redfield master equation (3.15):

$$\frac{d\rho_S^I(t)}{dt} = \mathcal{J}_{mi}\mathcal{J}_{nj} \sum_{\alpha\beta\gamma\delta} \left\{ \left[\left(\mathcal{S}_m^{\alpha\beta}\right)^I(t)\rho_S^I(t), \left(\mathcal{S}_n^{\gamma\delta}\right)^I(t) \right] K_V^{ij}(\omega_{\alpha\beta}) + \text{h.c.} \right\}. \tag{4.21}$$

Here $\mathcal{S}_{x,y,z}^{\alpha\beta} = |\psi_S^\alpha\rangle S_{x,y,z}^{\alpha\beta}\langle\psi_S^\beta|$, $S_{x,y,z}^{\alpha\beta} = \langle\psi_S^\alpha|S_{x,y,z}|\psi_S^\beta\rangle$, and $\omega_{\alpha\beta} = E_S^\beta - E_S^\alpha$. The spin-spin correlator function $K_V^{ij}(\omega_{\alpha\beta})$ is defined in Eq. (3.18). While Eq. (4.21) is formally similar to Eq. (3.15), there is a major difference between the former and the latter: in contrast to Eq. (3.15), the structure of the eigenstates $|\psi_S^\alpha\rangle$ and the respective energies E_S^α in Eq. (4.21) are both affected by the local anisotropy. Below, we will show that in many cases this feature has a dramatic influence on the character of the impurity dynamics and on the backscattering current.

Alternatively, Eq. (4.21) may be rewritten as

$$\frac{d\rho_S(t)}{dt} = -i\left[\mathcal{D}_z S_z^2 + \mathcal{D}_x S_x^2 + \mathcal{J}_{kz} S_k \frac{V}{2}, \rho_S(t)\right] + \tag{4.22}$$
$$+ \mathcal{J}_{mi}\mathcal{J}_{nj} \sum_{\alpha\beta\gamma\delta} \left\{ \left[\mathcal{S}_m^{\alpha\beta}\rho_S(t), \mathcal{S}_n^{\gamma\delta}\right] \mathcal{K}_V^{ij}(\omega_{\alpha\beta}) + \text{h.c.} \right\}/2.$$

Here we omitted the antihermitian part of the correlator K_V which accounts for the renormalization of the impurity Hamiltonian. Complemented by the equation for the backscattering current

$$I_{\text{bs}} = \frac{1}{2}\varepsilon_{zpl}\mathcal{J}_{mp}\mathcal{J}_{nq} \sum_{\alpha\beta\gamma\delta} \left(-i\langle\mathcal{S}_m^{\alpha\beta}\mathcal{S}_n^{\gamma\delta}\rangle\mathcal{K}_V^{ql}(\omega_{\gamma\delta}) + \text{c.c} \right). \tag{4.23}$$

Eq. (4.22) allows us to determine the correction to the ballistic conductance mediated by the magnetic impurity. The prescription is similar to those considered in Chapter 3. First, we solve Eq. (4.22) for the steady state density matrix $\rho_S^{(\text{st})}$ and then perform the averaging in Eq. (4.23) over $\rho_S^{(\text{st})}$. While the procedure is conceptually simple, it is a very complicated task to find $\rho_S^{(\text{st})}$ and I_{bs} in the general case, i.e. for arbitrary relations between temperature T, voltage V, and the anisotropy coefficients $\mathcal{D}_z$ and $\mathcal{D}_x$. Yet, a lot of progress can be made in various limiting cases. To identify different regimes of interest, let us compare the terms in Eq. (4.22). For the estimates, we denote the typical value of the anisotropy as $\mathcal{D}$. Given the fact that $\mathcal{D}_z \geq \mathcal{D}_x$, by definition we take

$\mathcal{D} \equiv \mathcal{D}_z$.

First of all, we note that the frequency dependence of the spin-spin correlator is substantiation for determination of the backscattering current only in the low-energy regime $\max\{T, V\} \lesssim \mathcal{D}$. If, on the contrary, $\max\{T, V\} \gg \mathcal{D}$, then one can safely substitute $\mathcal{K}_V(\omega_{\alpha\beta})$ by $\mathcal{K}_V^0$ in Eqs. (4.22) and (4.23). As a result, Eq. (4.22) simplifies to

$$\frac{d\rho_S}{dt} = -i\left[\mathcal{D}_z S_z^2 + \mathcal{D}_x S_x^2 + \mathcal{J}_{kz} S_k \frac{V}{2}, \rho_S\right] + \eta_{mn}\left(S_m \rho_S S_n - \frac{1}{2}\{\rho_S, S_n S_m\}\right) \quad (4.24)$$

with $\eta = \mathcal{J}\mathcal{K}_V^0 \mathcal{J}^T$, whereas the expression for I_{bs} (4.23) reduces to the one considered in the previous Chapter (see Eq. (3.30)). Intriguingly, in contrast to the naïve expectations, the anisotropy cannot be fully disregarded even in the case $\max\{T, V\} \gg \mathcal{D}$. Indeed, while the relaxation term in the master equation is independent of $\mathcal{D}$ in this limit, the anisotropy may still have a profound influence on the impurity dynamics through the Liouvillian term $-i\left[\mathcal{D}_z S_z^2 + \mathcal{D}_x S_x^2, \rho_S\right]$. There are two cases in which this term may be completely neglected: i) when the mean-field interaction $H_{\mathrm{mf}}^{\mathrm{e-i}} = \mathcal{J}_{kz} S_k V/2$ plays dominant role in determining the level structure of the magnetic impurity as compared to anisotropy, i.e. $V \gg \mathcal{D}/\mathcal{J}$, ii) when the relaxation term $\sim \mathcal{J}^2 \max\{T, V\}$ in Eq. (4.24) greatly surpasses the typical value of anisotropy $\mathcal{D}$. Combining these two conditions we establish that the anisotropy may be disregarded if the inequality

$$\max\left\{\mathcal{J}^2 T, \mathcal{J} V\right\} \gg \mathcal{D}. \quad (4.25)$$

is fulfilled. The condition (4.25) determines the range of applicability of the results presented in Chapter 3. Notice, that for the anisotropy produced by the interaction between the impurity and the bulk electrons (see Eqs. (4.8) and (4.12)) the temperature scale $T \sim \mathcal{D}/\mathcal{J}^2$ is of the order of $|M|(\xi/l_{\mathrm{imp}})^3$ which largely exceeds the band gap $|M|$. Therefore, the results for the correction to the linear conductance presented in Eqs. (3.32) and (3.35) are to be treated with care for the impurities with $S > 1/2$: they are relevant for temperatures at which the conductivity of the sample is primarily determined by its bulk. and not by the edge.

The three regions in the (V, T) plane with the different behavior of the backscattering current are presented in Fig. 4.1. The region I corresponds to the regime of low energies $\max\{T, V\} \ll \mathcal{D}$. The region II, i.e. $\max\{\mathcal{J}^2 T, \mathcal{J} V\} \ll \mathcal{D} \ll \max\{T, V\}$, describes the limit in which the relaxation is independent of the anisotropy whereas the Liouvillian dynamics is strongly influenced by the presence of non-zero $\mathcal{D}$. Finally, the region III is defined by $\max\{\mathcal{J}^2 T, \mathcal{J} V\} \gg \mathcal{D}$. Here the effects of the anisotropy are fully negligible and all of the results of Chapter 3 are reproduced.
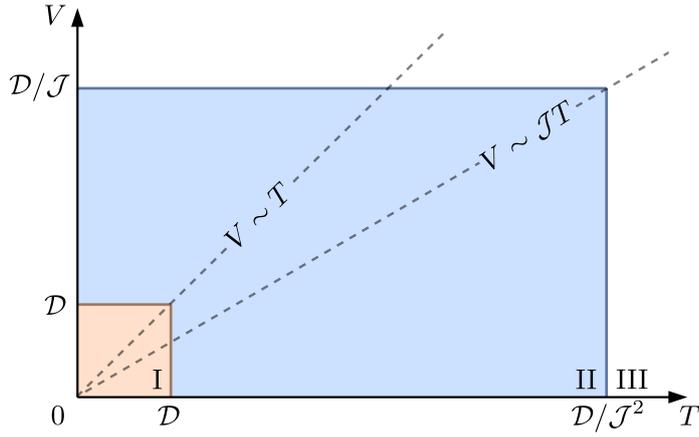
Figure 4.1: Three regions in the (V, T) plane. Region I: low energies, both the relaxation and the Liovillian dynamics are strongly affected by the anisotropy; region II: the relaxation rates are independent of the anisotropy; region III: the anisotropy is negligible. Dashed lines correspond to $V \sim T$ and $V \sim \mathcal{J}T$.

In the next sections, we consider the transport along the helical edge in regions I and II in details. For illustrative purposes, we focus on the cases of uniaxial anisotropy ($\mathcal{D}_x = 0$) and almost uniaxial anisotropy ($|\mathcal{D}_x| \ll |\mathcal{D}_z|$) only. We note that the pair of equations (4.22) and (4.23) in principle allows one to evaluate the backscattering current for the arbitrary ratio of anisotropy components $\mathcal{D}_x$ and $\mathcal{D}_z$ numerically.

4.3 Uniaxial anisotropy

In this section we develop a theory of the helical edge transport in the presence of the magnetic impurity with uniaxial anisotropy $H_{\mathrm{imp}} = \mathcal{D}_z S_z^2$. First, in subsection 4.3.1 we discuss the level structure of the total impurity Hamiltonian $H_{\mathrm{imp}}^{\mathrm{tot}}$. Then, in subsection 4.3.2 we focus on the regime of low energies $\max\{T, V\} \ll |\mathcal{D}_z|$ (region I in Fig. 4.1). The results differ for the impurities with integer and half-integer spin and, hence, are divided between two subsections. After that, in subsection 4.3.3 we discuss the regime of intermediate temperatures and voltages, $\max\{\mathcal{J}^2 T, \mathcal{J}V\} \ll |\mathcal{D}_z| \ll \max\{T, V\}$ (region II in Fig. 4.1), separately considering the cases of the impurity with integer and half-integer spin. We note that the consideration of the high-energy limit $\max\{\mathcal{J}^2 T, \mathcal{J}V\} \gg |\mathcal{D}_z|$ (region III in Fig. 4.1) is omitted in this section: the results in this regime coincide with the ones presented in Chapter 3.

4.3.1 Level structure

To begin with, we consider the level structure of the total Hamiltonian of the impurity

$$H_{\mathrm{imp}}^{\mathrm{tot}} = H_{\mathrm{imp}} + H_{\mathrm{mf}}^{\mathrm{e-i}}, \quad H_{\mathrm{imp}} = \mathcal{D}_z S_z^2, \quad H_{\mathrm{mf}}^{\mathrm{e-i}} = \mathcal{J}_{kz} S_k \frac{V}{2}. \tag{4.26}$$

At zero voltage, the mean-field electron-impurity interaction vanishes and $\left(H_{\text{imp}}^{\text{tot}}\right)\big|_{V=0} \equiv H_{\text{imp}}$. Hence, in this regime the energy levels are characterized by the well-defined z-projection of the impurity spin, i.e. $\left(H_{\text{imp}}^{\text{tot}}\right)\big|_{V=0} |\alpha\rangle = \mathcal{D}_z \alpha^2 |\alpha\rangle$, where $|\alpha\rangle \equiv |S_z = \alpha\rangle$. The states $|\pm\alpha\rangle$ with $\alpha > 0$ form doublets. Notice, that the state $|0\rangle$ of the impurity with integer spin does not have a degenerate partner. On the contrary, all of the states of the half-integer spin impurity are double-degenerate: this is a manifestation of Kramers theorem for a simple Hamiltonian $\left(H_{\text{imp}}^{\text{tot}}\right)\big|_{V=0}$.

A finite voltage applied along the edge induces the non-zero mean-field interaction $H_{\text{mf}}^{\text{e-i}}$. It splits all of the doublets $\{|+\alpha\rangle, |-\alpha\rangle\}$ with $\alpha > 0$. A secular Hamilotnian H_{sec}^α which governs the splitting of the pair $\{|+\alpha\rangle, |-\alpha\rangle\}$ is always diagonal for the impurity with integer S:

$$H_{\text{sec}}^\alpha = \begin{pmatrix} \mathcal{D}_z \alpha^2 + \mathcal{J}_{zz} \alpha V/2 & 0 \\ 0 & \mathcal{D}_z \alpha^2 - \mathcal{J}_{zz} \alpha V/2 \end{pmatrix}. \tag{4.27}$$

Here H_{sec}^α is presented in the basis $|+\alpha\rangle$, $|-\alpha\rangle$ for $\alpha = 1, 2, ..., S$. It implies that the doublet $\{|+\alpha\rangle, |-\alpha\rangle\}$ with the energy $\mathcal{D}_z \alpha^2$ splits into the states $|\psi_S^{\pm\alpha}\rangle = |\pm\alpha\rangle$ with the respective energies $E_S^{\pm\alpha} = \mathcal{D}_z \alpha^2 \pm \mathcal{J}_{zz} \alpha V/2$. This feature also holds true for the doublets $\{|+\alpha\rangle, |-\alpha\rangle\}$ with $\alpha \geq 3/2$ for the half-integer spin impurity. However, in the latter case the pair $\{|+1/2\rangle, |-1/2\rangle\}$ gets split by $H_{\text{mf}}^{\text{e-i}}$ non-trivially. Indeed, the corresponding secular Hamiltonian $H_{\text{sec}}^{1/2}$ is not diagonal in the basis $|+1/2\rangle$, $|-1/2\rangle$:

$$H_{\text{sec}}^{1/2} = \frac{1}{4} \begin{pmatrix} \mathcal{D}_z + \mathcal{J}_{zz}V & (S+1/2)(\mathcal{J}_{xz} - i\mathcal{J}_{yz}) \\ (S+1/2)(\mathcal{J}_{xz} + i\mathcal{J}_{yz}) & \mathcal{D}_z - \mathcal{J}_{zz}V \end{pmatrix}. \tag{4.28}$$

Therefore, the pair $\{|+1/2\rangle, |-1/2\rangle\}$ with the energy $\mathcal{D}_z/4$ breaks into

$$\left|\psi_S^{+1/2}\right\rangle = \cos\left(\frac{\theta_{1/2}}{2}\right)|+1/2\rangle + \sin\left(\frac{\theta_{1/2}}{2}\right) e^{i\phi_{1/2}}|-1/2\rangle, \tag{4.29}$$

$$\left|\psi_S^{-1/2}\right\rangle = \cos\left(\frac{\theta_{1/2}}{2}\right)|-1/2\rangle - \sin\left(\frac{\theta_{1/2}}{2}\right) e^{-i\phi_{1/2}}|+1/2\rangle \tag{4.30}$$

with $E_S^{\pm 1/2} = \left(\mathcal{D}_z \pm \sqrt{\mathcal{J}_{zz}^2 + (S+1/2)^2(\mathcal{J}_{xz}^2 + \mathcal{J}_{yz}^2)}\right)/4$ and

$$\tan\theta_{1/2} = (S+1/2)\frac{\sqrt{\mathcal{J}_{xz}^2 + \mathcal{J}_{yz}^2}}{\mathcal{J}_{zz}}, \quad \tan\phi_{1/2} = \frac{\mathcal{J}_{yz}}{\mathcal{J}_{xz}}. \tag{4.31}$$

As we will see later, the peculiar structure of the eigenstates $\left|\psi_S^{\pm 1/2}\right\rangle$ is of the large importance in the parameter region II, i.e. for $\max\{\mathcal{J}^2 T, \mathcal{J}V\} \ll |\mathcal{D}_z| \ll \max\{T, V\}$.

4.3.2 Transport at low energies

In this subsection we determine the backscattering current in the parameter region I, i.e. when $\max\{T, V\} \ll |\mathcal{D}_z|$. We mention that the results in this limit strongly depend on the parity of $2S$ and on the sign of the anisotropy. Therefore, below we consider all possible cases: transport in the presence of the impurity i) with the integer spin and easy-axis anisotropy ($\mathcal{D}_z < 0$), ii) with the integer spin and easy-plane anisotropy ($\mathcal{D}_z > 0$), iii) with the half-integer spin and easy-axis anisotropy, and, finally, iv) with the half-integer spin and easy-plane anisotropy.

Integer impurity spin

First of all, we discuss the case of **the easy-axis anisotropy** for the integer spin impurity. The inequalities $\mathcal{D}_z < 0$ and $\max\{T, V\} \ll |\mathcal{D}_z|$ guarantee that the impurity is restrained to occupy the doublet $\{|+S\rangle, |-S\rangle\}$ only. Thus, to describe the correction to the backscattering conductance it is possible to project the total Hamiltonian of the helical edge (4.16) onto the subspace formed by $|+S\rangle$ and $|-S\rangle$. Under the projection, the Hamiltonian (4.16) turns into

$$H_{\text{tot}}^{\text{eff}} = \mathcal{D}_z S^2 + \frac{1}{\nu}\hat{\mathcal{J}}_{ij}\hat{S}_i s_j + iv \int dy\, \Psi^\dagger(y)\sigma_z\partial_y\Psi(y), \quad \hat{S}_i = \hat{\sigma}_i/2, \tag{4.32}$$

where $\hat{\sigma}_{x,y,z}$ are the Pauli matrices in the basis $|+S\rangle, |-S\rangle$ and

$$\hat{\mathcal{J}} = \begin{pmatrix} 0 & 0 & 0 \\ 0 & 0 & 0 \\ 2S\mathcal{J}_{zx} & 2S\mathcal{J}_{zy} & 2S\mathcal{J}_{zz} \end{pmatrix}. \tag{4.33}$$

The transformation is justified with high accuracy controlled by a large parameter $|\mathcal{D}_z|/T$. From Eq. (4.32) we conclude that the problem of determining the backscattering current I_{bs} in the presence of the anisotropic spin S impurity was effectively mapped to those of a spin-1/2 impurity with a simple exchange matrix (4.33). Thus, the results of Chapter 3 may be employed to find I_{bs}. We note that $\hat{\mathcal{X}}_k = 2\varepsilon_{kmn}\hat{\mathcal{J}}_{mx}\hat{\mathcal{J}}_{ny} = 0$. Thus, from Eq. (3.30) we find

$$I_{\text{bs}} = -\frac{\pi^2}{4}\left(\hat{\mathcal{J}}_{zx}^2 + \hat{\mathcal{J}}_{zy}^2\right)G_0 V = -\pi^2 S^2\left(\mathcal{J}_{zx}^2 + \mathcal{J}_{zy}^2\right)G_0 V. \tag{4.34}$$

Remarkably, this result it is fully independent of temperature except for the weak logarithmic dependence due to the coupling constants renormalization. We note that I_{bs} vanishes for $\mathcal{J}_{zx} = \mathcal{J}_{zy} = 0$ in the considered limit. Since we assume that $\mathcal{J}$ has a general form we do not discuss the case

$\mathcal{J}_{zx} = \mathcal{J}_{zy} = 0$ below.

Next, we consider the low-energy transport in the case of **the easy-plane anisotropy** $\mathcal{D}_z > 0$. In this regime the impurity is frozen in its ground state $|0\rangle$ whereas the transitions to the excited states are exponentially suppressed with a large parameter $\mathcal{D}_z/T$. Consequently, the backscattering current evaluated to the second order in $\mathcal{J}$ with the help of Eqs. (4.22) and (4.23) is small as $\exp\{-\mathcal{D}_z/T\}$ as well. At the same time, *virtual transitions* of the magnetic impurity to the closest excited states $|\pm 1\rangle$ yield the contribution to the current of the fourth order in $\mathcal{J}$ which is not exponentially small. In order to estimate it, we project the exchange interaction $H^{\text{e-i}}_{\text{edge}} = \mathcal{J}_{ij}S_i s_j/\nu$ onto the ground state $|0\rangle$. To the second order in $\mathcal{J}$, we obtain the following effective low-energy Hamiltonian

$$H^{\text{e-i}}_{\text{eff}} = -\frac{1}{\mathcal{D}_z}\mathcal{J}_{ij}\mathcal{J}_{kl}s_j s_l \sum_{\alpha=\pm 1}\langle 0|S_i|\alpha\rangle\langle\alpha|S_k|0\rangle = -\frac{S(S+1)}{2\mathcal{D}_z}s_j s_l \sum_{k=x,y}\mathcal{J}_{kj}\mathcal{J}_{kl}. \qquad (4.35)$$

The resultant expression indicates that the magnetic impurity effectively mediates electron-electron interaction between the edge states in its vicinity. Its sophisticated spin structure allows for the non-zero backscattering current I_{bs} in the steady state regime. To evaluate I_{bs} one has to take the finite range of the electron-impurity interaction l_{imp} into account: for $l_{\text{imp}} = 0$ the effective Hamiltonian (4.35) yields no backscattering as dictated by the Pauli exclusion principle. Thus, we replace the spin density operators in Eq. (4.35) by

$$s_j = \frac{1}{2}\int dy c(y)\Psi^\dagger(y)\sigma_j\Psi(y), \qquad (4.36)$$

where $c(y)$ is a smooth symmetric function centred around the position $y_0 = 0$ of the impurity which satisfies $\int dy c(y) = 1$, $\int dy y^2 c(y) = l^2_{\text{imp}}$.

The presence of the effective electron-electron interaction (4.35) induces two-particle scattering processes which occur near the magnetic impurity. Three types of them contribute to the backscattering current. These are

$$\begin{aligned}
\text{(ia)} \quad & |\sigma_{z,1} = +1,\ \sigma_{z,2} = +1\rangle \rightleftarrows |\sigma_{z,1} = +1,\ \sigma_{z,2} = -1\rangle, \\
\text{(ib)} \quad & |\sigma_{z,1} = -1,\ \sigma_{z,2} = -1\rangle \rightleftarrows |\sigma_{z,1} = +1,\ \sigma_{z,2} = -1\rangle, \\
\text{(ii)} \quad & |\sigma_{z,1} = +1,\ \sigma_{z,2} = +1\rangle \rightleftarrows |\sigma_{z,1} = -1,\ \sigma_{z,2} = -1\rangle.
\end{aligned} \qquad (4.37)$$

Here $\sigma_{z,1}/2$ and $\sigma_{z,2}/2$ stand for the spin-z projections of the two interacting electrons. The latter are labelled by the indexes $1, 2$. The sketches of the interaction processes (ia), (ib), and (ii) are
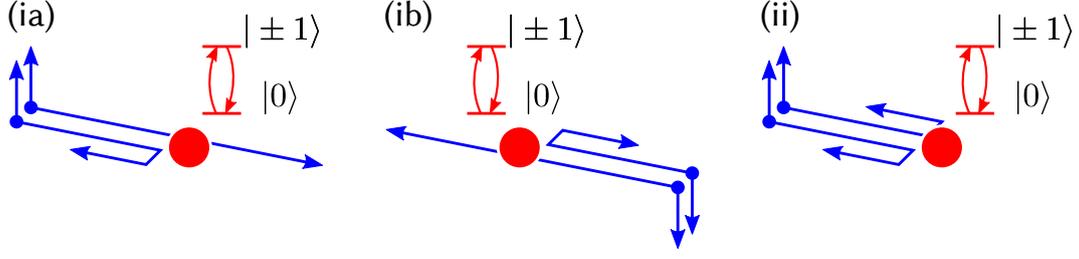
Figure 4.2: Three types of processes in which the impurity makes a virtual transition from its ground state $|0\rangle$ into the lowest excited states $|\pm 1\rangle$. (ia) and (ib) depict processes with one backscattered electron. (ii) depicts the process with two backscattered electrons.

presented in Fig. 4.2. The processes (ia) and (ib) describe the scattering events in which only one electron flips its spin and, due to the spin-momentum locking, changes its direction of motion. In the processes of type (ii) two electrons flip their spins and get backscattered synchronously.

We divide the backscattering current I_{bs} in a sum of two contributions: $I_{\text{bs}} = I_{\text{bs}}^{(\text{i})} + I_{\text{bs}}^{(\text{ii})}$, where $I_{\text{bs}}^{(\text{i})}$ is related to the scattering events of types (ia) and (ib) and $I_{\text{bs}}^{(\text{ii})}$ is due to the events of type (ii). Using the Fermi Golden rule, we estimate $I_{\text{bs}}^{(\text{i})}$ and $I_{\text{bs}}^{(\text{ii})}$ as

$$\frac{I_{\text{bs}}^{(\text{i})}}{G_0 V} \sim -\frac{S^2(S+1)^2}{\mathcal{D}_z^2 v^4} \sum_{j=x,y} \left(\sum_{l=x,y} \mathcal{J}_{lj} \mathcal{J}_{lz} \right)^2 \max\{|\mu|, T, V\}^2 \max\{T, V\}^4 \, l_{\text{imp}}^4, \qquad (4.38)$$

$$\frac{I_{\text{bs}}^{(\text{ii})}}{G_0 V} \sim -\frac{S^2(S+1)^2}{\mathcal{D}_z^2 v^4} \sum_{l,j,m,p,r,n=x,y} \mathcal{J}_{lj} \mathcal{J}_{lm} \mathcal{J}_{pr} \mathcal{J}_{pn} \mathcal{O}_{jr}^{mn} \max\{|V|, T\}^6 \, l_{\text{imp}}^4, \qquad (4.39)$$

where $\mathcal{O}_{jr}^{mn} = \delta_{jr}\delta_{mn} - \varepsilon_{jrz}\varepsilon_{mnz}$ and μ is the helical edge chemical potential. Interestingly, in the limit $\max\{T, V\} \ll |\mu|$ the single spin-flip processes are much more efficient compared to those with two simultaneous spin-flips, i.e. $\left| I_{\text{bs}}^{(\text{i})} \right| \gg \left| I_{\text{bs}}^{(\text{ii})} \right|$. Notice, the both $I_{\text{bs}}^{(\text{i})}$ and $I_{\text{bs}}^{(\text{ii})}$ are the power-law functions of voltage and temperature: there is no exponential suppression of the backscattering current, although I_{bs} is of the fourth order in $\mathcal{J}$. Finally, we mention that for $\mathcal{J} = \mathcal{J}^{(\text{iso})} = \text{diag}\{\mathcal{J}_\perp, \mathcal{J}_\perp, \mathcal{J}_z\}$ the backscattering current I_{bs} nullifies. This is a consequence of the fact that, even in the presence of $H_{\text{imp}} = \mathcal{D}_z S_z^2$, the Hamiltonian (4.16) with the exchange matrix $\mathcal{J}^{(\text{iso})}$ conserves $S_z + \Sigma_z$. Now, we switch to the case of the impurity with a half-integer spin.

Half-integer impurity spin

The result (4.34) for the backscattering current in the presence of **the easy-axis local anisotropy** ($\mathcal{D}_z < 0$) is trivially extended from the case of the integer spin impurity to the case of the half-integer spin impurity. However, there is no connection like that if the anisotropy is of **the easy-plane** type ($\mathcal{D}_z > 0$).

In the low-energy regime the half-integer spin impurity with $\mathcal{D}_z > 0$ is pinned to the two-

fold degenerate subspace $\{|+1/2\rangle, |-1/2\rangle\}$. To describe the backscattering current I_{bs} in this scenario we project the total Hamiltonian (4.16) onto the states $|+1/2\rangle$ and $|-1/2\rangle$ and obtain

$$H_{\text{tot}}^{\text{eff}} = \frac{\mathcal{D}_z}{4} + \frac{1}{\nu}\bar{\mathcal{J}}_{ij}\bar{S}_i s_j + iv \int dy \Psi^\dagger(y)\sigma_z \partial_y \Psi(y), \quad \bar{S}_i = \bar{\sigma}_i/2, \tag{4.40}$$

where

$$\bar{\mathcal{J}} = \begin{pmatrix} (S+1/2)\mathcal{J}_{xx} & (S+1/2)\mathcal{J}_{xy} & (S+1/2)\mathcal{J}_{xz} \\ (S+1/2)\mathcal{J}_{yx} & (S+1/2)\mathcal{J}_{yy} & (S+1/2)\mathcal{J}_{yz} \\ \mathcal{J}_{zx} & \mathcal{J}_{zy} & \mathcal{J}_{zz} \end{pmatrix}. \tag{4.41}$$

We immediately conclude that the problem of determining the backscattering current in the presence of the anisotropic impurity with the spin S was mapped to those with a spin-1/2 impurity and the exchange matrix $\bar{\mathcal{J}}$. As it was shown in Chapter 3 in the latter case it is possible to deduce *an exact* relation for I_{bs} (see Eq. (3.52)) which would be valid at arbitrary voltage and temperature. With its help we find

$$I_{\text{bs}} = \frac{\pi^2}{4}\left(\bar{\mathcal{X}}^T\bar{\Gamma}^{-1}\bar{\mathcal{X}}\frac{V}{2T}\coth\frac{V}{2T} - \bar{g}\right), \quad \bar{\mathcal{X}}_k = 2\varepsilon_{kmn}\bar{\mathcal{J}}_{mx}\bar{\mathcal{J}}_{ny}, \tag{4.42}$$

$$\bar{\Gamma}_{lk} = \frac{1}{\pi T}\left(\delta_{lk}\text{tr}\bar{\eta} - \frac{\bar{\eta}_{lk} + \bar{\eta}_{kl}}{2} + V\varepsilon_{lkj}\bar{\mathcal{J}}_{jz}\right), \quad \bar{\eta} = \bar{\mathcal{J}}\mathcal{K}_V^0\bar{\mathcal{J}}^T, \tag{4.43}$$

$\bar{g} = \left(\bar{\mathcal{J}}^T\bar{\mathcal{J}}\right)_{xx} + \left(\bar{\mathcal{J}}^T\bar{\mathcal{J}}\right)_{yy}$. We remind the reader that, as a function of voltage, the expression for I_{bs} saturates at $V \sim \bar{\mathcal{J}}T$ and not at $V \sim T$. Eqs. (4.42) and (4.43) finish the discussion of the low-energy transport.

4.3.3 Transport at intermediate temperatures and voltages

This subsection is dedicated to the discussion of the backscattering current in the regime of intermediate temperatures and voltages, i.e. $\max\{\mathcal{J}^2 T, \mathcal{J}V\} \ll |\mathcal{D}_z| \ll \max\{T, V\}$ (region II in Fig. 4.1). Below, we separately consider the cases of the magnetic impurity with integer and half-integer spin.

Integer impurity spin

As was discussed in section 4.3.1 at $V = 0$ the eigenstates of the impurity Hamiltonian $H_{\text{imp}}^{\text{tot}}$ can be characterized by the spin z-projection $S_z = \alpha$. The states with $\alpha \geq 1$ form doublets $\{|+\alpha\rangle, |-\alpha\rangle\}$. At finite voltage the mean-field interaction $H_{\text{mf}}^{\text{e}-\text{i}}$ splits them into the states $|+\alpha\rangle$ and $|-\alpha\rangle$ separated by the gap $\sim \mathcal{J}V$. Depending on the ratio between this splitting and the

level broadening due to the relaxation, which is controlled by the inverse Korringa time $\tau_K^{-1} \sim \mathcal{J}^2 \max\{T, V\}$, the behavior of the backscattering current may be different. Thus, in the following we first discuss the limit of well-separated energy levels and then switch to case of strongly smeared energy levels.

Integer impurity spin: well-split doublets

To begin with, we assume that $V \gg \mathcal{J}T$ (for the illustration, see Fig. 4.1). This condition guarantees that all of the doublets are well-split as compared to their smearing. Thus, the rotating wave approximation may be employed in this case to simplify the master equation (4.24) for the reduced density matrix of the magnetic impurity. The procedure is described in details in section 3.4. Here we only provide its sketch. First, we switch to the interaction representation in Eq. (4.24). Then we average the resultant equation over the time-scale Δt satisfying $(\mathcal{J}V)^{-1} \ll \Delta t \ll \tau_K$. In this way, we obtain the equation for the evolution of the diagonal elements of the density matrix ρ_S which is fully decoupled from the equation for the dynamics of the off-diagonal components:

$$\frac{dp_\alpha}{dt} = \sum_\beta \mathcal{W}_{\alpha\beta} p_\beta, \quad \mathcal{W}_{\alpha\beta} = w_{\alpha \leftarrow \beta} - \delta_{\alpha\beta} \sum_{\beta'} w_{\beta' \leftarrow \alpha}, \quad w_{\alpha \leftarrow \beta} = \eta_{mn} S_m^{\alpha\beta} S_n^{\beta\alpha}. \tag{4.44}$$

Here $p_\alpha(t) = \langle \psi_S^\alpha | \rho_S^I(t) | \psi_S^\alpha \rangle$, $S_{x,y,z}^{\alpha\beta} = \langle \psi_S^\alpha | S_{x,y,z} | \psi_S^\beta \rangle$, and $\eta = \mathcal{J}\mathcal{K}_V^0 \mathcal{J}^T$. We explicitly utilized the fact that for $\max\{T, V\} \gg |\mathcal{D}_z|$ the spin-spin correlation function $\mathcal{K}_V(\omega_{\alpha\beta})$ may be evaluated at zero frequency. As was discussed in section 4.3.1, *for the integer spin impurity* the eigenstates $|\psi_S^\alpha\rangle$ are trivial: they are characterized by the spin z-projection, $|\psi_S^\alpha\rangle = |\alpha\rangle$.

Next, we search for the stationary solution of Eq. (4.44) $p_\alpha^{(st)}$. With its help one may readily recover the steady state density matrix as $\rho_S^{(st)} = \sum_\alpha p_\alpha^{(st)} |\alpha\rangle\langle\alpha|$. By evaluating the transition rates $\omega_{\alpha \leftarrow \beta}$ we establish that in the basis $|S\rangle$, $|S-1\rangle$,..., $|-S\rangle$ the tridiagonal matrix $\mathcal{W}_{\alpha\beta}$ has the following matrix elements

$$\mathcal{W}_{\alpha,\alpha\mp1} = \eta_\pm \left(S(S+1) - \alpha(\alpha \mp 1)\right)/4, \tag{4.45}$$

$$\mathcal{W}_{\alpha,\alpha} = -W_{\alpha-1,\alpha} - W_{\alpha+1,\alpha}, \tag{4.46}$$

where $\eta_\pm = (\eta_{xx} \pm i\eta_{xy}) \mp i(\eta_{yx} \pm i\eta_{yy})$. From these equations we find

$$p_\alpha^{(st)} = \frac{1}{\mathcal{Z}} \left(\frac{\eta_+}{\eta_-}\right)^\alpha, \quad \alpha = S, S-1, ..., -S. \tag{4.47}$$

The multiplier $\mathcal{Z}$ guarantees $\sum_\alpha p_\alpha^{(st)} = 1$. The density matrix $\rho_S^{(st)}$ which corresponds to the

populations (4.47) may be written in a basis independent form as

$$\rho_S^{(\text{st})} = \frac{1}{\mathcal{Z}} \exp\left(\beta S_z\right), \quad \beta = 2\text{arth}\left(\frac{V}{2T}\frac{\mathcal{X}_{zz}}{\Gamma_{zz}}\right). \tag{4.48}$$

We recall that $\mathcal{X}_k = 2\varepsilon_{kmn}\mathcal{J}_{mx}\mathcal{J}_{ny}$ and the matrix Γ is defined in Eq. (3.27). The explicit form of Γ_{zz} is

$$\Gamma_{zz} = \sum_{k=x,y} \mathcal{J}_{kz}^2 + \frac{V}{2T}\coth\frac{V}{2T}\sum_{m,n=x,y} \mathcal{J}_{mn}^2. \tag{4.49}$$

We mention that, in contrast to the case of negligible anisotropy (see Eq. (3.44)), the density matrix (4.48) *does not* have a Gibbs form $\sim \exp\left\{-H_{\text{imp}}^{\text{tot}}/T_{\text{eff}}\right\}$ and, consequently, cannot be characterized by any effective temperature. Yet, in the chosen basis the ratio between the consecutive populations $p_{\alpha+1}^{(\text{st})}/p_\alpha^{(\text{st})} = e^\beta$, $\alpha = S - 1, S - 2, ..., -S$, is independent of α. Notice, that in the limit $V \gg T$ the factor $\exp\left(\beta\right)$ saturates at a finite value and the impurity does not get fully polarized.

Interestingly, for $V \gg \mathcal{J}T$ the impurity spin is directed along the z-axis in the regime of intermediate temperatures and voltages $\max\left\{\mathcal{J}^2T, \mathcal{J}V\right\} \ll |\mathcal{D}_z| \ll \max\left\{T, V\right\}$ (region II in Fig. 4.1). At the same time, for high energies $\max\left\{\mathcal{J}^2T, \mathcal{J}V\right\} \gg |\mathcal{D}_z|$ (region III in Fig. 4.1) the average spin $\langle \boldsymbol{S} \rangle$ is collinear with the mean-field interaction $H_{\text{mf}}^{\text{e}-\text{i}} = \mathcal{J}_{kz}S_kV/2$ as long as $V \gg \mathcal{J}T$ is fulfilled.

With the help of the expression (4.48) one can readily evaluate the averages $\langle S_k \rangle$ and $\langle \{S_m, S_n\} \rangle$ entering the formula for the backscattering current (3.30) and, thus, find the correction to the conductance analytically. The corresponding result is not illustrative and, hence, is not presented here.

Integer impurity spin: strongly smeared doublets

In this subsection we discuss the regime $V \ll \mathcal{J}T$. Together with $\max\left\{\mathcal{J}^2T, \mathcal{J}V\right\} \ll |\mathcal{D}_z| \ll \max\left\{T, V\right\}$ this condition implies $T \gg |\mathcal{D}_z|$. Hence, the stationary density matrix is close to equipartitioning $\rho_S^{(\text{st})} \simeq \rho_S^{(\text{eq})} = I_{(2S+1)\times(2S+1)}/(2S + 1)$. The deviations from $\rho_S^{(\text{eq})}$ are small as V/T. Thus, it is reasonable to decompose

$$\rho_S^{(\text{st})} = \rho_S^{(\text{eq})} + \frac{V}{T}\rho_S^{(1)} + ... \tag{4.50}$$

The matrix η may also be expanded as $\eta = \eta^{(0)} - i\eta^{(1)}V/T + ...$, where $\eta^{(0)}$ is a symmetric matrix and $\eta^{(1)}$ is an antisymmetric matrix. Next, we substitute the decompositions for $\rho_S^{(\text{st})}$ and η into Eq.

(4.24) (for $\mathcal{D}_x = 0$) and project the latter onto the states $|\alpha\rangle$ and $|\alpha'\rangle$. In this way, we establish

$$\left(\alpha^2 - \alpha'^2\right)\left(\rho_S^{(1)}\right)_{\alpha\alpha'} = \frac{\varepsilon_{mnk}S_k^{\alpha\alpha'}}{2S+1}\frac{\eta_{mn}^{(1)}}{\mathcal{D}_z} - \frac{i\eta_{mn}^{(0)}}{\mathcal{D}_z}\left(S_m\rho_S^{(1)}S_n - \frac{1}{2}\left\{S_nS_m, \rho_S^{(1)}\right\}\right)_{\alpha\alpha'}. \tag{4.51}$$

Here we neglected the mean-field interaction term: this is a justified approximation because the doublets are strongly smeared, i.e. $V \ll \mathcal{J}T$.

It is worth mentioning that the parameters $\eta_{jk}^{(0,1)}/\mathcal{D}_z$ which enter Eq. (4.51) are of the order of $\mathcal{J}^2T/\mathcal{D}_z$ and, thereby, are small. Hence, the components $(\rho_S^{(1)})_{\alpha\alpha'}$ with $|\alpha| \neq |\alpha'|$ are negligible in comparison to those with $|\alpha| = |\alpha'|$ as indicated by Eq. (4.51). Therefore, to the leading order in $\mathcal{J}^2T/\mathcal{D}_z$ it is possible to constrict Eq. (4.51) to the subspace $|\alpha| = |\alpha'|$ by representing $\rho_S^{(1)} = \sum_\alpha p_\alpha^{(1)}|\alpha\rangle\langle\alpha| + \sum_{\alpha\neq 0} q_\alpha^{(1)}|\alpha\rangle\langle-\alpha|$. Solving Eq. (4.51) for $p_\alpha^{(1)}$ and $q_\alpha^{(1)}$ we obtain

$$p_\alpha^{(1)} = \frac{\alpha}{2S+1}\frac{2\eta_{mn}^{(1)}\varepsilon_{mnz}}{\eta_{xx}^{(0)} + \eta_{yy}^{(0)}} = \frac{\alpha}{2S+1}\frac{\mathcal{X}_z}{(\Gamma_0)_{zz}}, \quad q_\alpha^{(1)} = 0. \tag{4.52}$$

We recall that $\Gamma_0 = \mathrm{tr}\left(\mathcal{J}\mathcal{J}^T\right) - \mathcal{J}\mathcal{J}^T$. Thus,

$$\rho_S^{(\mathrm{st})} \simeq \frac{I_{(2S+1)\times(2S+1)}}{2S+1} + \frac{V}{T}\frac{S_z}{2S+1}\frac{\mathcal{X}_z}{(\Gamma_0)_{zz}}. \tag{4.53}$$

With the help of (4.53) we evaluate the averages in the equation for the backscattering current (3.30) and, to the leading order in V/T, find

$$I_{\mathrm{bs}} = \pi^2\frac{S(S+1)}{3}\left(\frac{\mathcal{X}_z^2}{(\Gamma_0)_{zz}} - g\right)G_0V, \quad g = \left(\mathcal{J}^T\mathcal{J}\right)_{xx} + \left(\mathcal{J}^T\mathcal{J}\right)_{yy}. \tag{4.54}$$

Remarkably, the stationary density matrix (4.53) and, therefore, the backscattering current (4.54) which were derived in the regime $V \ll \mathcal{J}T$ match smoothly with $\rho_S^{(\mathrm{st})}$ and I_{bs} found in the limit $V \gg \mathcal{J}T$ (see Eq. (4.48)).

In conclusion, we mention that for $\max\{\mathcal{J}^2T, \mathcal{J}V\} \ll |\mathcal{D}_z| \ll \max\{T, V\}$ *none* of results presented above (see Eqs. (4.48), (4.53), and (4.54)) depend on *the sign* and *the magnitude* of the anisotropy $\mathcal{D}_z$. Nonetheless, the anisotropy is crucially important for the transport properties in the considered limit because it controls the structure of the energy levels of the magnetic impurity.

Half-integer impurity spin

Now, we describe the backscattering current mediated by a half-integer spin impurity in the regime $\max\{\mathcal{J}^2T, \mathcal{J}V\} \ll |\mathcal{D}_z| \ll \max\{T, V\}$. Qualitatively, this scenario is similar to those of an

integer spin impurity. Once again, the impurity energy levels at zero-voltage have a definite spin z-projection $S_z = \alpha$ and form doublets $\{|+\alpha\rangle, |-\alpha\rangle\}$ for any $\alpha \geq 1/2$. At $V \neq 0$ these doublets are split by $H_{\text{mf}}^{\text{e-i}}$. For $\alpha > 1/2$ the splitting is trivial and the pair $\{|+\alpha\rangle, |-\alpha\rangle\}$ breaks into $|+\alpha\rangle$ and $|-\alpha\rangle$ (for details, see section 4.3.1). However, this is not the case for $\alpha = 1/2$: the doublet $\{+1/2, -1/2\}$ splits into the two rotated combinations presented in Eqs. (4.29) and (4.30). The latter feature is specific for the half-integer spin impurity. Ultimately, it makes the steady state density matrix $\rho_S^{(\text{st})}$ somewhat more complicated than that for the impurity with integer spin. To illustrate this peculiarity, we determine $\rho_S^{(\text{st})}$ in the case of the well-separated energy levels $V \gg \mathcal{J}T$.

Once again, the condition $V \gg \mathcal{J}T$ allows us to employ the rotating wave approximation to describe the evolution of the impurity density matrix. With its help we establish that the stationary density matrix is diagonal in the basis of $H_{\text{imp}}^{\text{tot}}$ eigenstates: $\rho_S^{(\text{st})} = \sum_\alpha p_\alpha^{(\text{st})} |\psi_S^\alpha\rangle \langle \psi_S^\alpha|$. Here $|\psi_S^\alpha\rangle = |\alpha\rangle$ for $|\alpha| \geq 3/2$ whereas $\left|\psi_S^{\pm 1/2}\right\rangle$ are defined in Eqs. (4.29) and (4.30). By finding the steady state solution of the classical Markov equation (4.44) and establish

$$
p_\alpha^{(\text{st})} = \frac{1}{\mathcal{Z}}
\begin{cases}
(\eta_+/\eta_-)^\alpha, & \alpha \geq 3/2, \\[2mm]
a_1, & \alpha = +1/2, \\[2mm]
a_2, & \alpha = -1/2, \\[2mm]
b\,(\eta_+/\eta_-)^\alpha, & \alpha \leq -3/2,
\end{cases}
\tag{4.55}
$$

where $\eta_\pm$ are the same as for the integer spin impurity,

$$
a_1 = \frac{\cos^2\left(\frac{\theta_{1/2}}{2}\right) - b\sin^2\left(\frac{\theta_{1/2}}{2}\right)}{\cos\theta_{1/2}}, \quad a_2 = \frac{b\cos^2\left(\frac{\theta_{1/2}}{2}\right) - \sin^2\left(\frac{\theta_{1/2}}{2}\right)}{\cos\theta_{1/2}},
\tag{4.56}
$$

$$
b = \frac{\eta_{xx} + \eta_{yy} + \text{tr}(\chi\eta)}{\eta_{xx} + \eta_{yy} + \text{tr}(\chi^T\eta)}, \quad \chi = \frac{\Theta^T\cos^2\left(\frac{\theta_{1/2}}{2}\right) + \Theta\sin^2\left(\frac{\theta_{1/2}}{2}\right)}{2\sin^2\left(\frac{\theta_{1/2}}{2}\right)\cos^2\left(\frac{\theta_{1/2}}{2}\right)(S(S+1) - 3/4)},
\tag{4.57}
$$

and, finally, Θ is a 3×3 Hermitian matrix which has the following components

$$
\Theta_{11} = (S+1/2)^2(1 - \sin^2\theta_{1/2}\cos^2\phi_{1/2}), \quad \Theta_{22} = (S+1/2)^2(1 - \sin^2\theta_{1/2}\sin^2\phi_{1/2}),
$$

$$
\Theta_{33} = \sin^2\theta_{1/2}, \quad \Theta_{12} = (S+1/2)^2(\sin^2\theta_{1/2}\sin 2\phi_{1/2} + 2i\cos\theta_{1/2})/2,
$$

$$
\Theta_{13} = (S+1/2)\sin\theta_{1/2}(\cos\phi_{1/2}\cos\theta_{1/2} - i\sin\phi_{1/2}),
$$

$$
\Theta_{23} = -(S+1/2)\sin\theta_{1/2}(\sin\phi_{1/2}\cos\theta_{1/2} + i\cos\phi_{1/2}).
$$

While the components $p_\alpha^{(\mathrm{st})}$ with $|\alpha| \geq 3/2$ have a similar form as compared to the integer spin case (see Eq. (4.47)), the components with $\alpha = \pm 1/2$ have a sophisticated structure. This is a manifestation of the non-trivial splitting character of the doublet $\{+1/2, -1/2\}$. As always, the steady state density matrix $\rho_S^{(\mathrm{st})} = \sum_\alpha p_\alpha^{(\mathrm{st})} |\psi_S^\alpha\rangle \langle \psi_S^\alpha|$, in principle, allows us to evaluate the impurity averages in the equation for the backscattering current (3.30) and, hence, to determine the correction to the ballistic conductance. The explicit form of these averages lacks demonstrativeness and, therefore, is not presented here.

For the impurity with the half-integer spin the regime of strongly smeared energy levels $V \ll \mathcal{J}T$ may also be analysed with the help of Eq. (4.51). Once again, we readily conclude that the correction to the stationary density matrix of the first order in V/T has the diagonal and "anti-diagonal" components only: $\rho_S^{(1)} = \sum_\alpha p_\alpha^{(1)} |\alpha\rangle\langle\alpha| + \sum_{\alpha\neq 0} q_\alpha^{(1)} |\alpha\rangle\langle-\alpha|$. However, unlike in the case of the integer spin impurity, both $p_\alpha^{(1)}$ and $q_\alpha^{(1)}$ are present in a steady state solution. This feature hinders the derivation of a concise analytical expression for the backscattering current in the considered regime. Nonetheless, Eq. (4.51) may be easily solved numerically. We mention that, in contrast to Eq. (4.24) which yields $(2S+1)^2 \times (2S+1)^2$ linear system for $\rho_S^{(\mathrm{st})}$, the system of equations for $p_\alpha^{(1)}$ and $q_\alpha^{(1)}$ based on Eq. (4.51) has the dimensionality $(4S+1) \times (4S+1)$ and, hence, presents a much simpler problem for the impurities with $S \gg 1$.

To conclude this section, in Fig. 4.3 we provide the exemplary voltage dependences of the backscattering correction to the ballistic conductance $\Delta G(V) = I_{\mathrm{bs}}/V$ on V in the presence of the uniaxial easy-plane anisotropy of the magnetic impurity. The curves are plotted for the impurity with integer spin (Fig. 4.3(a)) and the half-integer spin (Fig. 4.3(b)) in the regimes $T \ll \mathcal{D}_z$ (solid lines) and $\mathcal{J}^2 T \ll \mathcal{D}_z \ll T$ (dashed lines). The data for the charts was obtained numerically with the help of Eqs. (4.22) and (4.23).

For $T \ll \mathcal{D}_z$ the backscattering current due to the impurity with integer spin is exponentially small[2] as long as $V \lesssim \mathcal{D}_z$ (see the solid curve in Fig. 4.3(a)). In this case the impurity is pinned to its ground state $|0\rangle$. At $V \simeq \mathcal{D}_z$ the absolute value of $\Delta G(V)$ starts to increase abruptly: now, the helical electrons have enough energy to cause the transitions of the impurity to the excited levels. There are several peaks in the dependence of $\Delta G(V)$ on V in the vicinity of $V \sim \mathcal{D}_z$. They are located at $V \simeq D_z|\alpha^2 - (\alpha-1)^2| = D_z|2\alpha - 1|$, $\alpha = S, S-1, ..., -S+1$. Since $T \ll \mathcal{D}_z \ll \mathcal{D}_z/\mathcal{J}$ the correction $\Delta G(V)$ reaches saturation at $V \sim \mathcal{D}_z/\mathcal{J}$.

At higher temperatures, i.e. $T \gg \mathcal{D}_z$, the backscattering mediated correction to the conductance

---

[2]The numeric plots are based on Eqs. (4.22) and (4.23) and, hence, do not take into account the contributions to the backscattering current mediated by the virtual transitions of the impurity to the excited levels.
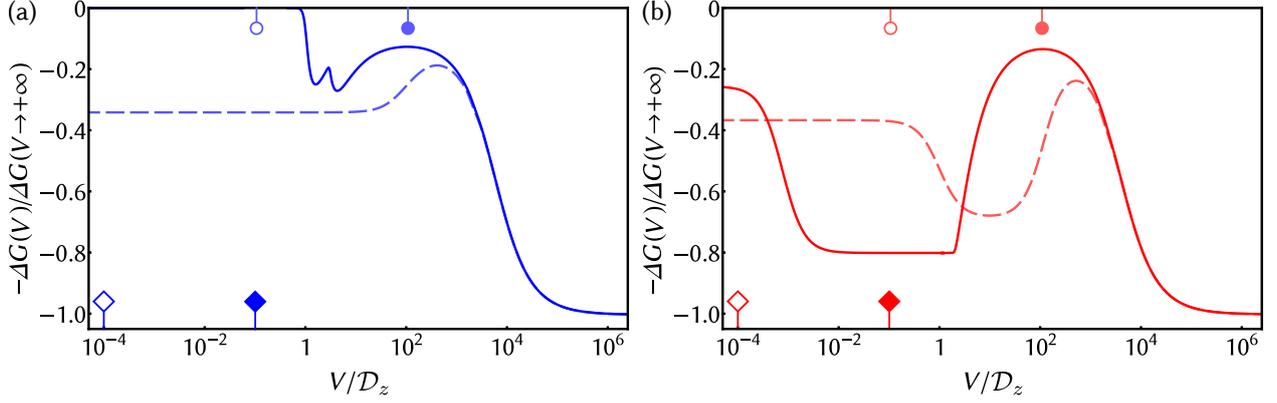
Figure 4.3: Correction $\Delta G(V)$ to the conductance as a function of voltage in the presence of the local easy-plane anisotropy $\mathcal{D}_z S_z^2$. $\Delta G(V)$ is measured in the units of $\Delta G(V \to +\infty)$. The non-zero dimensionless couplings are $\mathcal{J}_{xx} = \mathcal{J}_{yy} = 10^{-3}$, $\mathcal{J}_{xz} = 0.8\mathcal{J}_{xx}$, $\mathcal{J}_{zx} = 0.3\mathcal{J}_{xx}$, $\mathcal{J}_{zz} = 0.9\mathcal{J}_{xx}$. The solid curves are plotted for $T = 0.05\mathcal{D}_z$. The dashed curves correspond to $T = 50\mathcal{D}_z$. The results in (a) are presented for $S = 2$. In (b) $S = 3/2$. Solid (empty) diamonds depict $V \sim T$ ($V \sim \mathcal{J}T$) for $T = 0.05\mathcal{D}_z$. Solid (empty) circles depict $V \sim T$ ($V \sim \mathcal{J}T$) for $T = 50\mathcal{D}_z$.

is non-vanishing in the limit $V \to 0$ (see the dashed curve in Fig. 4.3(a)). In this regime, the peaks at $V \sim \mathcal{D}_z$ are smeared. Interestingly, for the impurity *with integer spin* there is no crossover behavior for $T \gg \mathcal{D}_z$ at the voltage $V \sim \mathcal{J}T$. This is in accordance with our predictions relying on Eqs. (4.48) and (4.53).

As it was expected, in the regime $T \ll \mathcal{D}_z$ the impurity with half-integer spin behaves as a spin-1/2 impurity for $V \lesssim \mathcal{D}_z$ (see the solid curve in Fig. 4.3(b)). In particular, similarly to $S = 1/2$, $\Delta G(V)$ saturates to a plateau at $V \sim \mathcal{J}T$. This plateau breaks when the voltage reaches $\mathcal{D}_z$ and the dependence of ΔG on V exhibits a cusp. It is connected with the fact that the edge electrons start to mediate the transitions of the impurity between its energy levels. Finally, $\Delta G(V)$ becomes constant at $V \sim \mathcal{D}_z/\mathcal{J}$.

For $T \gg \mathcal{D}_z$ the correction to the conductance due to the impurity with half-integer spin shows two crossovers before saturating at $V \sim \max\{T, \mathcal{D}_z/\mathcal{J}\}$: one is located at $V \sim \mathcal{J}T$ and the other one – at $V \sim T$ (see the dashed curve in Fig. 4.3(b)).

4.4 Non-uniaxial anisotropy

So far, we have only been discussing the transport along the edge of the topological insulator assuming that the local anisotropy of the magnetic impurity is uniaxial: $H_{\text{imp}} = \mathcal{D}_z S_z^2$. At the same time, a simple realistic model of the impurity in the CdTe/HgTe/CdTe quantum well indicates (see Eq. (4.15)) that the anisotropy might be more complicated than that. In this section we revise the problem of determining the backscattering current for the impurity Hamiltonian of the form

$H_{\text{imp}} = \mathcal{D}_x S_x^2 + \mathcal{D}_z S_z^2$. We recall that *any* quadratic anisotropy $H_{\text{imp}} = \mathcal{D}_{qp} S_q S_p$ may be reduced to the two-component structure above by a proper redefinition of the exchange matrix $\mathcal{J}$ (see section 4.2).

Throughout this section, we will suppose that the non-uniaxial admixture $\mathcal{D}_x S_x^2$ is small: $|\mathcal{D}_x| \ll |\mathcal{D}_z|$. Furthermore, we will focus on qualitatively new backscattering regimes only leaving minor effects, e.g. parametrically small corrections to the results presented in section 4.3, aside. We begin the discussion by examining the level structure of the impurity – as we have already seen the latter plays a decisive role in determining the character of the backscattering.

4.4.1   Level structure

The level structure of the total Hamiltonian $H_{\text{imp}}^{\text{tot}} = \mathcal{D}_x S_x^2 + \mathcal{D}_z S_z^2 + \mathcal{J}_{kz} S_k V / 2$ is strongly sensitive to the parity of $2S$. Thus, we first focus on the case of the impurity with half-integer spin.

Level structure of the half-integer spin impurity

At $V = 0$ the Hamiltonian $H_{\text{imp}}^{\text{tot}}$ is time-reversal symmetric. Therefore, for the impurity with the half-integer spin the Kramers theorem holds and every energy level is two-fold degenerate. As a result, for *any* $\mathcal{D}_x$ a series of doublets is formed. For instance, for $\mathcal{D}_x = 0$ these are the pairs $\{|+\alpha\rangle, |-\alpha\rangle\}$ with energies $\mathcal{D}_z \alpha^2$, where $\alpha = 1/2, 3/2, ..., S$ denotes the value of S_z. If a finite but small $\mathcal{D}_x$ is introduced, then each doublet exhibits an overall energy shift without getting split. In the process, the corresponding wave functions acquire the corrections of the order of $\mathcal{D}_x/\mathcal{D}_z$. The presence of these small contributions $\sim \mathcal{D}_x/\mathcal{D}_z$ is the only difference in the level structure between the case of the non-uniaxial anisotropy with $|\mathcal{D}_x| \ll |\mathcal{D}_z|$ and the case of uniaxial anisotropy. Accordingly, *for the impurity with the half-integer spin* all of the results for the backscattering current are qualitatively similar to those presented in section 4.3: at non-zero $\mathcal{D}_x$ the latter acquire the corrections of the order of $\sim \mathcal{D}_x/\mathcal{D}_z$ only. We do not discuss these fine effect below. Instead, we switch to the case of the integer spin impurity in which even a small $\mathcal{D}_x$ might have a profound influence on the backscattering current for certain voltages and temperatures.

Level structure of the integer spin impurity

At $V = 0$ and $\mathcal{D}_x = 0$ the energy levels of the integer spin impurity form doublets $\{|+\alpha\rangle, |-\alpha\rangle\}$ in which $\alpha = 1, 2, ..., S$ denotes the spin z-projection S_z. In contrast to the case of the half-integer S, the finite $\mathcal{D}_x$ lifts the degeneracy of these doublets. To the lowest non-vanishing order in $\mathcal{D}_x/\mathcal{D}_z$ the splitting of a pair $\{|+\alpha\rangle, |-\alpha\rangle\}$ with $\alpha > 0$ is governed by the following secular Hamiltonian

(in the basis $|+\alpha\rangle, |-\alpha\rangle$):

$$H_{\text{sec}}^{\alpha} = \begin{pmatrix} \mathcal{D}_z \alpha^2 + \Delta_\alpha & \delta_\alpha \\ \delta_\alpha & \mathcal{D}_z \alpha^2 + \Delta_\alpha \end{pmatrix}, \quad \Delta_\alpha = \mathcal{D}_x \left(S(S+1) - \alpha^2 \right)/2,$$

$$\delta_\alpha = \mathcal{D}_x \left(\frac{\mathcal{D}_x}{\mathcal{D}_z} \right)^{\alpha-1} \frac{\langle \alpha | S_x^2 | \alpha - 2 \rangle \langle \alpha - 2 | S_x^2 | \alpha - 4 \rangle ... \langle -\alpha + 2 | S_x^2 | -\alpha \rangle}{\left(\alpha^2 - (\alpha-2)^2 \right) \left(\alpha^2 - (\alpha-4)^2 \right) ... \left(\alpha^2 - (-\alpha+2)^2 \right)}. \tag{4.58}$$

Hence, the doublet $\{|+\alpha\rangle, |-\alpha\rangle\}$ with the energy $\mathcal{D}_z \alpha^2$ breaks into a symmetric superposition $[|+\alpha\rangle + |-\alpha\rangle]/\sqrt{2}$ and an antisymmetric superposition $[|+\alpha\rangle - |-\alpha\rangle]/\sqrt{2}$. The respective energies $\mathcal{D}_z \alpha^2 + \Delta_\alpha \pm \delta_\alpha$ are divided by a gap $2\delta_\alpha$. The numeric multiplier in the expression for δ_α is of the order of unity for the impurities with $S \sim 1$ and, therefore, $\delta_\alpha \sim \mathcal{D}_x \left(\mathcal{D}_x / \mathcal{D}_z \right)^{\alpha-1}$. We mention that the overall shift in the energy of doublet Δ_α does not affect the backscattering current significantly and will be disregarded below.

A non-zero voltage applied to the edge induces the effective Zeeman field $H_{\text{mf}}^{\text{e-i}} \sim \mathcal{J}V$ and, thus, provides another mechanism for the doublets splitting. To understand the implications of the finite V let us consider a fixed doublet $\{|+\alpha\rangle, |-\alpha\rangle\}$ with $\alpha > 0$. If the voltage is low enough, i.e. $|\delta_\alpha| \gg \mathcal{J}V$, then the pair $|\pm\alpha\rangle$ splits predominantly due to $\mathcal{D}_x S_x^2$. As a result, the eigenfunctions of $H_{\text{imp}}^{\text{tot}}$ are given by

$$|\psi_S^{\pm\alpha}\rangle = \frac{|+\alpha\rangle \pm |-\alpha\rangle}{\sqrt{2}}. \tag{4.59}$$

On the contrary, if the voltage is rather high: $|\delta_\alpha| \ll \mathcal{J}V$, then the splitting is mainly controlled by the mean-field interaction $H_{\text{mf}}^{\text{e-i}}$ and, hence, the doublet $\{|+\alpha\rangle, |-\alpha\rangle\}$ breaks into $|\psi_S^{\pm\alpha}\rangle = |\pm\alpha\rangle$. Therefore, the hierarchy of voltages arises.

- If $\mathcal{D}_z \gg \mathcal{J}V \gg |\delta_1|$ then all of the doublets are split by the effective field $H_{\text{mf}}^{\text{e-i}}$ and the wave functions $|\psi_S^{\alpha}\rangle$ of $H_{\text{imp}}^{\text{tot}}$ are approximately given by $|\psi_S^{\alpha}\rangle = |\alpha\rangle$, $\alpha = S, S-1, ..., -S$.

- If $|\delta_1| \gg \mathcal{J}V \gg |\delta_2|$ then $|\psi_S^{\alpha}\rangle = |\alpha\rangle$ for $|\alpha| > 1$ and $\alpha = 0$ whereas

$$|\psi_S^{\pm 1}\rangle = \frac{|+1\rangle \pm |-1\rangle}{\sqrt{2}}.$$

- If $\delta_2 \gg \mathcal{J}V \gg \delta_3$ then $|\psi_S^{\alpha}\rangle = |\alpha\rangle$ for $|\alpha| > 2$ and $\alpha = 0$ whereas

$$|\psi_S^{\pm 1}\rangle = \frac{|+1\rangle \pm |-1\rangle}{\sqrt{2}}, \quad |\psi_S^{\pm 2}\rangle = \frac{|+2\rangle \pm |-2\rangle}{\sqrt{2}},$$

and so on.

As a result of the competition between the splitting mechanisms qualitatively new backscattering regimes emerge. In the next section, we investigate them.

4.4.2 Backscattering current due to the impurity with integer spin

The manifestations of the non-uniaxial admixture to the anisotropy are exceptionally rich in the regime of the intermediate temperatures and voltages $\max\{\mathcal{J}^2 T, \mathcal{J}V\} \ll |\mathcal{D}_z| \ll \max\{T, V\}$ (region II in Fig. 4.1). Below, we will restrict the discussion to this case. The transport at low energies $\max\{T, V\} \ll |\mathcal{D}_z|$ in the presence of a finite $\mathcal{D}_x$ is beyond the scope of the thesis.

To begin with, we assume that the voltage is sufficiently high $V \gg \mathcal{J}T$. In this regime all energy levels are well-separated and each doublet's splitting exceeds the broadening due to the Korringa-type relaxation $\sim \tau_K^{-1} \sim \mathcal{J}^2 \max\{T, V\}$. The classical Markov equation (4.44) may be used to establish the steady state density matrix $\rho_S^{(\text{st})}$ of the magnetic impurity. First, we find $\rho_S^{(\text{st})}$ when the voltage belongs to the interval $|\mathcal{D}|_z \gg \mathcal{J}V \gg |\delta_1|$. In this case, all of the doublets are split predominantly by the mean-field interaction $H_{\text{mf}}^{\text{e}-\text{i}}$. Hence, all signatures of the non-uniaxial admixture $\mathcal{D}_x S_x^2$ to the anisotropy effectively drop from Eq. (4.44). Thus, the answer (4.48) for uniaxial anisotropy is recovered:

$$\rho_S^{(\text{st})} = \sum_\alpha p_\alpha^{(\text{st})} |\alpha\rangle\langle\alpha|, \quad p_\alpha^{(\text{st})} = \exp\left(\beta\alpha\right)/\mathcal{Z}, \quad \beta = 2\text{arth}\left(\frac{V}{2T}\frac{\mathcal{X}_{zz}}{\Gamma_{zz}}\right). \tag{4.60}$$

After that, we consider the voltage interval $|\delta_1| \gg \mathcal{J}V \gg |\delta_2|$. In this limit, all doublets but $\{|+1\rangle, |-1\rangle\}$ are split by $H_{\text{mf}}^{\text{e}-\text{i}}$ whereas the latter breaks into the symmetric and antisymmetric combinations due to $\mathcal{D}_x S_x^2$ (see Eq. (4.59)). Taking this feature into the account, we solve Eq. (4.44) and find the steady state density matrix. It is diagonal in the basis of the states with a fixed spin z-projection and has the following form:

$$\rho_S^{(\text{st})} = \sum_\alpha p_\alpha^{(\text{st})} |\alpha\rangle\langle\alpha|, \quad p_\alpha^{(\text{st})} = \frac{1}{\mathcal{Z}} \begin{cases} \exp\left(\beta(\alpha-1)\right), & \alpha > 1, \\ 1, & |\alpha| \leq 1, \\ \exp\left(\beta(\alpha+1)\right), & \alpha < -1. \end{cases} \tag{4.61}$$

Thus, in the regime $|\delta_1| \gg \mathcal{J}V \gg |\delta_2|$ the states with $\alpha = -1$, 0, 1 are populated equally. The consequences of such peculiar structure of $\rho_S^{(\text{st})}$ for the backscattering current are particularly vivid for the impurity with $S = 1$. In this case $\rho_S^{(\text{st})} = \rho_S^{(\text{eq})} = I_{3\times3}/3$. Then, with the help of Eq. (3.30),

for the correction to the ballistic current we immediately find:

$$I_{\mathrm{bs}} = -\frac{2\pi^2}{3} \left\{ \left(\mathcal{J}^T \mathcal{J} \right)_{xx} + \left(\mathcal{J}^T \mathcal{J} \right)_{yy} \right\} G_0 V. \tag{4.62}$$

Remarkably, the expression (4.62) remains finite even for the exchange interaction matrix $\mathcal{J}^{(\mathrm{iso})} =$ diag $\{\mathcal{J}_\perp, \mathcal{J}_\perp, \mathcal{J}_z\}$. As was discussed before, $H_{\mathrm{edge}}^{\mathrm{e-i}} = \mathcal{J}_{ij}^{(\mathrm{iso})} S_i s_j / \nu$ commutes with $S_z + \Sigma_z$ for $\mathcal{J} = \mathcal{J}^{(\mathrm{iso})}$ and, hence, cannot induce the backscattering by itself. However, the presence of $\mathcal{D}_x S_x^2$ breaks the conservation of $S_z + \Sigma_z$ and, thus, allows for non-zero I_{bs}.

In principle, all further intervals $|\delta_\alpha| \gg \mathcal{J}V \gg |\delta_{\alpha+1}|$ with $\alpha > 1$ may be analysed in a manner similar to that described above. For example, by solving the master equation for the voltages $|\delta_2| \gg \mathcal{J}V \gg |\delta_3|$ we establish that the structure of the steady state density matrix resembles the one presented in Eq. (4.61), although the populations of *five* intermediate states are equal:

$$p_\alpha^{(\mathrm{st})} = \frac{1}{\mathcal{Z}} \left\{ e^{\beta(S-2)}, ..., e^\beta, 1, 1, 1, 1, 1, e^{-\beta}, ..., e^{-\beta(S-2)} \right\}_\alpha. \tag{4.63}$$

Yet, in the present thesis we do not discuss the voltage intervals $|\delta_\alpha| \gg \mathcal{J}V \gg |\delta_{\alpha+1}|$ with $\alpha > 1$ thoroughly.

Now, we proceed to the case $\mathcal{J}V \ll T$. Crucially, only *some* of the doublets are strongly smeared by the relaxation in this regime. Indeed, while the splitting of the pair $\{|+\alpha\rangle, |-\alpha\rangle\}$, which is given by $\delta_\alpha \sim \mathcal{D}_x (\mathcal{D}_x/\mathcal{D}_z)^{\alpha-1}$, differs parametrically between the doublets, the level broadening $\sim \mathcal{J}^2 T$ is the same – at least on a parametric level – for all of the states. Therefore, if, for instance, $|\mathcal{D}_z| \gg \mathcal{J}^2 T \gg |\delta_1|$, then all of the doublets are strongly smeared by relaxation. If $|\delta_1| \gg \mathcal{J}^2 T \gg |\delta_2|$, then the states $|\psi_S^{+1}\rangle$ and $|\psi_S^{-1}\rangle$ (see Eq. (4.59)) are well-separated whereas the broadening of the doublets $\{|+\alpha\rangle, |-\alpha\rangle\}$ with $\alpha > 1$ exceeds the splitting. Similarly, if $|\delta_2| \gg \mathcal{J}^2 T \gg |\delta_3|$ then the first two doublets, $\{|+1\rangle, |-1\rangle\}$ and $\{|+2\rangle, |-2\rangle\}$ are well-split while the other ones – with $\alpha > 2$ – are strongly smeared, and so on. As a result, in the regime $\mathcal{J}V \ll T$ the hierarchy of *temperatures* alike that of the voltages for $\mathcal{J}V \gg T$ is present.

In order to evaluate the backscattering current, we first determine the steady state density matrix $\rho_S^{(\mathrm{st})}$ with the help of Eq. (4.51) modified by the presence of $\mathcal{D}_x S_x^2$. For $|\mathcal{D}_z| \gg \mathcal{J}^2 T \gg |\delta_1|$ the result for $\rho_S^{(\mathrm{st})}$ matches with (4.53). Then the backscattering current is given by Eq. (4.54). For the temperature satisfying $|\delta_1| \gg \mathcal{J}^2 T \gg |\delta_2|$ we find

$$\rho_S^{(\mathrm{st})} \simeq \frac{I_{(2S+1)\times(2S+1)}}{2S+1} + \frac{V}{T} \sum_\alpha p_\alpha^{(1)} |\alpha\rangle\langle\alpha|, \tag{4.64}$$

where

$$p_\alpha^{(1)} = \begin{cases} \frac{\alpha-1}{2S+1}\frac{\mathcal{X}_z}{(\Gamma_0)_{zz}}, & \alpha > 1, \\[2mm] 0, & |\alpha| \leq 1, \\[2mm] \frac{\alpha+1}{2S+1}\frac{\mathcal{X}_z}{(\Gamma_0)_{zz}}, & \alpha < -1. \end{cases} \tag{4.65}$$

Then, using Eq. (4.53) we obtain

$$I_{\mathrm{bs}} = \pi^2 \frac{S(S+1)}{3}\left(\frac{2(S-1)}{2S+1}\frac{\mathcal{X}_z^2}{(\Gamma_0)_{zz}} - g\right)G_0 V, \quad g = \left(\mathcal{J}^T\mathcal{J}\right)_{xx} + \left(\mathcal{J}^T\mathcal{J}\right)_{yy}. \tag{4.66}$$

The regimes $|\delta_\alpha| \gg \mathcal{J}^2 T \gg |\delta_{\alpha+1}|$ may be considered in a similar way. We leave them outside the framework of the present thesis.

In conclusion of this section, we mention that the results discussed above indicate that a series of *qualitatively* new regimes of the backscattering emerge in the (V, T) plane for the impurity with integer spin in the presence of non-uniaxial admixture to the anisotropy. Hence, the region II of the diagram 4.1 gets subdivided into the region II_0 defined by $|\mathcal{D}_z| \gg \max\{\mathcal{J}^2 T, \mathcal{J}V\} \gg |\delta_1|$, the region II_1 which corresponds to $|\delta_1| \gg \max\{\mathcal{J}^2 T, \mathcal{J}V\} \gg |\delta_2|$, and so on. These new regions are depicted in Fig. 4.4.
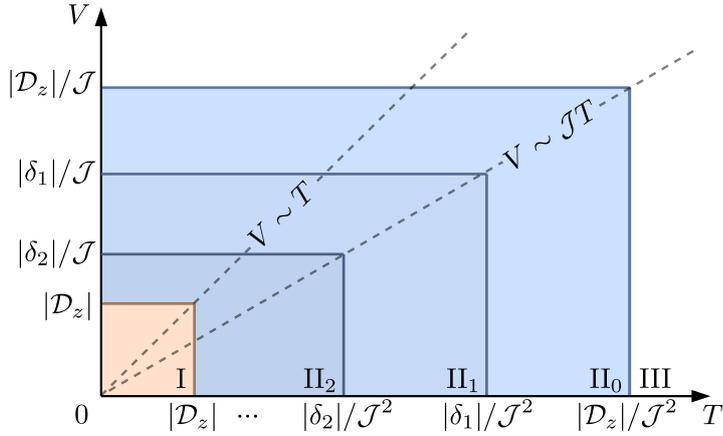

Figure 4.4: Regions in the (V, T) plane. Finite $\mathcal{D}_x$ splits the region II of Fig. 4.1 into the regions II_0, II_1, II_2, and so on.

Chapter 5

Conclusions

In the thesis, we conducted a comprehensive study of the transport along the edge of a 2D topological insulator in the presence of a sole quantum magnetic impurity with arbitrary spin S. No constrictive assumptions about the relative magnitude of the applied voltage V and temperature T were made. For the impurities with $S > 1/2$ the local magnetic anisotropy was taken into account. Below, we highlight the main *novel* results of the work.

- In Chapter 3 we considered the helical edge transport assuming that the local anisotropy of the magnetic impurity may be ignored. We have shown that the backscattering current I_{bs} mediated by the impurity is determined by the stationary state of the latter (see Eq. (3.30)). In order to evaluate the corresponding spin averages we derived, the master equation (3.19) for the reduced density matrix of the impurity ρ_S.

- With the help of Eqs. (3.30) and (3.19) we evaluated the correction to the ballistic conductance in the linear limit $V \ll \mathcal{J}T$ (see Eq. 3.32). No assumptions about the the exchange interaction constants $\mathcal{J}_{ij}$ ($i, j = x, y, z$) apart from $\mathcal{J} \ll 1$ were made.

- We established that in the non-linear limit $V \gg \mathcal{J}T$ the steady state density matrix $\rho_S^{(\mathrm{st})}$ of the magnetic impurity has a Gibbs structure (3.44). It is characterized by the effective non-equilibrium temperature (3.45). Using $\rho_S^{(\mathrm{st})}$ we found the explicit expression (3.49) for the backscattering current in the regime $\mathcal{J}T \ll V \ll T$.

- For the impurity with $S = 1/2$ we found the backscattering current I_{bs} analytically for any voltage V and temperature T (see Eq. 3.52).

- In Chapter 4 we examined the influence of the local magnetic anisotropy of the impurity on the transport properties of the helical edge. We established that the anisotropy of typical

magnitude $\mathcal{D}$ may be fully neglected in the regime $\max\{\mathcal{J}^2 T, \mathcal{J}V\} \gg \mathcal{D}$ only. In case the condition is not fulfilled, the anisotropy strongly affects the backscattering current.

- In section 4.1 we estimated the anisotropy produced by the indirect exchange interaction of the magnetic impurity with itself (see Eqs. (4.6) and (4.8)) for the 2D topological insulator based on the CdTe/HgTe/CdTe quantum well.

- In section 4.3 we considered the case of the uniaxial anisotropy of the impurity, i.e. $H_{\text{imp}} = \mathcal{D}_z S_z^2$. First, we analysed the low-energy limit $\max\{T, V\} \ll |\mathcal{D}_z|$. For the easy-axis anisotropy we obtained the explicit expression (4.34) for the backscattering current. If the anisotropy is of the easy-plane type, the results differ for the impurities with integer and half-integer spin. For integer S we have shown that the backscattering is mainly induced by the virtual transition of the impurity to the excited states (see Eqs. (4.38) and (4.39)). For half-integer S we have mapped the problem to the transport in the presence of a spin-1/2 impurity and obtained Eq. (4.42) for I_{bs}. Then we discussed the limit of intermediate voltages and temperatures $\max\{\mathcal{J}^2 T, \mathcal{J}V\} \ll |\mathcal{D}_z| \ll \max\{T, V\}$. We found the corresponding stationary state of the density matrix of the impurity (see Eqs. (4.48), (4.53), and (4.55)).

- Finally, in section 4.4 we analysed the influence of a small non-uniaxial admixture $\mathcal{D}_x S_x^2$ to the anisotropy with $|\mathcal{D}_x| \ll |\mathcal{D}_z|$ on the helical edge transport. For the impurity with the integer spin we established that qualitatively new backscattering regimes emerge in the (V, T) plane (see Fig. 4.4).

In the future, we will examine the influence of electron-electron interaction on the transport properties of the edge of the topological insulator in the presence of an anisotropic magnetic impurity. Furthermore, we will try to take more than one impurity into account.

Bibliography

[1] C. L. Kane and E. J. Mele. Z_2 topological order and the quantum spin Hall effect. *Phys. Rev. Lett.*, 95:146802, 2005.

[2] X.-L. Qi and S.-C. Zhang. Topological insulators and superconductors. *Rev. Mod. Phys.*, 83:1057, 2011.

[3] M. Z. Hasan and C. L. Kane. *Colloquium*: Topological insulators. *Rev. Mod. Phys.*, 82:3045, 2010.

[4] Y. Ando. Topological insulator materials. *Journal of the Physical Society of Japan*, 82(10):102001, 2013.

[5] Y. Xia, D. Qian, D. Hsieh, L. Wray, A. Pal, H. Lin, A. Bansil, D. Grauer, Y. S. Hor, R. J. Cava, and M. Z. Hasan. Topological insulator materials. *Journal of the Physical Society of Japan*, 82(10):102001, 2013.

[6] T. Sato, K. Segawa, H. Guo, K. Sugawara, S. Souma, T. Takahashi, and Y. Ando. Direct evidence for the Dirac-cone topological surface states in the ternary chalcogenide TlBiSe$_2$. *Phys. Rev. Lett.*, 105:136802, 2010.

[7] M. König, H. Buhmann, L. W. Molenkamp, T. Hughes, C.-X. Liu, X.-L. Qi, and S.-C. Zhang. The quantum spin Hall effect: Theory and experiment. *J. Phys. Soc. Jpn*, 77:031007, 2008.

[8] B. A. Bernevig, T. L. Hughes, and S.-C. Zhang. Quantum spin Hall effect and topological phase transition in HgTe quantum wells. *Science*, 314(5806):1757, 2006.

[9] M. König, S. Wiedmann, C. Brüne, A. Roth, H. Buhmann, L. W. Molenkamp, X.-L. Qi, and S.-C. Zhang. Quantum spin Hall insulator state in HgTe quantum wells. *Science*, 318(5851):766, 2007.

[10] M. König, M. Baenninger, A. G. F. Garcia, N. Harjee, B. L. Pruitt, C. Ames, P. Leubner, C. Brüne, H. Buhmann, L. W. Molenkamp, and D. Goldhaber-Gordon. Spatially resolved study of backscattering in the quantum spin Hall state. *Phys. Rev. X*, 3:021003, 2013.

[11] L. Du, I. Knez, G. Sullivan, and R.-R. Du. Robust helical edge transport in gated InAs/GaSb bilayers. *Phys. Rev. Lett.*, 114:096802, 2015.

[12] C. Sabater, D. Gosálbez-Martínez, J. Fernández-Rossier, J. G. Rodrigo, C. Untiedt, and J. J. Palacios. Topologically protected quantum transport in locally exfoliated bismuth at room temperature. *Phys. Rev. Lett.*, 110:176802, 2013.

[13] Z. Fei, T. Palomaki, S. Wu, W. Zhao, X. Cai, B. Sun, P. Nguyen, J. Finney, X. Xu, and D. H. Cobden. Edge conduction in monolayer WTe_2. *Nature Physics*, 13:677, 2017.

[14] G. M. Gusev, Z. D. Kvon, E. B. Olshanetsky, A. D. Levin, Y. Krupko, J. C. Portal, N. N. Mikhailov, and S. A. Dvoretsky. Temperature dependence of the resistance of a two-dimensional topological insulator in a HgTe quantum well. *Phys. Rev. B*, 89:125305, 2014.

[15] R. A. Niyazov, D. N. Aristov, and V. Yu. Kachorovskii. Tunneling Aharonov-Bohm interferometer on helical edge states. *arXiv:1804.01115*, 2018.

[16] N. Kainaris, I. V. Gornyi, S. T. Carr, and A. D. Mirlin. Conductivity of a generic helical liquid. *Phys. Rev. B*, 90:075118, 2014.

[17] J. I. Väyrynen, M. Goldstein, and L. I. Glazman. Helical edge resistance introduced by charge puddles. *Phys. Rev. Lett.*, 110:216402, 2013.

[18] J. I. Väyrynen, M. Goldstein, Y. Gefen, and L. I. Glazman. Resistance of helical edges formed in a semiconductor heterostructure. *Phys. Rev. B*, 90:115309, 2014.

[19] J. Maciejko, Ch. Liu, Y. Oreg, X.-L. Qi, C. Wu, and S.-C. Zhang. Kondo effect in the helical edge liquid of the quantum spin Hall state. *Phys. Rev. Lett.*, 102:256803, 2009.

[20] Y. Tanaka, A. Furusaki, and K. A. Matveev. Conductance of a helical edge liquid coupled to a magnetic impurity. *Phys. Rev. Lett.*, 106:236402, 2011.

[21] J. I. Väyrynen, F. Geissler, and L. I. Glazman. Magnetic moments in a helical edge can make weak correlations seem strong. *Phys. Rev. B*, 93:241301, 2016.

[22] L. Kimme, B. Rosenow, and A. Brataas. Backscattering in helical edge states from a magnetic impurity and Rashba disorder. *Phys. Rev. B*, 93:081301, 2016.

[23] P. D. Kurilovich, V. D. Kurilovich, I. S. Burmistrov, and M. Goldstein. Helical edge transport in the presence of a magnetic impurity. *JETP Letters*, 106(9):593, 2017.

[24] B. A. Volkov and O. A Pankratov. Two-dimensional massless electrons in an inverted contact. *JETP Lett.*, 42:178, 1985.

[25] V. D. Kurilovich, P. D. Kurilovich, and I. S. Burmistrov. Indirect exchange interaction between magnetic impurities near the helical edge. *Phys. Rev. B*, 95:115430, 2017.

[26] M. V. Entin, M. M. Mahmoodian, and L. I. Magarill. Linearity of the edge states energy spectrum in the 2D topological insulator. *Europhysics Letters*, 118(5):57002, 2017.

[27] P. D. Kurilovich, V. D. Kurilovich, and I. S. Burmistrov. Indirect exchange interaction between magnetic impurities in the two-dimensional topological insulator based on CdTe/HgTe/CdTe quantum wells. *Phys. Rev. B*, 94:155408, 2016.

[28] G. M. Minkov, A. V. Germanenko, O. E. Rut, A. A. Sherstobitov, M. O. Nestoklon, S. A. Dvoretski, and N. N. Mikhailov. Spin-orbit splitting of valence and conduction bands in hgte quantum wells near the dirac point. *Phys. Rev. B*, 93:155304, 2016.

[29] S. A. Tarasenko, M. V. Durnev, M. O. Nestoklon, E. L. Ivchenko, J.-W. Luo, and A. Zunger. Split Dirac cones in HgTe/CdTe quantum wells due to symmetry-enforced level anticrossing at interfaces. *Phys. Rev. B*, 91:081302, 2015.

[30] M. V. Durnev and S. A. Tarasenko. Magnetic field effects on edge and bulk states in topological insulators based on HgTe/CdHgTe quantum wells with strong natural interface inversion asymmetry. *Phys. Rev. B*, 93:075434, 2016.

[31] D.L. Cox and A. Zawadowski. Exotic kondo effects in metals: Magnetic ions in a crystalline electric field and tunnelling centres. *Advances in Physics*, 47(5):599, 1998.

[32] Á. Rivas and S.F. Huelga. *Open Quantum Systems: An Introduction*. SpringerBriefs in Physics. Springer Berlin Heidelberg, 2011.

[33] J. Korringa. Nuclear magnetic relaxation and resonnance line shift in metals. *Physica*, 16:601, 1950.

[34] M. Esposito, U. Harbola, and S. Mukamel. Nonequilibrium fluctuations, fluctuation theorems, and counting statistics in quantum systems. *Rev. Mod. Phys.*, 81:1665, 2009.

[35] J. Lambe and C. Kikuchi. Paramagnetic resonance of CdTe: Mn and CdS: Mn. *Phys. Rev.*, 119:1256, 1960.